

https://dspace.org/

Application of Micro Computed-Tomography in the characterisation of Early Triassic coprolite microstructures and microfossils from the Burgersdorp Formation (Tarkastad Subgroup, Beaufort Group) of South Africa

Montgomery, Chandelé

2022

https://hdl.handle.net/10539/37004

Downloaded from a DSpace repository. https://dspace.org/



Application of Micro Computed-Tomography in the characterisation of Early Triassic coprolite microstructures and microfossils from the Burgersdorp Formation (Tarkastad Subgroup, Beaufort Group) of South Africa.

By

Chandelé Montgomery (1349460)
ORCID number: 0000-0002-3718-1648

A **dissertation** submitted to the Faculty of Science, University of the Witwatersrand, Johannesburg, in fulfilment of the requirements for the degree of **Master of Science** in **Palaeontology**.

Supervisor: Prof. Jonah N. Choiniere
Co-supervisor: Dr. P. John Hancox
Johannesburg, 2022





1. DECLARATION

I declare that this dissertation is my own, unaided work. It is being submitted for the Degree of Master of Science at the University of the Witwatersrand, Johannesburg. It has not been submitted before for any degree or examination at any other University.



C. Montgomery

Signed on the 24th day of June 2022 at the Evolutionary Studies Institute, University of the Witwatersrand, Johannesburg

2. ABSTRACT

Driefontein 11, a farm in the Free State province of South Africa, is a fossiliferous Early Triassic locality with a diverse and prolific coprolite assemblage. This study used micro-CT to characterise the coprofabrics and coprolite inclusions of 47 coprolites from this assemblage, and assesses how well these variables correlate with their respective morphotype assignations. Three different coprofabrics were characterised: homogenous massive, heterogenous massive and heterogenous zoned. Homogenous massive coprofabrics are indicative of coprolite perpetrators with high digestive efficacy, whereas both types of the heterogenous coprofabrics are indicative of individuals with varying digestive strategies. The coprolites document several microfossil inclusions including fish, tetrapods and the second instance of Early Triassic beetles and freshwater bivalves. The coprolite ordination shows that there is no unambiguous correlation between morphotypes or coprofabrics and microfossil inclusions. This contribution is a first step in the understanding of the fauna that inhabited this Early Triassic ecosystem and their feeding ecology.

3. ACKNOWLEDGEMENTS

In my academic career thus far, I have found this research to be one of the most challenging yet rewarding experiences. I wish to extend my sincere gratitude to several individuals without whom this research would not have been a success.

First and foremost, I would like to thank my supervisors Prof. Jonah N. Choiniere and Dr. P. John Hancox. It has been an extraordinarily trying two years and I am deeply grateful for your patience, encouragement, and understanding. Your belief in both me and my peers pushes us to achieve our absolute best and for that I will be forever grateful. I have found in you not only role models but lifelong confidantes and mentors.

To numerous colleagues and members of staff at the Evolutionary Studies Institute, particularly PhD student Gideon Chinamatira for the time he dedicated to CT-scanning my specimens and Dr. Frank H. Neumann for his help and guidance in the initial development of this project. Postgraduate students Frederick B. Tolchard, Atashni Moopen and SoRi La have been invaluable partners and a point of social contact during a time where such things are scares.

Thanks to my family and friends, who believe in me without reservation and have supported me in following my passions. Your kindness and generosity have meant so much to me. To my parents, I am grateful for all the sacrifices you've made to enable me to pursue my dreams. To my sister, thank you for brightening even my darkest days. To my friends, thank you for keeping me sane and loving me unconditionally.

Lastly, I would like to acknowledge the financial aid from GENUS: DSI-NRF Centre of Excellence in Palaeosciences that made this research possible.

4. CONTENTS

1. DECLARATION i
2. ABSTRACT i
3. ACKNOWLEDGEMENTS i
4. CONTENTS ii
5. LIST OF FIGURES iv
6. LIST OF TABLES v
7. INTRODUCTION 1
8. LITERATURE REVIEW 4
   - 8.1. History of Study 4
   - 8.2. Utility of Coprolites 6
9. GEOLOGICAL SETTING 8
10. MATERIALS AND METHODS 13
    - 10.1. Materials 13
    - 10.2. Methods 13
      - 10.2.1. Microtomography (micro-CT) 13
      - 10.2.2. Coprolite Microstructure and Microfossil Analyses 14
      - 10.2.3. Coprolite ordination 15
11. RESULTS 23
    - 11.1. Coprofabrics 23
      - 11.1.1. Homogenous Coprofabrics 23
      - 11.1.2. Heterogenous Coprofabrics 24
    - 11.2. Inclusions 31
      - 11.2.1. Invertebrates 31
      - 11.2.2. Vertebrates 36

11.3. Coprolite Ordination 39
12. DISCUSSION 43
12.1. Coprofabrics 43
12.2. Inclusions 45
12.2.1. Bivalves 45
12.2.2. Arthropods 46
12.2.3. Pisces 47
12.2.4. Tetrapods 48
12.3. Digestive Strategies 49
12.4. Comparison of classic and non-destructive methods 50
13. CONCLUSION 52
14. APPENDIX. 53
14.1. Appendix A 53
14.2. Appendix B 54
14.3. Appendix C 70
15. REFERENCES 72

5. LIST OF FIGURES

Figure 1: Lithostratigraphy, vertebrate biostratigraphy and geochronology of the Beaufort and Stormberg groups (Karoo Supergroup), east of 24°E, in the Main Karoo Basin, South Africa. 9

Figure 2: Locality map and geological setting of Driefontein 11 farm in the eastern Free State of South Africa. Adapted from Yates et al. (2012)..... 11

Figure 3: Stratigraphic log of the Driefontein strata. Adapted from Jenkins, et al., in press..... 12

Figure 4: Longitudinal CT-slice images of coprolites with massive, homogenous coprofabrics. 24

Figure 5: CT-slice images of coprolites with massive, heterogenous coprofabrics.. 26

Figure 6: CT-slice images of coprolites with muddled zoned, heterogenous coprofabrics. 27

Figure 7: CT-slice images of coprolites with muddled zoned, heterogenous coprofabrics. 28

Figure 8: CT-slice images of coprolites with zoned, heterogenous coprofabrics both in longitudinal..... 29

Figure 9: CT-slice images of coprolites with zoned, heterogenous coprofabrics. 30

Figure 10: Contents of coprolite BP/21/422, assigned to morphotype 1. 32

Figure 11: Contents of coprolite BP/21/161, assigned to morphotype 2. 33

Figure 12: Contents of coprolite BP/21/2, assigned to the existing ichnotaxon *Alococoprus triassicus*. 35

Figure 13: Contents of coprolite BP/21/263, assigned to morphotype 4. 37

Figure 14: Contents of coprolite BP/21/421, assigned to morphotype 4. 38

Figure 15: Non-metric Multidimensional Scaling (NMDS) ordination. The graph represents the relationships among coprolite heterogenous coprofabrics according to the coprolite inclusions per specimen.. 41

Figure 16: Non-metric Multidimensional Scaling (NMDS) ordination. The graph represents the relationships among coprolite morphotypes according to the coprolite inclusions per specimen. 42

6. LIST OF TABLES

Table 1: Summary of coprolite ichnotaxa and morphotypes along with their potential perpetrators (Montgomery, 2019). 3

Table 2: List of coprolites micro-CT scanned from the Driefontein collection. 17

Table 3: Species found in the lowest most subzone of Cynognathus Assemblage Zone at Driefontein. 53

Table 4: Coprolites from the farm Driefontein 11 coprolite collection with their corresponding inchnotaxa/morphotypes. 54

7. INTRODUCTION

Real-time observational data are critical for the study, conceptualisation and categorisation of animal behaviour and interactions (Hsieh and Plotnick, 2020). Such data are rare in the fossil record, representing a critical barrier for assessing the behavioural repertoires of extinct animals (Benton, 2010, Hsieh and Plotnick, 2020). As a result, most of our current understanding of the behaviour of extinct fauna comes from indirect evidence, such as statistical analyses of associated and/or co-occurring fossils (such as potential predators and prey animals), theoretical models, trace fossil analyses, and inferred functional morphology and phylogeny (Benton, 2010, Hsieh and Plotnick, 2020).

Fossil faeces (formally known as coprolites) are the end-point of digestion, and serve as proxies that provide direct evidence of feeding behaviour, diet and digestion for the animals (Thulborn, 1991, Hunt et al., 1994, Chin and Kirkland, 1998, Hunt et al., 2013b, Niedźwiedzki et al., 2016a, 2016b, Barrios-de Pedro and Buscalioni, 2018, Hunt and Lucas, 2020 , Hunt and Lucas, 2021). Over the past decade, studies on coprolites have shown that their utility extends beyond this. They act as micro-lagerstätte (Seilacher et al., 2001, Qvarnström et al., 2016, Cueille et al., 2020, Dentzien-Dias et al., 2020), preserving otherwise poorly preserved microfossils, they delimit a hierarchy of ichnocoenosis and ichofacies (Hunt et al., 1998, 2007, 2013a, Hunt and Lucas, 2017); and researchers use them in studies on biochronology, biogeography and faunal turnovers (Hunt, 1992, Chin and Kirkland, 1998, 2003, Hunt et al., 2005a, 2013b, 2018, Knaust, 2020, Hunt and Lucas, 2020).

In my Honours research I characterised the external morphologies of a coprolite assemblage from the farm Driefontein 11 in the Free State province of South Africa. I examined 2000 coprolite specimens, assigning them to eleven distinct morphotypes (Montgomery, 2019; see Table 1). This M.Sc. study aims to characterise their coprofabrics and material inclusions to assess how well the material inclusions correlate with their respective morphotype and coprofabric assignations. Classical inference of digestive strategies and diet from coprolite assemblages involves investigation of external macroscopic properties, destructive petrographic thin sections and external and/or internal Scanning Electron Microscopic (SEM)

properties (e.g., Eriksson et al., 2011, Barrios-de Pedro and Buscalioni, 2018, Barrios-de Pedro et al., 2019, Qvarnström et al., 2019a). This study goes beyond these classical methods by exploring the use of microtomography (micro-CT) to non-destructively characterise internal microstructures (coprofabrics) and produce three-dimensional (3D) reconstructions of material inclusions. Imaging of coprolites using x-ray radiation has been applied with increasing frequency over the past decade, often with excellent results (e.g., Qvarnström et al., 2017, 2019a, Cueille et al., 2020, Qvarnström et al., 2021).

Table 1: Summary of coprolite ichnotaxa and morphotypes identified in my Honours project along with their potential perpetrators (Montgomery, 2019). Scale bars = 1 cm.

Morphotypes	Morphology	Images	Perpetrators
Alocoprus triassicus	Longitudinally striated, arcuate shape in lateral view, sub-rounded in cross-section.		Erythrosuchid archosaurs 
Eucoprus cylindratus	Cylindrical, elongate, sub-rounded in cross-section.		Vertebrate indeterminate
Hyronocoprus amphipola	Spiraled, amphipolar, anisopolar, elongate.		Dipnoan *Ptychoceratodus phillips* and/or Actinopterrygian *Saurichtys* sp. 
Morphotype 1	Oval, anisopolar, short and fat or long and slender.		Fish 
Morphotypes 2	Elongate, oval, anisopolar, dorsoventrally flattened.		Vertebrate indeterminate
Morphotypes 3	Hook-shaped, pointed terminal end that is arcuate, oval in cross-section.		Vertebrate indeterminate

Morphotypes	Morphology	Images	Perpetrators
Morphotype 4	Spherical, small (<1.5 cm), either round with a distinct ventral surface or discoidal.		Small fishes/invertebrates 
Morphotype 5	Twisted (long axes of segments are not parallel), initial end is rounded, sub-rounded in cross-section.		Vertebrate indeterminate
Morphotype 6	Anisopolar, amphipolar, elongate, few, shallowly angled spirals.		Dipnoan *Ptychoceratodus phillips* and/or Actinopterrygian *Saurichtys* sp. 
Morphotype 7	Anisopolar, amphipolar, few, steeply angled spirals concentrated at terminal end.		Dipnoan *Ptychoceratodus phillips* and/or Actinopterrygian *Saurichtys* sp. 
Morphotype 8	Twisted (long axes of segments are not parallel), dorsoventrally flattened, oval in cross-section.		Vertebrate indeterminate

8. LITERATURE REVIEW

8.1. History of Study

The first studies of that included coprolites date to the late 17th and early 18th century (see Duffin, 2009, 2012), but they were incorrectly identified as identified as either cones or catkins that belong to some unknown plant (e.g., Woodward, 1695; Burtin, 1784; Mantell, 1822). It was naturalist William Buckland that correctly identified their animal origin, linking them specifically to animal excrement which had undergone subsequent fossilisation (Buckland, 1829). Drawing inspiration from the Greek words “copros” and ”lithos” (meaning “dung” and “stone” respectively), he later coined the term “coprolite” for these trace fossils (Buckland, 1829).

Following this recognition by Buckland, coprolites have been studied with intermittent interest over the last two centuries. There is now an extensive and growing literature on coprolites, with the discovery of late Paleozoic and Mesozoic localities with coprolite assemblages in North America (e.g., Hunt, 1992, Krishnaswamy et al., 1994, Chin et al., 2003, Hunt and Lucas, 2005a, Hunt and Lucas, 2005c, Chin et al., 2009, Chin, 2007, Hunt et al., 2007, Cantrell et al., 2012, Hunt et al., 2012b, 2012c, 2013a, 2018), South America (e.g., Souto, 2001, 2007, Schwanke and Souto, 2007, Souto, 2008, Alves, 2010, Souto, 2010, Souto and Schwanke, 2010, Souto and Fernandes, 2015, Dentzien-Dias et al., 2012, 2013, 2017, 2021), and Europe (e.g., Silantiev et al., 2000a, b, Diedrich, 2009, Duffin, 2012, Bajdek, 2013, Niedźwiedzki et al., 2016a, b, Qvarnström et al., 2016, Bajdek et al., 2017, Qvarnström et al., 2017, 2018, Barrios-de Pedro et al., 2018, 2019, Bajdek et al., 2019, Qvarnström et al., 2019a-c, Bajdek and Bienkowska-Wasiluk, 2020, Duffin and Ward, 2020, Qvarnström et al., 2021) renewing interest in the last few decades.

The oldest identified vertebrate coprolites are from the Early Ordovician (e.g., Conway Morris and Robison, 1986, Tolmacheva, 1996, Tolmacheva and Purnell, 2002, Stewart and Nicoll, 2003), rare occurrences are documented through the middle/late Ordovician (e.g., Caster and Kjellesyig-Waering, 1964 , Selden, 1979, Aldridge et al., 2006, Briggs et al., 2015, Liu et al., 2017, Hawkins et al., 2018), Silurian (e.g., Strickland and Hooker, 1853, Gilpin, 1886, Murchison, 1867, Rolfe, 1973, Selden, 1984, Gilmore, 1992, Turner and Peterson, 1999), into the Devonian

where they become more common (e.g., Branson, 1914, Rayner, 1963, Trewin, 1986, McAllister, 1996, Bartels et al., 1998, Maisey and Melo, 2005, Wagner et al., 2006, Trewin, 2008, Newman and Davidson, 2010, Hunt et al., 2012b, Kühl et al., 2012, Zatoń and Rakociński, 2014) and into the Carboniferous where larger morphotypes appear (e.g., Buckland, 1836, Price, 1927, Bayer, 1934, Johnson, 1934, Zidek, 1980, McAllister, 1988, Shabica and Godfrey, 1997, Falcon-Lang et al., 2006, Lucas, 2006, Mansky et al., 2012, Hunt et al., 2012b-i, Krzykawski et al., 2014, Lomax et al., 2016, Chipman et al., 2020, Bingham-Koslowski et al., 2021, Hunt and Lucas, 2021).

Permian coprolite abundances are highly variable and geographically wide-spread (Hunt and Lucas, 2013, Hunt and Lucas, 2021). The non-marine red beds of southwestern America are particularly abundant in coprolites and these coprolite assemblages have allowed for specimens from their assemblages to be assigned to ichnotaxa (Hunt et al., 1998, Hunt and Lucas, 2013, Hunt and Lucas, 2021). The current list of ichnotaxa include *Alococopros triassicus* (Cantrell et al., 2012), *Dakyronocopros arroyoensis* (Hunt and Lucas, 2005a, Cantrell et al., 2012) *Heteropolacoprus sp.* (Williams, 1972, McAllister, 1985 , Hunt et al., 2012c, 2012d), *Heteropolacopros texaniensis* (Hunt and Lucas, 2005a, Cantrell et al., 2012, Hunt et al., 2013a), *Hyronocopros amphipola* (Hunt et al., 2005a, 2013a) *Liassocoprus sp.* (Gaudy, 1887, Hunt et al., 2012c, 2012d), *Malericoprus sp.* (Hunt et al., 2012c, 2012d), *Megaheteropolacopros sidmcadamsi* (Hunt and Lucas, 2005a, Hunt et al., 2005b, 2013a), *Saurocoprus sp.* (Hunt et al., 2012c, 2012d), *Strophocoprus sp*. (Hunt et al., 2012c, 2012d) and *Strophocoprus valensis* (Hunt and Lucas, 2005a, Hunt et al., 2005b, 2013a).

Much like the Permian coprolites, Triassic coprolites are abundant in non-marine red beds (Hunt and Lucas, 2021). At present, most Triassic coprolites mentioned or described in the literature come from Upper Triassic deposits (Hunt et al., 2007, Hunt et al., 2013b, Zatoń et al., 2015). Less research has been done on Lower Triassic coprolites, with the only well-described specimens coming from Australia (Northwood, 1997, 2005) where three morphotypes were recognised: amphipolar; longitudinally striated; and indeterminate. Hunt et al. (2007) subsequently assigned

these Lower Triassic amphipolar coprolites to the ichnotaxon *Hyronocopros amphipola* and the longitudinally striated specimens to *Alococopros triassicus*. Lower Triassic coprolites from rocks of the Karoo Supergroup of South Africa were briefly mentioned by Bender and Hancox (2004), where their abundance and inclusions were noted, and by Yates et al. (2012), who reported on two freshwater bivalve species preserved in coprolites that gave evidence of the “Lilliput effect” affecting the Early Triassic recovery fauna at Driefontein.

8.2. Utility of Coprolites

It was in the 1990s that studies on some distinctive and recurring coprolite morphologies demonstrated that they have restricted stratigraphic ranges (Hunt, 1992, Hunt et al., 1993, 1998). This indicated to researchers that coprolites could be useful in studies on biostratigraphy, biogeography and biochronology (Hunt et al., 1993, 1998). Hunt and colleagues (1998) however indicated that the lack of a classification scheme for coprolites hindered their utility, not only in terms of biostratigraphy, biogeography and biochronology but also other potential palaeobiological applications. They therefore strongly advocated for the use of binomial nomenclature (e.g., Hunt and Lucas, 2017, Hunt et al., 2018, Hunt and Lucas, 2021b) to refer to distinct, recurring coprolite morphologies, naming what are now widely considered to be the first valid coprolite ichnotaxa (Hunt et al., 1998).

Assigning coprolites to ichnotaxa requires a good understanding of who produced them. Assigning producers, however, is challenging because a single individual can produce faeces of various sizes and morphologies and conversely, because different animals can also produce similar-looking faeces. This means that a coprolite morphotype is not necessarily unique to an individual taxon, prompting most authors to advocate for the use of morphotypes instead (e.g., Duffin, 2010, Eriksson et al., 2011, Laojumpon et al., 2012, Hansen et al., 2016, Francischini et al., 2016, Milàn et al., 2018, Rakshit et al., 2019, Rummy et al., 2021). The morphotypes allow for differentiation in a coprolite assemblage and then if researchers have a good understanding of the body- and trace fossil record and the contents of the coprolites,

researchers can identify their potential producers and make use of ichnotaxonomy. As a result, most modern studies on coprolite assemblages utilize only morphotypes, (few utilize formal ichnotaxonomy and morphotypes) for biostratigraphy, biogeography and biochronology investigations (e.g., Hunt, 1992, Chin and Kirkland, 1998, 2003, Hunt et al., 2005a, 2013b, 2018, Knaust, 2020, Hunt and Lucas, 2020), as well as the building of palaeoenvironmental transects (Hunt and Lucas, 2017).

The soft nature of faeces before fossilisation means they are subject to rapid degradation by both biotic and abiotic processes (Seilacher et al., 2001, Chin et al., 2003, Hollocher and Hollocher, 2012, Qvarnström et al., 2016). Rapid burial during early taphonomic stages minimises mechanical degradation and can partially or completely inhibit microbial decomposition (Hollocher et al., 2001, Chin, 2002, Dentzien-Dias et al., 2017, Rodrigues et al., 2018). Bacterial autolithification is encouraged instead, a process during which bacteria whose metabolic pathways produce phosphates and iron sulphides as side products mineralise the faeces (Seilacher et al., 2001, Chin et al., 2003, Hollocher and Hollocher, 2012, Qvarnström et al., 2016, Hunt et al., 1994). This means that under the right environmental conditions (oxygenation, pH, temperature), coprolites and their organic inclusions have a high preservation potential (Hunt et al., 1994, Seilacher et al., 2001, Chin et al., 2003, Hollocher and Hollocher, 2012, Qvarnström et al., 2016, Qvarnström et al., 2019c). Coprolites are self-contained potential lagerstätte because they provide a rare, unique preservation environment; preserving parts of the ecosystem and structures not normally part of the fossil record (Chin and Kirkland, 1998, 2003, Dentzien-Dias et al., 2013, Bajdek et al., 2015, Qvarnström et al., 2016, Dentzien-Dias et al., 2017, Qvarnström et al., 2017, 2019c, 2019b, 2021).

9. GEOLOGICAL SETTING

The rocks of the Karoo Supergroup cover more than half of the current land surface of South Africa (~300 000 km^2, Smith, 1990). They represent sediment accumulation across Gondwana when it was still part of the supercontinent Pangea. Because the sedimentary succession accumulated inland, in front of the Cape Fold Mountain, on the cratonic side of the fold-thrust belt, the Karoo Basin is considered an intracratonic, retro-arc, foreland basin (Johnson, 1991, Catuneanu et al., 2005). Accumulation started with the formation of the supercontinent in the Late Carboniferous (~300 Ma) and continued until the break-up of Pangea in the Early Jurassic (~190) Ma, after which the emplacement of basaltic lavas replaced sedimentation (Catuneanu et al., 1998, Catuneanu et al., 2005, Smith et al., 2020).

The Beaufort Group (Fig. 1) of the Karoo Basin is renowned globally as the reference section for the terrestrial environmental succession of the Permo-Triassic (P-T) extinction and the faunal recovery that followed (Hancox et al., 1995, Hancox and Rubidge, 2001, Bender and Hancox, 2004, Neveling et al., 2005, Smith and Botha, 2005, Nicolas and Rubidge, 2010). This is because this single area of deposition documents the gap usually present in other global successions between the Permian and Triassic faunas. The Beaufort Group is dominated by mudstones and siltstones, with subordinate lenticular and tabular sandstones deposited by a variety of fluvial systems, but not all the lithostratigraphic subdivisions of the Beaufort Group extend basin-wide (Catuneanu et al., 2005). They grade eastwards over a palaeohigh known as the “Willowmore Arch” (Van Eeden, 1972), therefore formations for the lithological units west of longitude 24°, east of longitude 24° and Free State/KwaZulu-Natal differ (Catuneanu et al., 2005).

Historically, this division of formations has made the correlation of units difficult on lithological grounds. The rich diversity of tetrapod fossils with a wide distribution across the Beaufort Group proved to be an effective way of subdividing thick monotonous mudstone successions (vertebrate biozones; Kitching, 1977, Keyser and Smith, 1978, Rubidge et al., 1995, Smith et al., 2020) that allow for an effective means of correlating units. The updated and refined Beaufort Group vertebrate biostratigraphic subdivisions (Fig. 1) are listed in stratigraphic order: *Eodicynodon*,

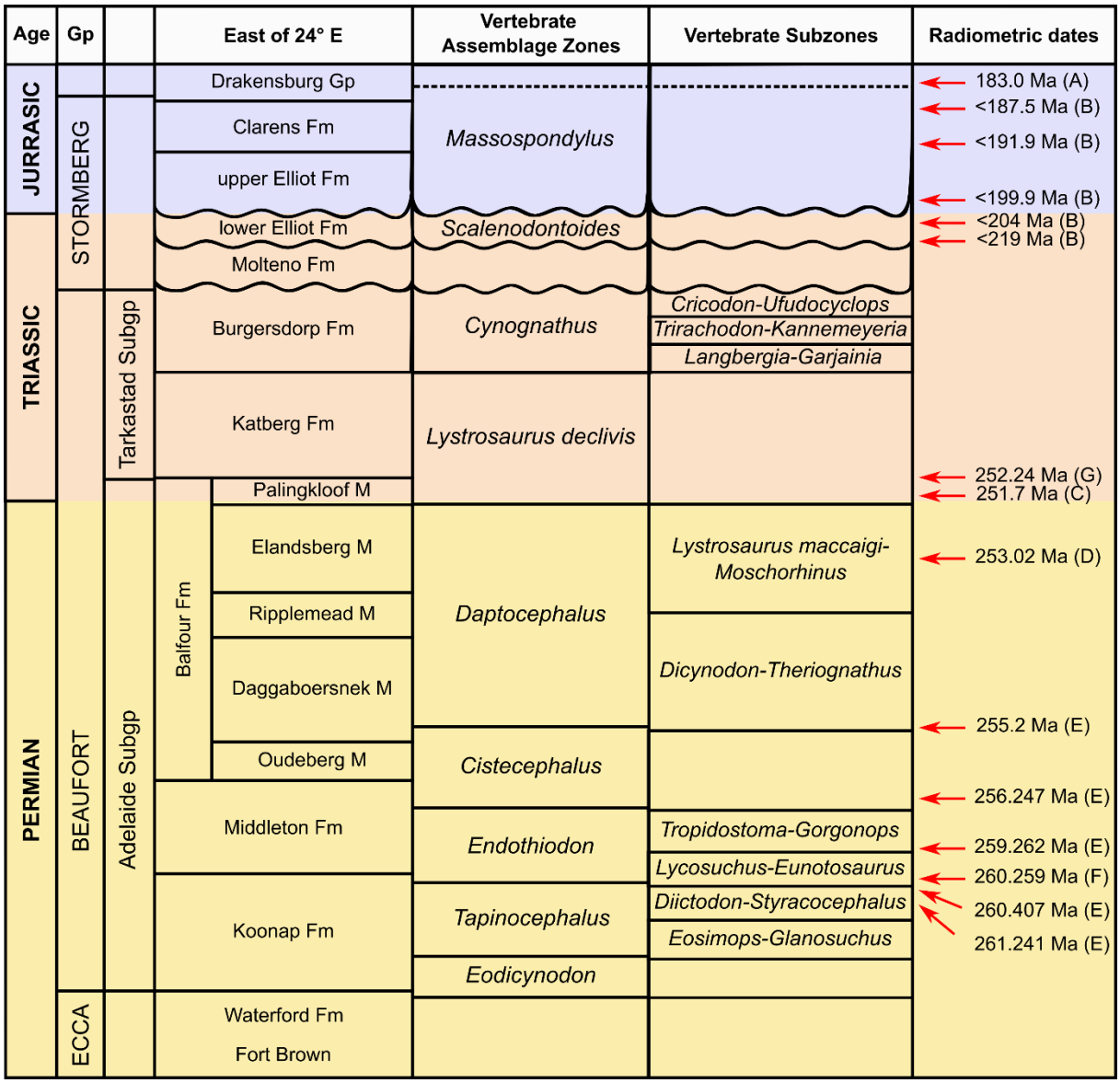

Figure 1: Lithostratigraphy, vertebrate biostratigraphy and geochronology of the Beaufort and Stormberg groups (Karoo Supergroup), east of 24°E, in the Main Karoo Basin, South Africa. Radiometric age determinations from; (A) Duncan et al., (1997), (B) Bordy et al., (2020), (C) Botha et al., (2020), (D) Gastaldo et al., (2015), (E) Rubidge et al., (2013), (F) Day et al., (2015), (G) Gastaldo et al., (2020). Dates prefaced by < are maximum depositional ages based on detrital zircon analyses. Wavy lines represent unconformities. Gp=Group, Subgp=Subgroup, Fm=Formation, M=Member. Adapted from Smith et al., (2020).

Taphinocephalus, *Endothiodon*, *Cistecephalus*, *Daptocephalus*, *Lystrosaurus declivis* and *Cynognathus* Assemblage Zones (AZ) (Smith et al., 2020).

Biostratigraphic ranges indicate that extinction at the end P-T extinction occurred in three phases as different ecotypes were affected at different times (Smith and Botha-Brink, 2014). Changes in the sedimentological facies through the P-T boundary support this theory of a three-phased extinction, indicating climatic drying followed by increased seasonality and then the onset of an unpredictable monsoon-type rainfall regime (Smith and Ward, 2001, Smith and Botha-Brink, 2014). The P-T boundary is thought to coincide with the faunal turnover between the *Daptocephalus* AZ and *Lystrosaurus* AZ, with the faunal recovery during the Early Triassic continuing through to the lowermost subzone of the overlying *Cynognathus* AZ (see Fig. 1; Smith, 1995, Irmis and Whiteside, 2012, Fröbisch, 2013, Irmis et al., 2013, Viglietti et al., 2016, 2021). The macro- and micro-fossils collected from the Burgersdorp Formation (Beaufort Group) have led to a three-fold subdivision of the *Cynognathus* AZ (Fig. 1) into a lower *Langbergia-Garjainia* Subzone, a middle *Trirachodon-Kannemeyeria* Subzone and an upper *Cricodon-Ufudocyclops* Subzone (Hancox et al., 2020).

The coprolites in this study are from an Early Triassic post P-T extinction recovery site on the farm Driefontein 11 in the Bethlehem District of the Free State Province, South Africa (Fig. 2). The fossiliferous donga exposures on this farm are considered the stratotype locality for the *Langbergia-Garjainia* Subzone (Hancox et al., 2020). Mapping of the local stratigraphy (Hancox et al., 2020) shows that the site consists of a lower, horizontally-laminated to massive, dark reddish-brown siltstone and mudstone-dominated unit (Fig. 3, 10R 3/4), which is overlain by light grey fine-grained sandstones (Fig. 2, 5Y 7/1) and intraformational lag on internal scour surfaces (Fig. 3, Sei); and an upper unit of dark reddish-brown siltstone and mudstone which is intercalated with thin (>1m) sandstones (Fig. 3, 10R 3/4). These are here interpreted as having formed in lacustrine, channel belt, and overbank depositional settings respectively.

The lag deposit (Fig. 3, Sei) is exceptionally fossil-rich, reaching clast-on-clast density in some places and this is where the bulk of the material has been collected

from as float (Hancox et al., 2020). This diverse fossil assemblage includes thousands of isolated cranial bones, teeth, scales, and coprolites (Hancox et al., 1995, Shishkin et al., 1995, Hancox and Rubidge, 1997, 1998b, Damiani and Welman, 2001, Neveling, 2002, 2004, Bender and Hancox, 2004, Neveling et al., 2005, Yates et al., 2012, Montgomery, 2019, Hancox et al., 2020). This has led to the identification of several taxa including numerous amphibians, actinopterygians, chondrichthyans, dipnoans, procolophonids, archosauromorphs, cynodonts and therocephalians as well as four coprolite ichnotaxa; *Alococopros triassicus*, *Heteropolacopros*, *Hyronocopros amphipola,* and *Eucoprus cylindratus* and an arthropod trackway (Hancox et al., 1995, Shishkin et al., 1995, Hancox and Rubidge, 1997, Hancox, 1998a, Damiani and Welman, 2001, Neveling, 2002, Bender and Hancox, 2003, 2004, Neveling, 2004, Neveling et al., 2005, Yates et al., 2012, Hancox et al., 2020; see Appendix A for full faunal list).

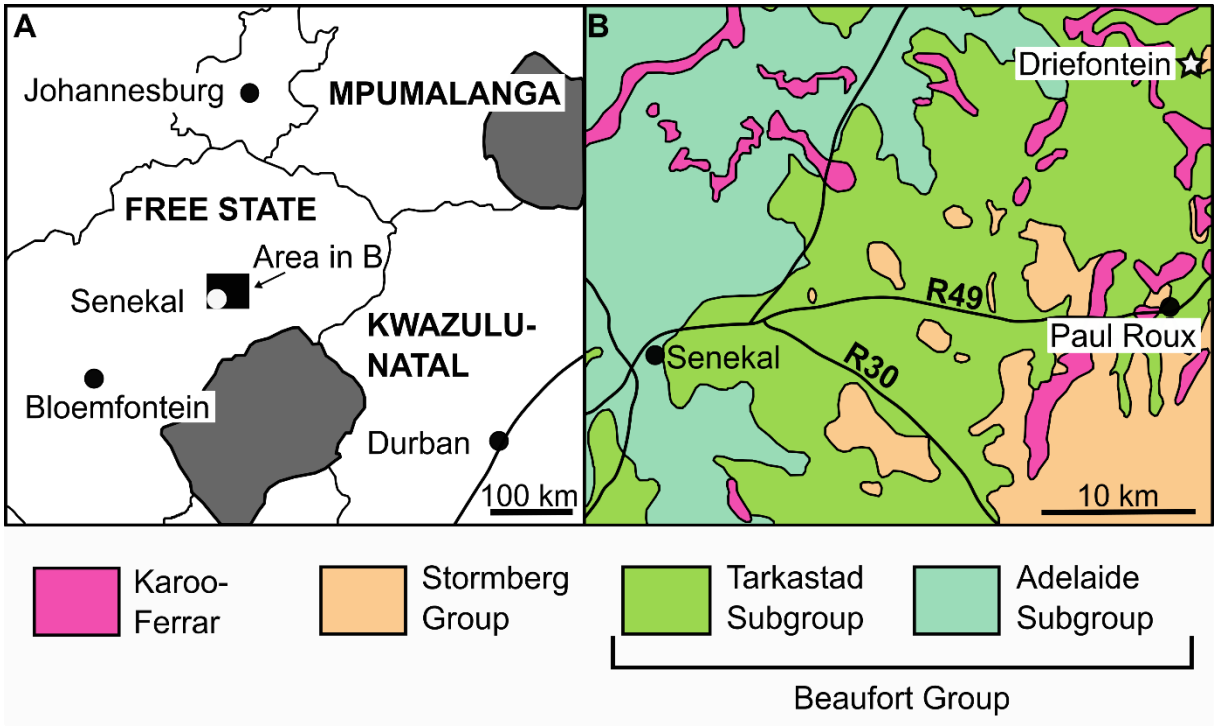

Figure 2: Locality map and geological setting of Driefontein 11 farm in the eastern Free State of South Africa. Adapted from Yates et al. (2012)

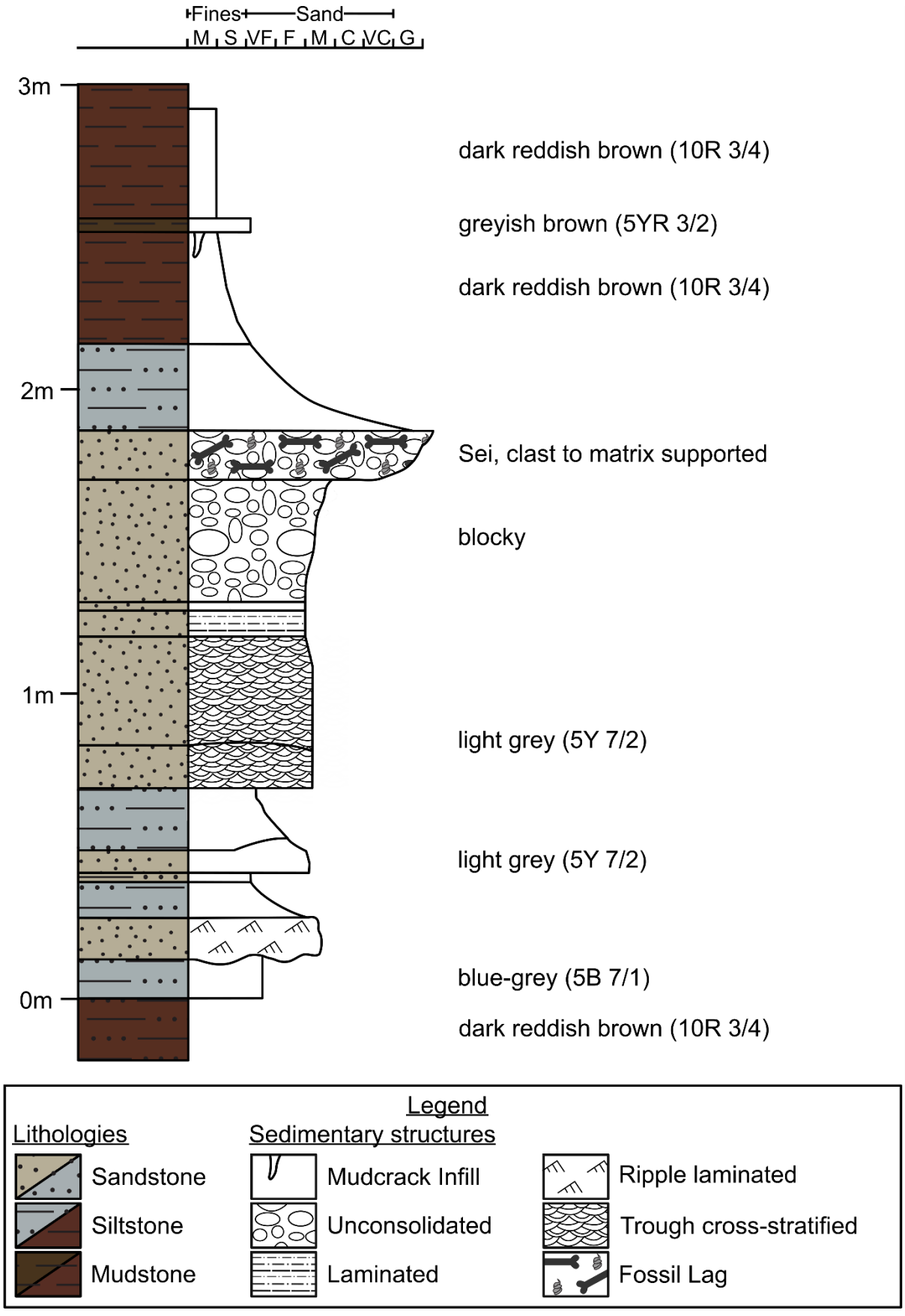

Figure 3: Stratigraphic log of the Driefontein strata. Adapted from Jenkins, et al., in press.

10. MATERIALS AND METHODS

10.1. Materials

The 47 coprolites described here, are all from the farm Driefontein 11 in the Nketoana Local Municipality, Free State Province, South Africa. The coprolites were collected *in situ* from the lower fines and overbank fines (Fig. 3, 10R 3/4) and as float from the lag deposit (Fig. 3, Sei) by Dr. P. John Hancox and colleagues. The coprolites in this study are part of the extremely large collection of coprolites (~30, 000 specimens) retrieved from Driefontein 11 over the last three decades and are housed at the Evolutionary Studies Institute (ESI), University of the Witwatersrand (WITS), Johannesburg, South Africa. The specimens have been catalogued into a new dedicated coprolite series (BP/21/) created with the support and guidance of Dr. Bernhard Zipfel, University Curator of Collections at the ESI (see Table 3 for full list). Each of these catalogue entries represent one coprolite specimen.

In my Honours research (Montgomery, 2019) I sorted the large Driefontein collection into distinct morphotypes based on obvious morphological differences and size. Eleven morphotypes (see Table 1) were identified from the 30,000 coprolites, three of which were assigned to previously defined ichnotaxa namely, *Alococopros triassicus*, *Eucoprus cylindratus* and *Hyronocoprus amphipola*. The 47 coprolites in this study are a representative sample of the morphotypes identified in my Honours research.

10.2. Methods

10.2.1. Microtomography (micro-CT)

CT-scanning of 47 coprolites allowed for non-destructive investigation of the microstructures and microfossils contained within coprolites. The coprolites were scanned in the Nikon Metrology XTH 225/320 LC dual source micro-CT system, at the MicroFocus CT scanning facility, ESI, WITS, Johannesburg, South Africa. This scanner uses the manufacturer's Inspect-X software for controlling the machine and for image reconstruction. For maximum operational flexibility, the machine is

equipped with both rotating and static reflection 225 kV targets and a more powerful 320 kV static target to enable denser fossils to be penetrated.

To obtain detailed 3D images of the coprolites, 3141 projections were created of the rotating specimens with varying parameters for the beam energy (kV) and current (µA) of the X-ray source (see Table 2 for scanning parameters). The magnification of the projected fossil images on the panel resulted in relatively small isotropic voxel (3D pixel) size (µm), giving very fine special resolution (see Table 2 for isotropic voxel sizes). Automated protocols for correcting beam hardening and reducing noise were applied during the reconstructions of the projections. Visualisation and analysis software package VGStudio Max (version 3.2) from Volume Graphics was used to study the resulting CT-slice images and generate 3D reconstructions of microfossil inclusions.

10.2.2. Coprolite Microstructure and Microfossil Analyses

Coprolite microstructures are studied with the aim of establishing the link between the feeding behaviours, dietary composition, and digestive strategies of the perpetrators. This has been done in other studies by characterising the coprofabrics (spatial and geometric configuration of all the coprolite elements) using petrographic thin sections (Eriksson et al., 2011, Barrios-de Pedro et al., 2020, Qvarnström et al., 2019b) and thus focus on mineral composition and grain size of the ground mass along with the presence/absence of inclusions and the type of inclusions. In this study however I have used CT-slice images (non-destructive means) to characterise coprofabric.

Coprolite microfossils were studied with the aim of identifying the inclusions to the lowest taxonomic level possible. Most studies do this by studying the inclusions visible on the external surface or by employing destructive techniques. In this study I used the region-growing tools in VGStudio Max to isolate regions of interest in the CT-slice images for microfossil inclusions, which I then reconstructed in 3D. The reconstructions were then used to identify the taxa from the assemblage to the lowest taxonomic level where possible.

A multivariate dataset was created in excel (see Appendix B, Table 4) that consists of nominal, numeric and binary variables. Nominal variables include the ichnotaxa/morphotype (identified in my Honours research [Montgomery, 2019]) and the coprofabrics. The numeric variables are the maximum length and diameter in centimetres (cm) per coprolite specimen. Lastly, the types of inclusions (arthropods, bacteria, bones, gastroliths, scales, shells, teeth and unknown) and the taphonomic features (microvesicles, cracks, secondary precipitation, and invertebrate burrows) are recorded as binary variables where “0” means the variable is not present in the coprolite and “1” means it is present.

10.2.3. Coprolite ordination

To make meaningful comparisons between coprofabrics and coprolite morphotypes, and to determine if coprolites are indicative of the perpetrators’ diets, statistical analysis was carried out. The statistical analysis was carried out using the raw data on the type of coprolite inclusions documented per specimen (see Appendix B, Table 4). Coprolite specimens that do not contain inclusions were excluded from this analysis. I ordinated the binary data to assess variance in inclusions using non-metric multidimensional scaling (NMDS). This method is a preferred approach for teasing out structural patterns from large, multidimensional (multivariate) datasets and visualising the patterns in two dimensions (Ramette, 2007, Dexter et al., 2018), like this dataset (see Appendix B, Table 4).

The following methods were performed in RStudio v.2022.02.0.443 (RStudio Team, 2022) to compare the coprolite morphotypes using the raw inclusion dataset. First, the function *dist* (method = “binary”) was used to calculate the dissimilarities and construct a specimen distance matrix. The resulting distance matrix was subjected to NMDS analysis with the function the R *vegan* package *metaMDS* and to alleviate any issues of non-convergence 100 iterations were performed. The resultant value of ordination stress was used to assesses how faithfully the multidimensional relationships among the coprolite inclusions are represented in the two-dimensional ordination plot. A stress value of less than 0.2 is required for useful two-dimensional

visualisations (Zuschin et al., 2006, Tyler and Kowalewski, 2014, Dexter et al., 2018). The *metaMDS* results were used to generate two plots, one that highlights potential groupings based on the coprofabrics defined in this study and the other based on the morphotype assignations. These plots we produced by using the *ggplot* function + *geom_polygon* + geom_jitter (see Appendix C for full R script).

Table 2: List of coprolites micro-CT scanned from the Driefontein collection, along with their maximum length and diameter (cm) and their scanning parameters namely, beam energy (kV), current (µA), frame rate (fps), frame averaging (fa), filters and voxel size (mm).

Sample #	Maximum Length (cm)	Maximum Diameter (cm)	Beam Energy (kV)	Current (µA)	Frame Rate (fps)	Frame Averaging (fa)	Filters	Isotropic Voxel Size (µm)
BP/21/1	4.45	2.3	135	170	1	2	1.2 Cu	288.251329
BP/21/108	1.96	1.04	130	170	0.7	2	1.2 Cu	26.718
BP/21/109	2.17	0.73	140	140	1	2	1.2 Cu	12.58
BP/21/12	2.49	1.76	140	150	1	2	1.2 Cu	20.233
BP/21/147	4.37	1.98	135	170	1	2	1.2 Cu	36.956721
BP/21/161	5.31	2.41	140	150	1	2	1.2 Cu	29.865
BP/21/170	5.02	2.39	135	170	1	2	1.2 Cu	46.360716

Sample #	Maximum Length (cm)	Maximum Diameter (cm)	Beam Energy (kV)	Current (µA)	Frame Rate (fps)	Frame Averaging (fa)	Filters	Isotropic Voxel Size (µm)
BP/21/186	4.16	2.59	135	170	1	2	1.2 Cu	35.798718
BP/21/190	4.79	2.29	135	170	1	2	1.2 Cu	36.956721
BP/21/191	3.54	2.81	135	170	1	2	1.2 Cu	35.798718
BP/21/2	4.69	1.4	100	140	1	2	0.5 Cu	32.441541
BP/21/243	2.48	2.17	140	140	1	2	1.2 Cu	17.324
BP/21/262	1.66	1.35	140	140	1	2	1.2 Cu	15.835346
BP/21/263	1.46	0.63	100	140	1	2	0.5 Cu	16.724088
BP/21/272	2.71	0.83	140	140	1	2	1.2 Cu	17.828919

Sample #	Maximum Length (cm)	Maximum Diameter (cm)	Beam Energy (kV)	Current (µA)	Frame Rate (fps)	Frame Averaging (fa)	Filters	Isotropic Voxel Size (µm)
BP/21/273	2.51	0.73	130	170	0.7	2	1.2 Cu	26.718
BP/21/275	1.88	0.73	100	140	1	2	0.5 Cu	14.805602
BP/21/289	1.98	1.94	130	170	0.7	2	1.2 Cu	26.718
BP/21/302	0.42	0.42	135	135	0.7	2	1.2 Cu	23.648287
BP/21/31	4.87	2.48	100	140	1	2	0.5 Cu	32.441541
BP/21/314	0.73	0.52	135	135	0.7	2	1.2 Cu	23.648287
BP/21/316	1.77	0.83	130	180	1	2	0.5 Cu	34.383664
BP/21/319	1.35	0.42	140	140	1	2	1.2 Cu	14.037

Sample #	Maximum Length (cm)	Maximum Diameter (cm)	Beam Energy (kV)	Current (µA)	Frame Rate (fps)	Frame Averaging (fa)	Filters	Isotropic Voxel Size (µm)
BP/21/320	1.25	0.62	140	140	1	2	1.2 Cu	10.988
BP/21/322	0.94	0.52	140	140	1	2	1.2 Cu	11.419006
BP/21/325	4.89	2.18	135	170	1	2	1.2 Cu	36.956721
BP/21/326	1.98	0.73	100	140	1	2	0.5 Cu	14.805602
BP/21/329	5.41	2.39	100	140	1	2	0.5 Cu	32.441541
BP/21/33	4.25	2.6	135	170	1	2	1.2 Cu	27.523652
BP/21/330	1.87	0.62	140	140	1	2	1.2 Cu	12.850744
BP/21/353	5.62	2.51	135	170	1	2	1.2 Cu	46.360716

Sample #	Maximum Length (cm)	Maximum Diameter (cm)	Beam Energy (kV)	Current (µA)	Frame Rate (fps)	Frame Averaging (fa)	Filters	Isotropic Voxel Size (µm)
BP/21/379	1.97	1.87	140	140	1	2	1.2 Cu	17.323514
BP/21/421	0.4	0.6	100	140	1	2	0.5 Cu	20.126086
BP/21/422	1	0.6	100	140	1	2	0.5 Cu	20.126086
BP/21/423	6.86	3.12	90	110	1	2	3 Al	25.08753
BP/21/424	1.87	0.72	130	160	1	1	0.5 Cu	33.053
BP/21/426	1.97	1.04	130	170	0.7	2	1.2 Cu	26.718
BP/21/427	1.25	0.83	130	180	1	2	0.5 Cu	34.383664
BP/21/428	2.08	0.83	140	140	1	2	1.2 Cu	15.848

Sample #	Maximum Length (cm)	Maximum Diameter (cm)	Beam Energy (kV)	Current (µA)	Frame Rate (fps)	Frame Averaging (fa)	Filters	Isotropic Voxel Size (µm)
BP/21/429	1.14	0.52	140	140	1	2	1.2 Cu	11.468
BP/21/430	1.03	0.2	140	140	1	2	1.2 Cu	10.988
BP/21/431	1.56	1.24	140	140	1	2	1.2 Cu	17.414598
BP/21/432	1.04	1.24	140	145	1	2	1.2 Cu	17.427313
BP/21/54	4.37	2.39	130	160	1	2	0.5 Cu	33.053153
BP/21/55	3.95	1.87	100	140	1	2	0.5 Cu	32.447876
BP/21/56	2.71	2.58	130	160	1	2	0.5 Cu	33.053153
BP/21/96	2.27	1.23	140	140	1	2	1.2 Cu	12.187

11. RESULTS

In general, the CT scans show marked variation in ground mass density in the majority of coprolites. These variations in density allow for the characterization of different coprofabrics (Fig. 4-9). Coprolite inclusions are abundant, of diverse nature, and often heterogeneously distributed. They include fully articulated bivalve molluscs, arthropod beetles missing their abdomens, fragmentary vertebrate jaw elements, ribs and long bones, and an abundance of fish scales (Fig. 10-14). The NMDS analysis shows that while the majority of the coprolite specimens have no variation in inclusion types, others show either intramorphotype and/or intermorphotype variation in inclusion types (Fig. 16) and that there is a large overlap in the space occupied by coprolite specimens with heterogeneous massive and heterogenous zoned coprofabrics (Fig. 15).

11.1. Coprofabrics

11.1.1. Homogenous Coprofabrics

The ground mass of a small portion (15%) of the Driefontein 11 coprolites have no internal structure, habit or layering (hereafter “massive”) and show no density differences (hereafter “homogenous”) and are thus considered to have a massive homogenous coprofabric (Fig. 4). These specimens contain no microfossil inclusions but coprolite BP/21/329 (Fig. 4C) does contain spherical inclusions with a low-density rim and anastomosing high density network that travels through that rim that is connected to a higher density core (~1.5 mm in diameter). These are potentially gastroliths but this cannot be confirmed at the current resolving power. Secondary mineral precipitation has infilled internal microfractures in coprolites BP/21/1 (Fig. 4A), BP/21/31 (Fig. 4B) and BP/21/329 (Fig. 4C), and overprinted some of the ground mass in coprolite BP/21/1 (Fig. 4A) in a dendritic pattern. Coprolites BP/21/108 (Fig. 4E) and BP/21/302 (Fig. 4F) possess internal microvesicles, while a tunnel runs through coprolite BP/21/302 (Fig. 4F), and elongate, often shallow tunnels that open the surface are present in BP/21/302 (Fig. 4G).

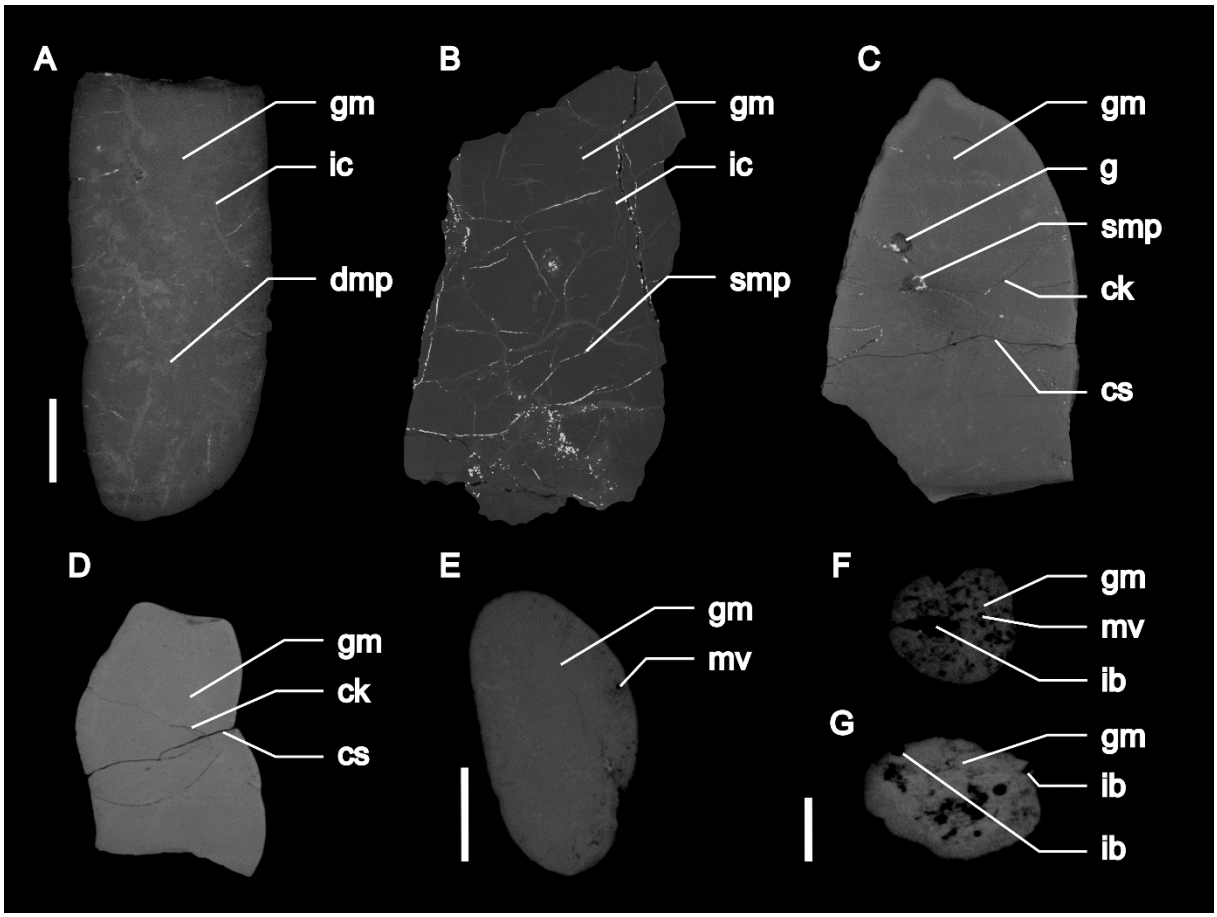

Figure 4: Longitudinal CT-slice images of coprolites BP/21/1 (A), BP/21/31 (B), BP/21/329 (C), BP/21/56 (D), BP/21/108 (E), BP/21/302 (F) and BP/21/314 (G) from Driefontein 11 with massive, homogenous coprofabrics. A-D: Scale bar = 8 mm, E: Scale bar = 4.5 mm, F-G: Scale bar = 2 mm. Abbreviations: ck, crack; cs, cleavage scar; dmp, dendritic mineral precipitation; g, gastrolith; gm, ground mass; ib, invertebrate burrow; ic, infilled crack; mv, microvesicles; smp, secondary mineral precipitation.

11.1.2. Heterogenous Coprofabrics

The majority of the coprolites (85%) from Driefontein 11 have a ground mass with spatial density differences (heterogenous). These heterogenous coprolites are either massive (Fig. 5), or they are zoned (Fig. 6-9), with the density differences arranged as concentric layers. Where the layering is defined by outer boundaries displacing inner layers (Fig. 5E, F; 6C) the coprofabric is defined as zoned, folded and heterogenous. In some coprolites there is a distinct outer layer, and the inner ground mass has a spotted density distribution (Fig. 6B, D-F), these coprofabrics are defined

as zoned, mottled and heterogenous. Lastly, the layering is not always defined by distinct density differences but rather graduated ones (Fig. 7, 8), these coprofabrics are defined as zoned, muddled and heterogenous.

Microfossil inclusions are common with no distinct arrangement and distribution in massive, heterogenous coprofabrics (Fig. 5) but in zoned, heterogenous coprofabrics (Fig. 6-9) they are arranged according to the concentric layering. In some of these coprolites the boundaries between the inclusions and the ground mass are well defined (Fig. 5E, F; 6A; 7C; 8I; 9C) but in most the boundaries are indefinite (Fig. 5B; 6C; 7E; 8G; 9A-E). Sometimes the inclusions are preserved as negative moulds (Fig. 5B, E; 6B, C, E; 8J; 9B). Small spherical inclusions (~1.5 mm in diameter) with a low-density rim and anastomosing high density network that travels through that rim are visible in BP/21/423 (Fig. 7A), BP/21/12 (Fig. 8E) and BP/21/431 (Fig. 8H). These are potentially gastroliths but this cannot be confirmed at the current resolving power. Internal microvesicles (Fig. 5C-E, G-I; 6A-E; 7A, B; 8A, B, D; 9B, C, E) and fracturing (Fig. 5A, D, H; 6B, E; 7A, B; 8A, E, F) are present in some specimens from both coprofabrics. Elongate, narrow tunnels that open onto the external surfaces are observed in BP/21/289 and BP/21/190 (Fig. 7D; 8D) and a larger tunnel, traveling all the way through the coprolite is present in BP/21/429 (Fig. 8I). Secondary mineral precipitation has infilled internal fractures in coprolites BP/21/289 (Fig. 7E) and BP/21/12 (Fig. 8E) and replaced original gastrolith minerology in coprolite BP/21/12 (Fig. 8E) and microfossil inclusions in coprolite BP/21/55 (Fig. 6A), BP/21/54 (Fig. 8G), BP/21/272 (Fig. 9A) and BP/21/421 (Fig. 9C).

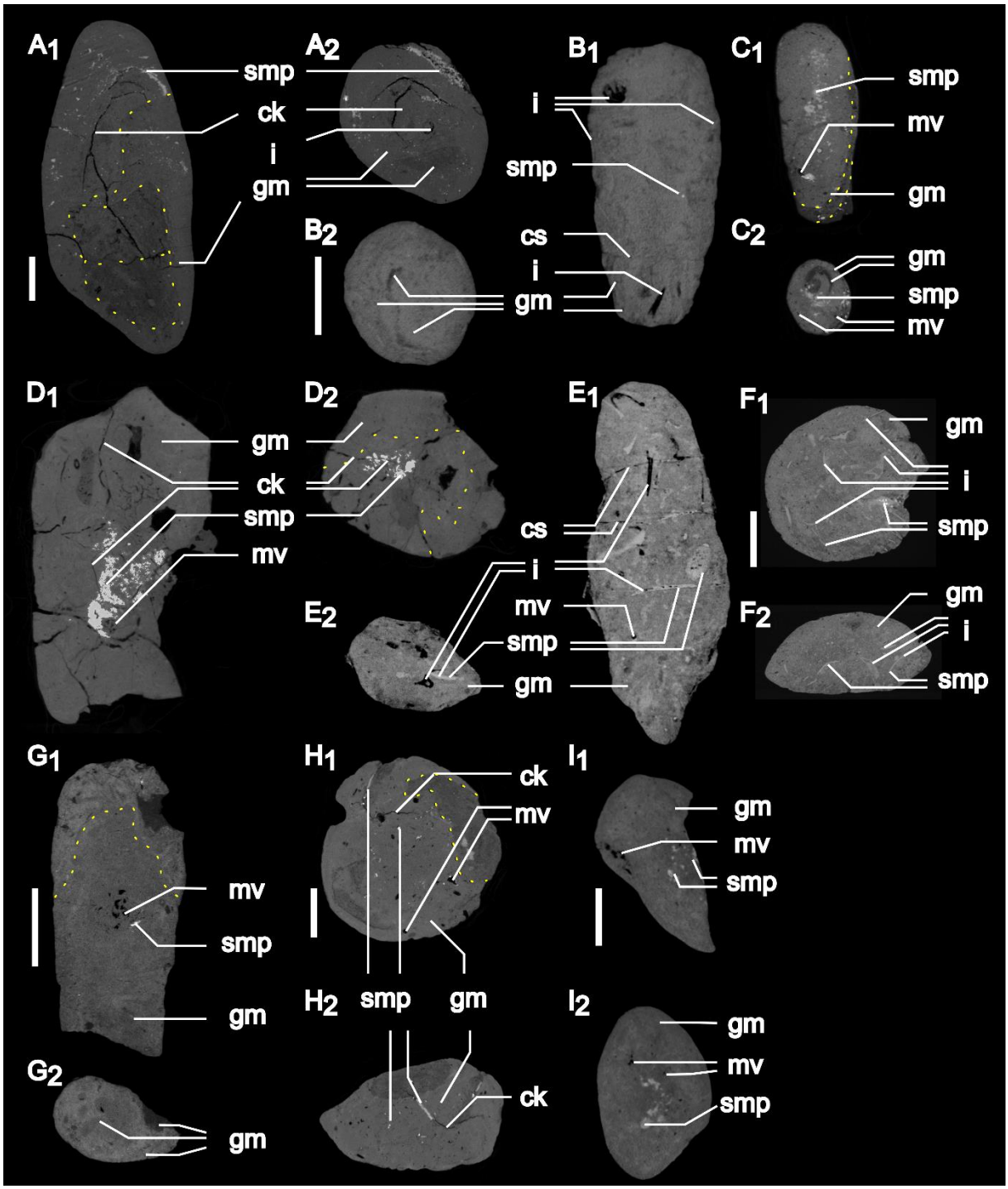

Figure 5: CT-slice images of coprolites BP/21/161 (A), BP/21/316 (B), BP/21/320 (C), BP/21/426 (D), BP/21/428 (E), BP/21/263 (F), BP/21/96 (G), BP/21/379 (H) and BP/21/427 (I) from Driefontein 11 with massive, heterogenous coprofabrics both in longitudinal (A_1, B_1, C_1, D_1, E_1, F_1, G_1, H_1, I_1) and transverse (A_2, B_2, C_2, D_2, E_2, F_2, G_2, H_2, I_2) views. A: Scale bar = 5 mm, B-I: Scale bar = 4 mm, J: Scale bar = mm Abbreviations: ck, crack; cs, cleavage scar; gm, ground mass; i, inclusions; ic, infilled crack; mv, microvesicles; smp, secondary mineral precipitation. Yellow dotted lines demarcate density differences in the coprolite ground mass.

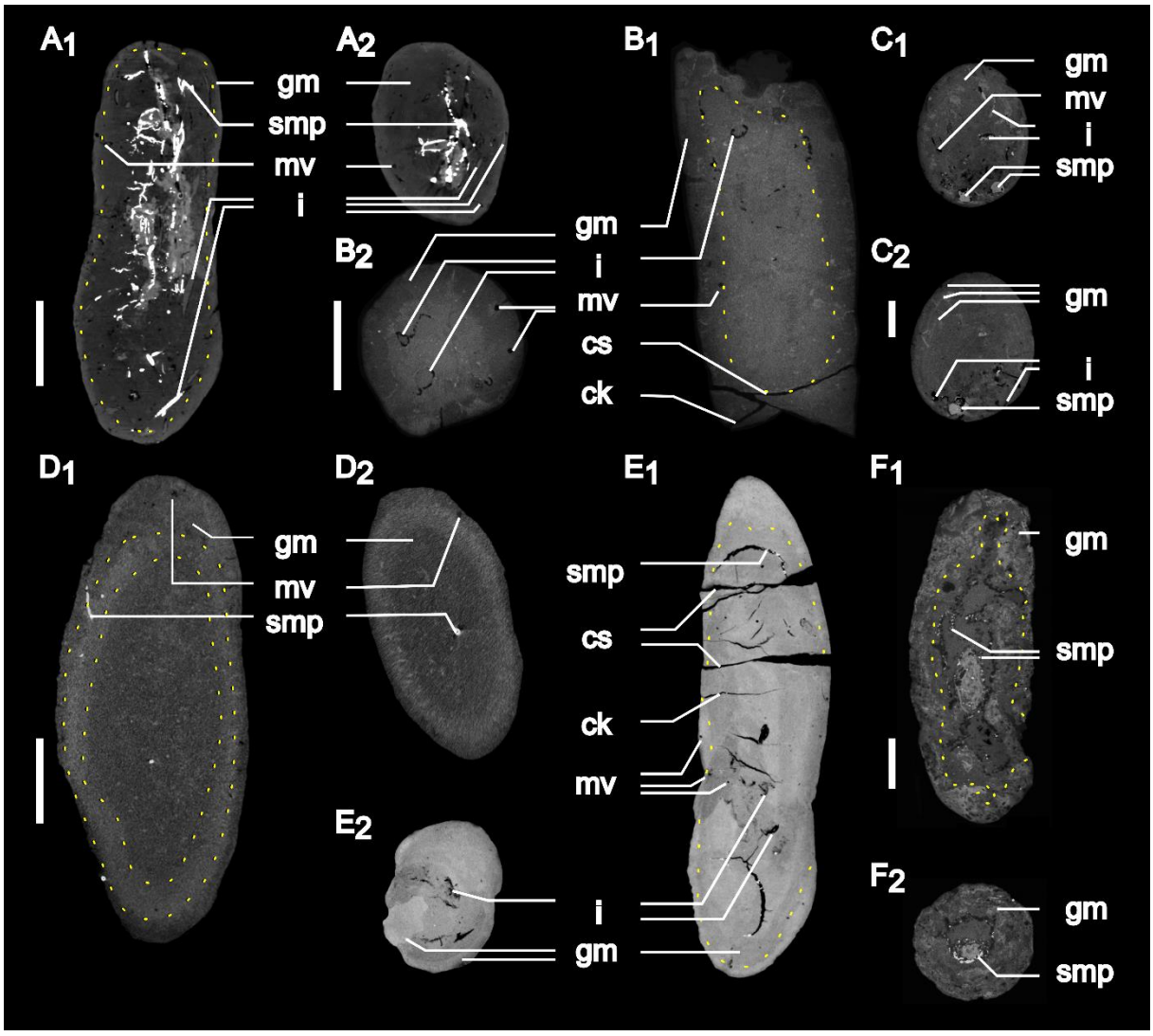

Figure 6: CT-slice images of coprolites from Driefontein 11 with muddled zoned, heterogenous coprofabrics both in longitudinal (A_1, B_1, C_1, D_1, E_1, F_1) and transverse (A_2, B_2, C_2, D_2, E_2, F_2) views. BP/21/55 (A), BP/21/33 (B), BP/21/262 (C), BP/21/147 (D) and BP/21/423 (G) are coprolites with zoned, heterogenous coprofabrics. BP/21/2 (E), BP/21/275 (F) are coprolites with folded, zoned, heterogenous coprofabrics. A-B: Scale bar = 8 mm, C: Scale bar = 4 mm, D-E: Scale bar = 8 mm, F: Scale bar = 3 mm. Abbreviations: ck, crack; cs, cleavage scar; gm, ground mass; i, inclusions; mv, microvesicles; smp, secondary mineral precipitation. Yellow dotted lines demarcate density differences in the coprolite ground mass.

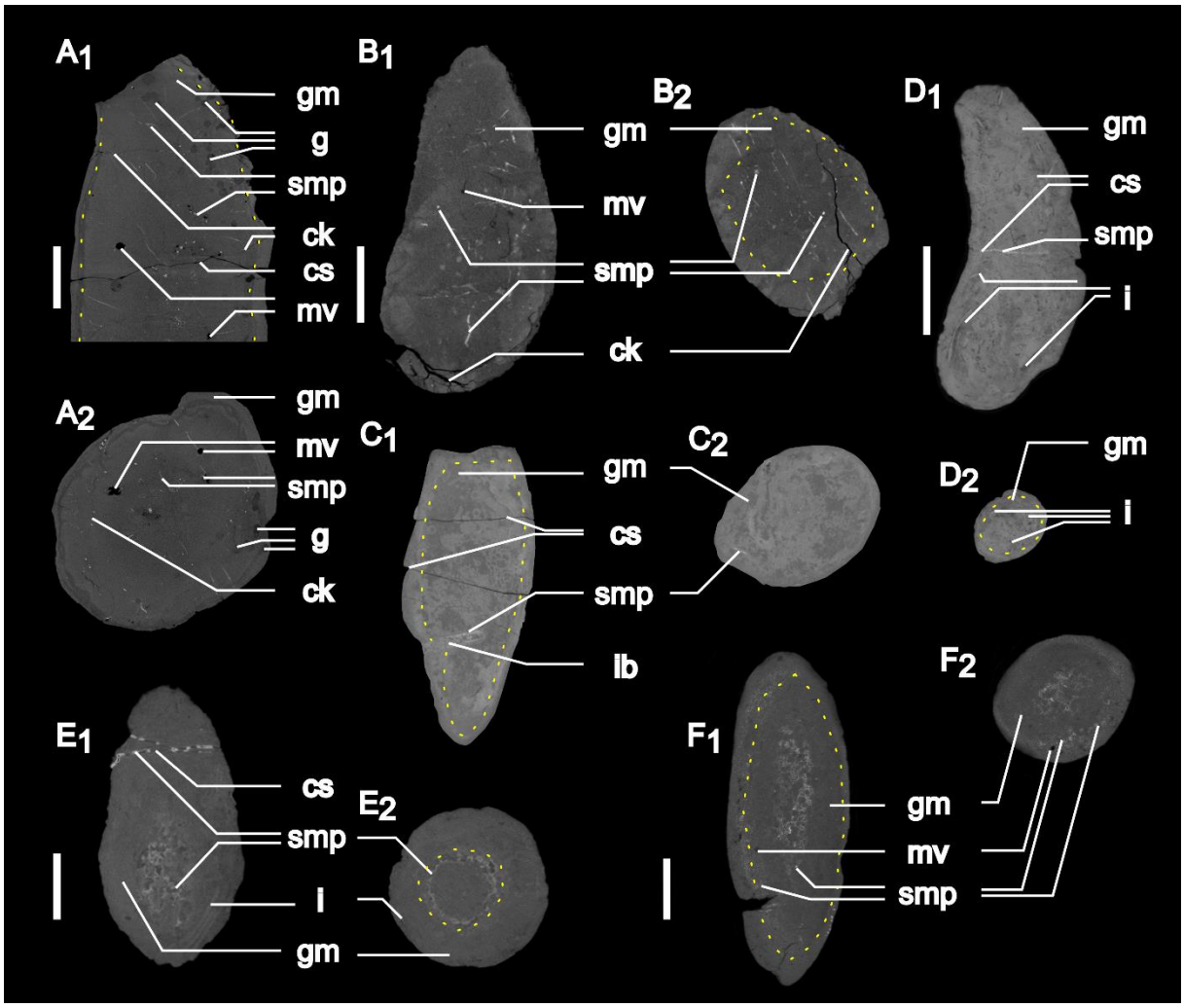

Figure 7: CT-slice images of coprolites from Driefontein 11 with muddled zoned, heterogenous coprofabrics both in longitudinal (A_1, B_1, C_1, D_1, E_1, F_1) and transverse (A_2, B_2, C_2, D_2, E_2, F_2) views. BP/21/423 (A) is a coprolite with zoned, heterogenous coprofabric. BP/21/427 (C) is coprolite with folded, zoned, heterogenous coprofabric. BP/21/170 (B), BP/21/186 (D), BP/21/289 (E) and BP/21/109 (F) are coprolites with mottled, zoned, heterogenous coprofabrics. A: Scale bar = 8 mm, B-D: Scale bar = 10 mm, E: Scale bar = 4 mm, F: Scale bar = 3 mm. Abbreviations: ck, crack; cs, cleavage scar; g, gastroliths; gm, ground mass; i, inclusions; ib, invertebrate burrow; mv, microvesicles; smp, secondary mineral precipitation. Yellow dotted lines demarcate density differences in the coprolite ground mass.

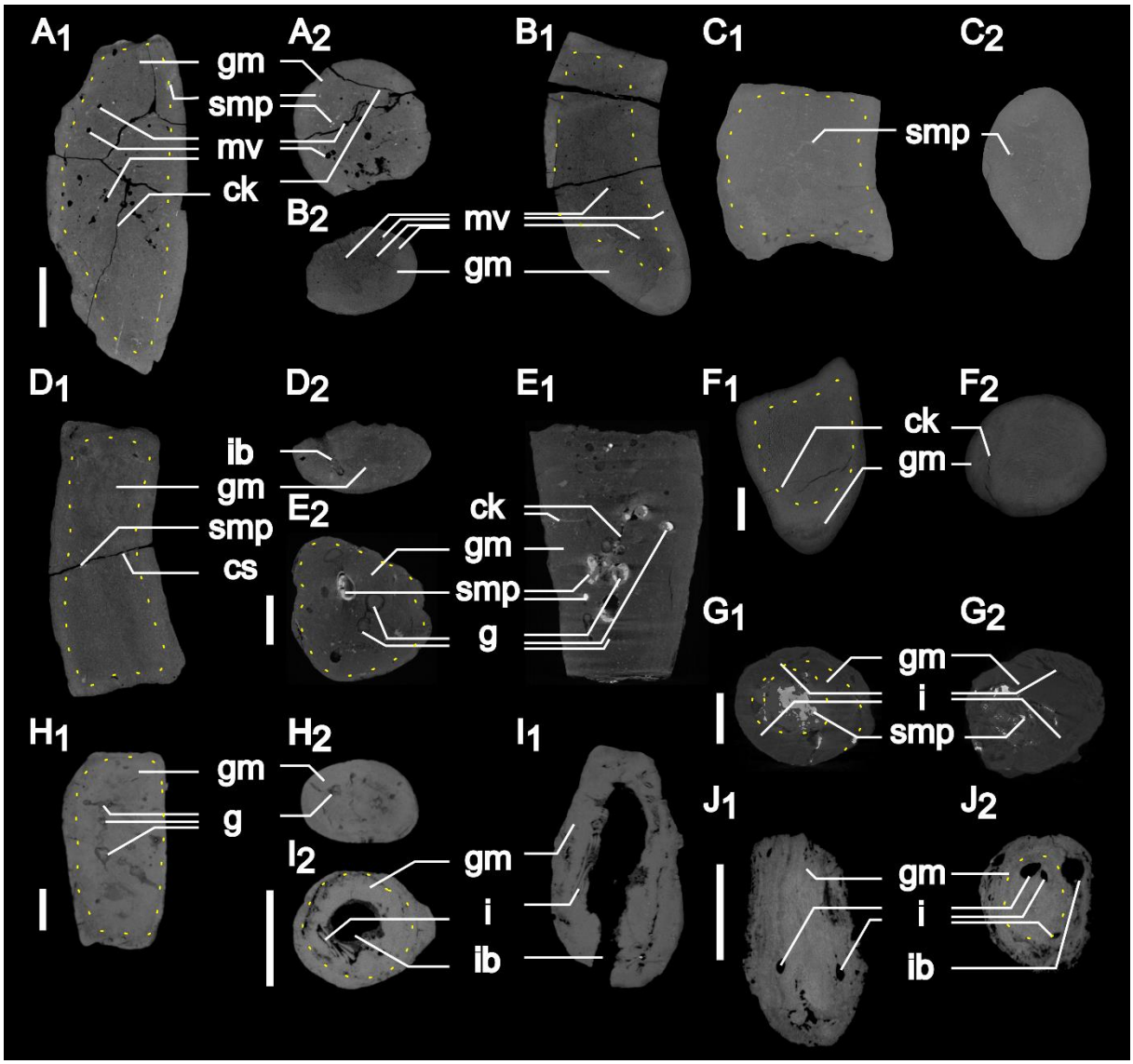

Figure 8: CT-slice images of coprolites from Driefontein 11 with zoned, heterogenous coprofabrics both in longitudinal (A1, B1, C1, D1, E1, F1, G1, H1, I1, J1) and transverse (A2, B2, C2, D2, E2, F2, G2, H2, I2, J2) views. (A) BP/21/353, (B) BP/21/325, (C) BP/21/191, (D) BP/21/190, (E) BP/21/12, (F) BP/21/243, (G) BP/21/54, (H) BP/21/431, (I) BP/21/429, (J) BP/21/422. A-D: Scale bar = 10 mm, E-J: Scale bar = 5 mm. Abbreviations: ck, crack; cs, cleavage scar; g, gastroliths; gm, ground mass; i, inclusions; ib, invertebrate burrow; mv, microvesicles; smp, secondary mineral precipitation. Yellow dotted lines demarcate density differences in the coprolite ground mass.

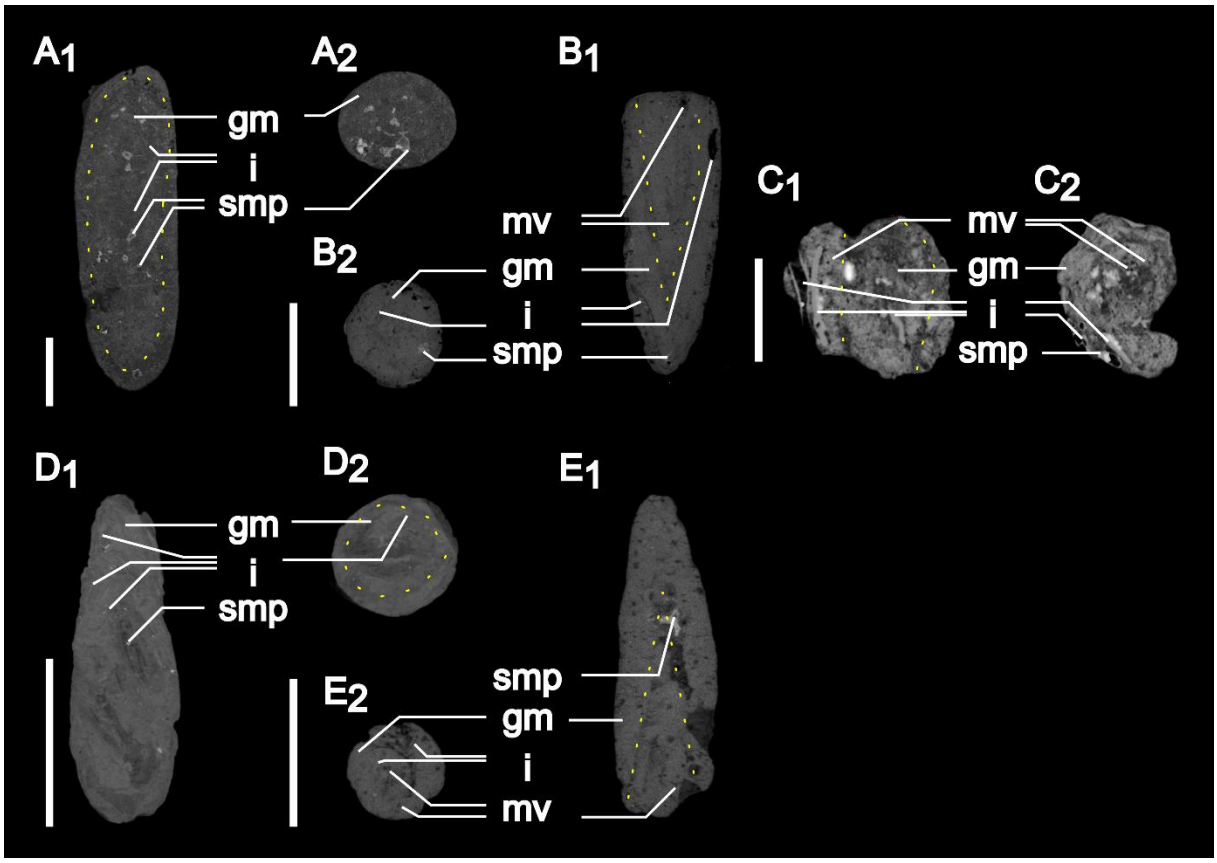

Figure 9: CT-slice images of coprolites BP/21/272 (A), BP/21/319 (B), BP/21/421 (C), BP/21/330 (D) and BP/21/430 (E) from Driefontein 11 with zoned, heterogenous coprofabrics both in longitudinal (A_1, B_1, C_1, D_1, E_1) and transverse (A_2, B_2, C_2, D_2, E_2) views. A-E: Scale bar = 5 mm. Abbreviations: gm, ground mass; i, inclusions; mv, microvesicles; smp, secondary mineral precipitation. Yellow dotted lines demarcate density differences in the coprolite ground mass.

11.2. Inclusions

Thirty-three coprolites from the representative sample of the Driefontein 11 coprolite assemblage contain microfossil remains of varying amounts, sizes, distribution, and type. Most of these coprolite specimens (58%) contain inclusions that have either large degrees of digestion or are highly fragmented, making them difficult to near-impossible to identify. Five coprolites (BP/21/422, BP/21/2, BP/21/161, BP/21/263 and BP/21/421; Fig.10-13) contain elements belonging to several prey items, that allow for systematic identification. Invertebrates identified include at least two unionoid taxa (Fig. 10) and five arthropod taxa (Fig. 11, 12), three of which belong to the order Coleoptera (Fig. 12). Vertebrates identified include fishes represented by an abundance of scale inclusions, a dipnoan lungfish (Fig. 13) and two indeterminate tetrapods (Fig. 13, 14). The following section reviews their morphology.

11.2.1. Invertebrates

Mollusca

Class Bivalvia

At least twelve fully articulated bivalves are preserved in coprolite BP/21/422 (Fig. 10). Some moulds of bivalves are present on the external surfaces, but the majority of the specimens are preserved internally. Most of the bivalves are similar in size (0.09-1.3 mm in length, 0.08-1.2 mm in breadth), and differences in the hinge and umbo morphology are indicative of at least two different taxa, A-B (Fig. 10C, D). In both taxa A and B the anterior end is distinctly truncated with a rounded margin, while the posterior end protrudes well beyond the hinge with a wide, oval and rounded-triangular margin (Fig. 10C_2, D_2). Meaning the shells of both taxa are equivalve and inequilateral, elliptical, and flat. Taxon A specimens (Fig. 10C) have a short and narrow hinge plate, and a protruding umbo that is dorso-laterally (Fig. 10C_2) located. Taxon B specimens have a broad and long hinge plate with a protruding umbo that is mediolaterally (Fig. 10D_2) located. Low resolution obscures details of the hinge such that it cannot be determined if it was edentulous or not.

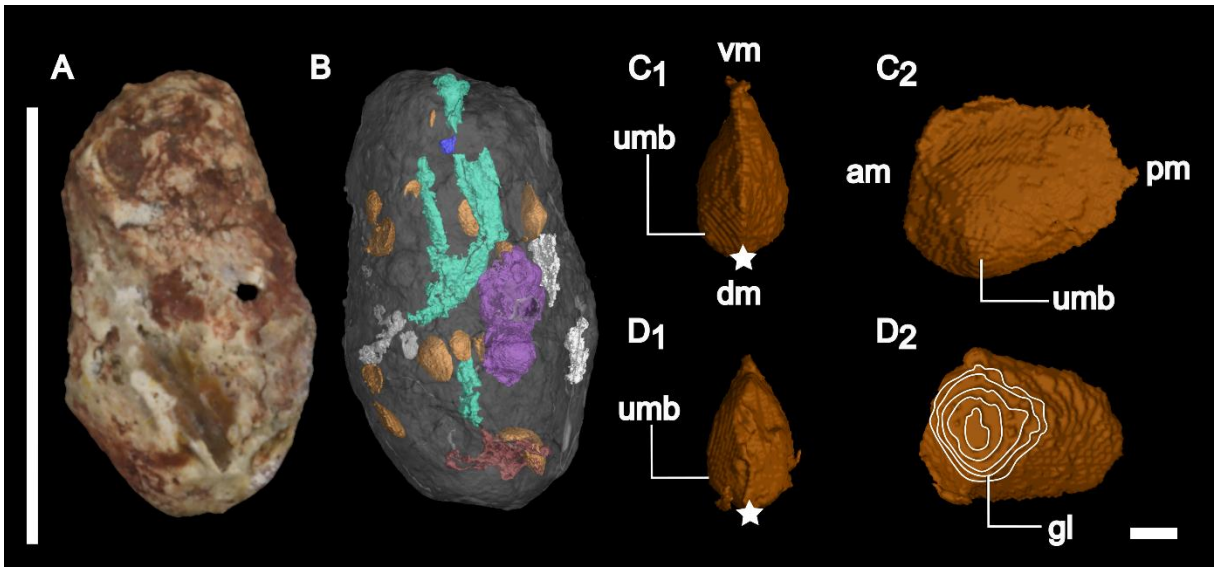

Figure 10: Contents of coprolite BP/21/422, assigned to morphotype 1. (A) Lateral view of coprolite BP/21/422, (B) Semi-transparent rendering of coprolite with at least twelve articulated bivalves along with other currently unidentifiable inclusions, (C) Taxa A and (D) Taxa B in anterior (C_1,D_1) and lateral (C_2, D_2) view. A-B: Scale bar = 1 cm, C-D: Scale bar = 0.3 mm. Abbreviations: am, anterior margin; dm, dorsal margin; gl = growth lines; pm, posterior margin; umb, umbo; vm, ventral margin.

Arthropoda

Arthropod remains are present in coprolite BP/21/161 (Fig. 11). It contains at least two different arthropod taxa. It is unclear whether the body segment that represents Taxon A (Fig. 11C) is the thorax or abdomen of this arthropod due to the lack of any diagnostic features. The element is approximately 6 mm long and 1.37 mm wide, folded over and consists of ten segments each approximately 0.6 mm long. Due to the lack of any distinct anterior or posterior features it is also not possible to orient the element. Taxon B (Fig. 11E) is represented by a fully articulated leg that is approximately 6.42 mm long. Whether it is a left or right leg is unclear. The trochanter is small (diameter is 0.34 mm), the femur is narrow and elongate (2.12 mm), the tibia is slender, slightly bent inward (2.64 mm) and the tarsus is short (1.01 mm) but the number of tarsomeres and any subdivisions is not clearly visible due to limited resolution. BP/21/161 also preserves several negative moulds of crescent shapes, all similar in size (~ 1.53 mm) and with a crescent morphology (Fig. 11D). These are

tentatively identified as eggs but due to the lack of visible diagnostic features it is impossible to say if they belong to arthropods of parasites.

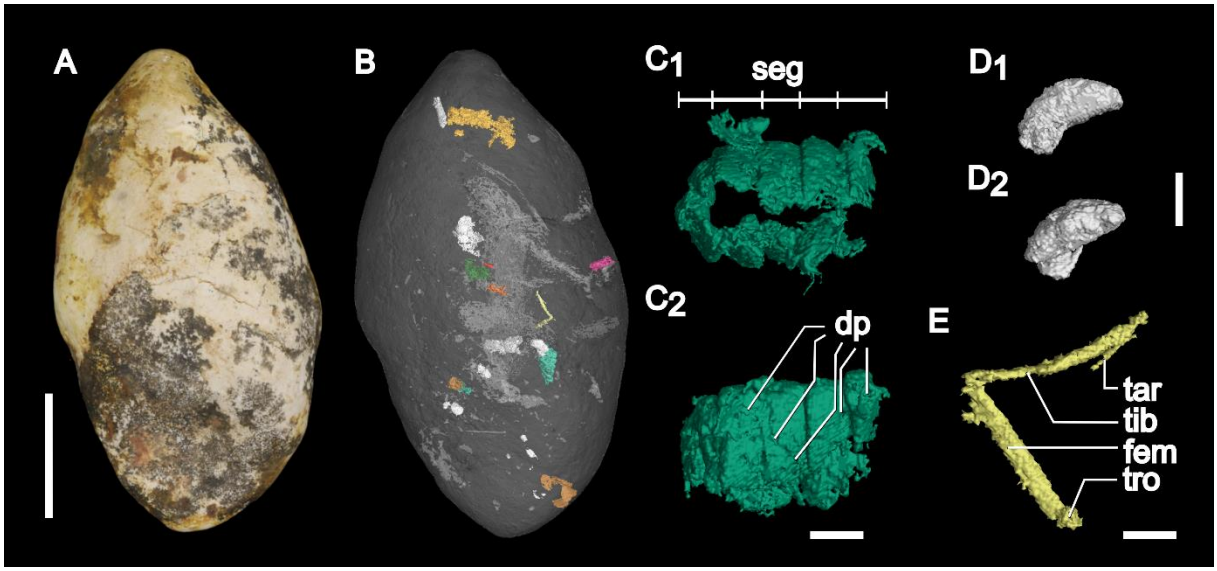

Figure 11: Contents of coprolite BP/21/161, assigned to morphotype 2. (A) Ventral view of BP/21/161, (B) Semi-transparent rendering of coprolite with arthropod remains along with other currently unidentifiable inclusions, (C) segmented arthropod body in lateral (C1) and dorsal (C2) view that represent Taxa A, (D) tentative arthropod egg in lateral (D1) and dorsal (D2) view that represents Taxa B, (E) articulated arthropod leg in lateral view. A-B: Scale bar = 1 cm, C-E: Scale bars = 0.75 mm. Abbreviations: ae, anterior end; dp, digestive pitting; fem, femur; pe, posterior end; seg, segments; tar, tarsus; tib, tibia; tro, trochanter.

Order Coleoptera

The remains of at least eleven beetles in various states of preservation are present in coprolite BP/21/2 (Fig. 12). The majority of these are highly digested and can only be identified as possible beetle remains because some leg segments and a vague head and thorax are still visible (Fig. 12F). Three of the beetle inclusions (Fig. 12C-E) are fairly well preserved, missing their abdomens, some legs, mouth parts and either their entire antennae or segments of them. These three beetle inclusions are approximately the same width (1.2-1.4 mm) but vary in length (2-3.3 mm) depending on where they were broken posteriorly. Their morphological features are also variable, which indicates that there are at least three beetles with varying morphologies present. Specimen A (Fig. 12C) consists of an articulated head (1.07

mm) and thorax (1.64 mm). The head is just as wide as the thorax and subquadrate, narrowing slightly anteriorly before terminating in line with the antennae in a flat, wide anterior margin. Based on the left scapus, the antennae are inserted antero-dorsally in a depressed area between the eyes. No other segments of the antennae have been preserved. Specimen B (Fig. 12D) consists of an articulated head (0.98 mm) and thorax (1.4 mm). The posterior margin of the head is subquadrate and just as wide as the thorax. It gradually narrows anteriorly behind the eyes and then strongly narrows into a rounded anterior margin in front of the eyes. The insertion site of the antennae is unclear. Specimen C (Fig. 12E) consists of an articulated head (1.43 mm) and thorax (1.91 mm). The posterior margin of the head is subquadrate and slightly wider than the thorax. The head gradually widens anteriorly until it reached the approximate middle along the lateral margin where it starts to narrow before the eyes, creating a rounded shape, after which it strongly narrows after the eyes into a rounded triangular shape. The position of the eyes is unclear, but the antennae insert antero-dorsally in a depression, the right antennae socket is visible, and a large portion of the left antenna is preserved. Due to low resolution the exact morphology of any legs, antennae, mouth parts and the different constituents of the thorax in all three taxa remain unclear.

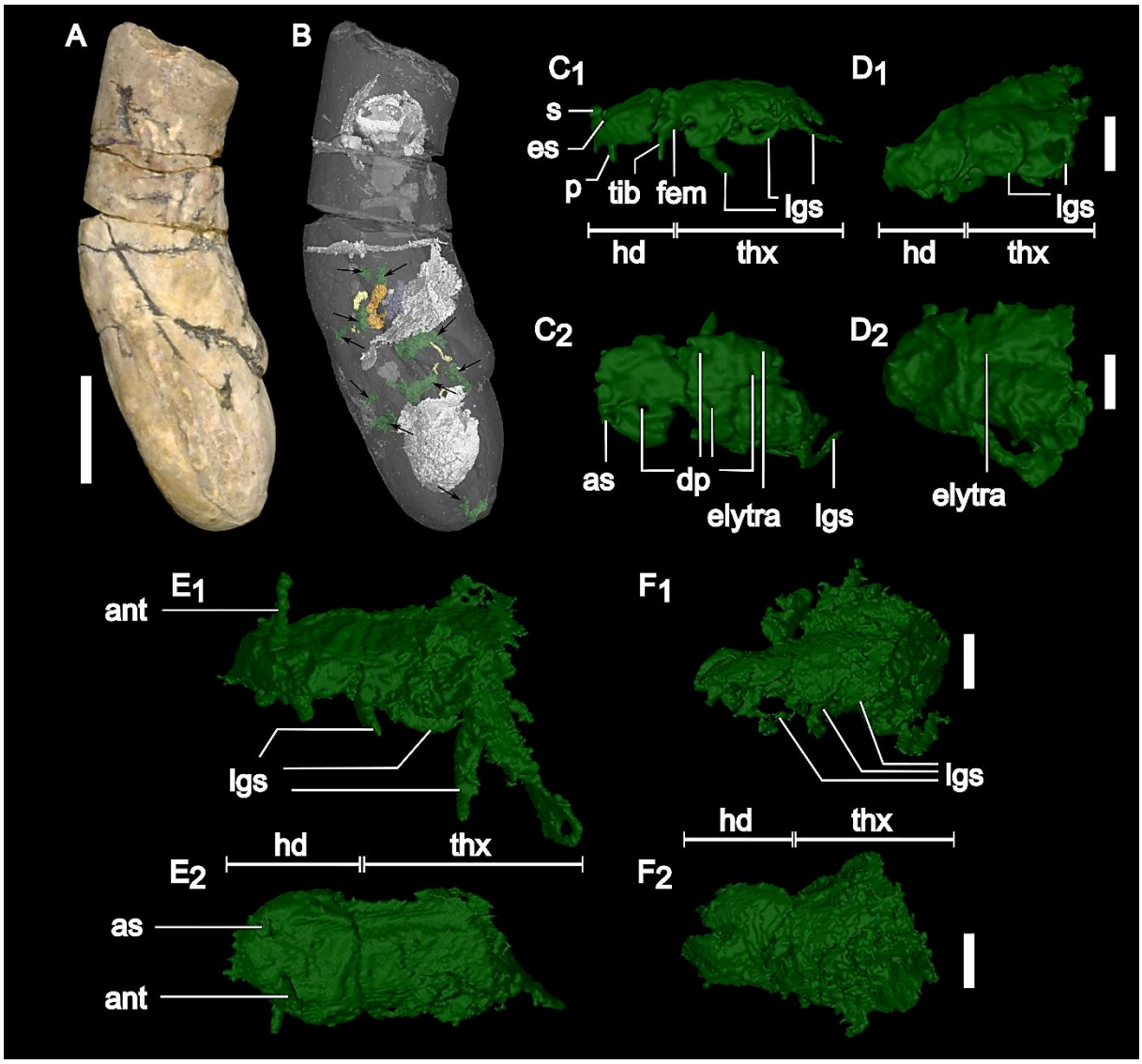

Figure 12: Contents of coprolite BP/21/2, assigned to the existing ichnotaxon *Alococoprus triassicus*. (A) Lateral view of BP/21/2, (B) Semi-transparent rendering of coprolite with at least eleven beetles (in green and indicated with black arrows) along with other currently unidentifiable inclusions, (C) specimen A, (D) specimen B, (E) specimen C and (F) unidentifyable taxa of beetles in various states of preservation, (C_1,D_1,E_1,F_1) lateral view, (C_2,D_2,E_2,F_2) dorsal view. A-B: Scale bar = 1 cm, C-F: Scale bar = 0.65 mm. Abbreviations: ant, antenna; as, antenna socket; dp, digestive pitting; es, eye socket; fem, femur; hd, head; lgs, legs; s, scape; thx, thorax; tib, tibia.

11.2.2. Vertebrates

Pisces

Scales are the dominant identifiable inclusion in the coprolite assemblage, making up 23.53% of the inclusions. They are visible in the CT-slice images and thin, elongate inclusions that taper towards the ends (Fig. 4E, F; 5A, 6D, E; 7G, I; 8B-D). Coprolite BP/21/263 (Fig. 13B) shows the dominant ganoid scale morphotypes found across the sample. This coprolite contains at least 20 scales, seemingly randomly arranged, none of which are visible on the external surface (Fig. 13A). There is some variation in scale shape and size. Highly fragmented scales are present, along with rhomboidal scales, between 1.95-2.81 mm long and 1.39-1.16 mm wide, with posterior pegs (Fig. 13$D_{1,3}$) and some lacking such pegs (Fig. 13D_2). Overall, they lack sculpture and some of the scales have rounded edges (Fig. 13$D_{1,2}$).

Superclass Osteichthyes
Class Sarcopterygii
Order Dipnoi

A fragmentary tooth plate (Fig. 13C) measuring 4.58 mm in length and 1.9 mm in width, with a roughly triangular shape and bearing three slightly curved, slender, and acute ridges is present in coprolite BP/21/263 (Fig. 13A, B). The occlusal surface is narrow and slightly convex, with three acute ridges that all radiate out from the inner angle ($\alpha = 94.5°$). The crests of the ridges meet at the mediolingual junction, with the last ridge of the tooth plates forming the lingual edge. In general, the ridges are slightly curved, with the first (Z_1) and last (Z_3) ridge curving posteriorly and the middle (Z_2) ridge curving anteriorly (Fig. 13C_1). Inter-ridge furrows are wide, rounded, and quite deep, with the last furrow broader than the other. A moderate tip of the inner angle is present at the mediolingual junction.

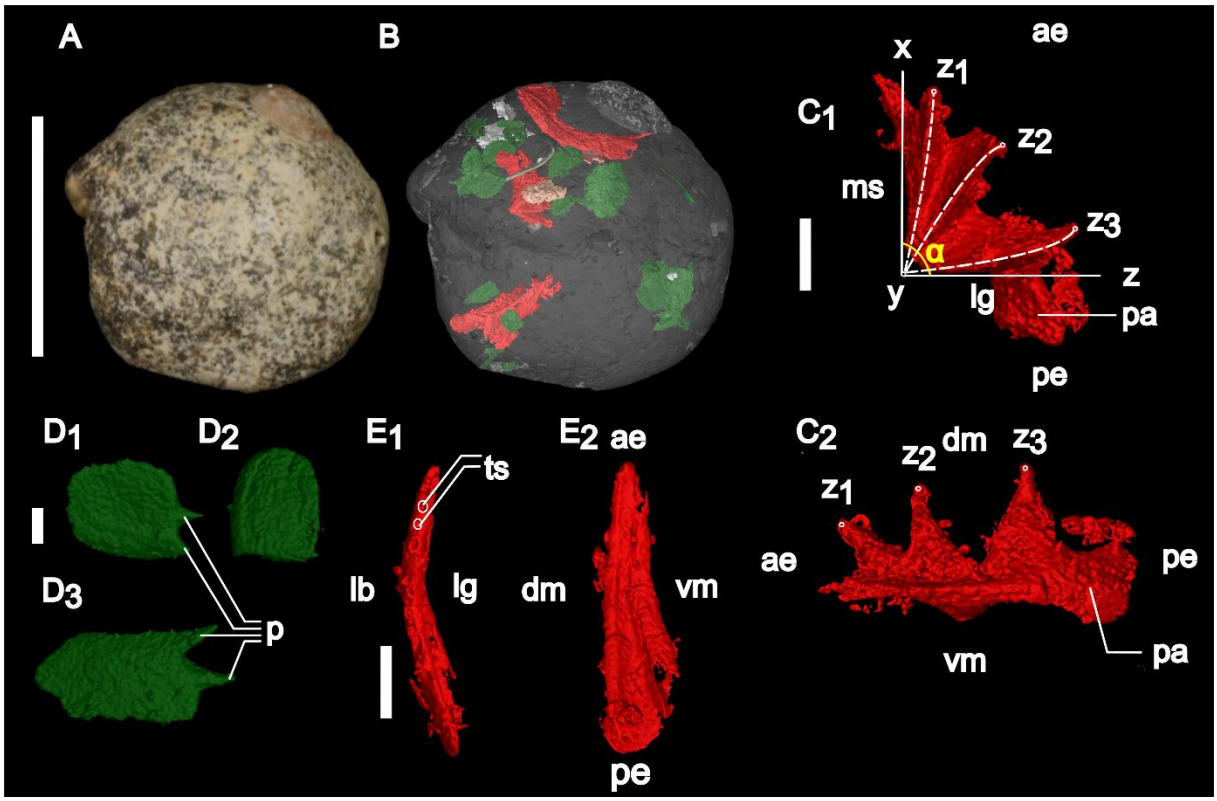

Figure 13: Contents of coprolite BP/21/263, assigned to morphotype 4. (A) Dorsal view of BP/21/263, (B) Semi-transparent rendering of coprolite with a lungfish tooth plate, tetrapod jaw, ribs, fish scales and other currently unidentifiable inclusions, (C) right lower dipnoan tooth plate in occlusal (C1) and labial (C2) view, (D) different scale morphotypes present and (E) left tetrapod mandible in occlusal (E1) and lingual (E2) view. A-B: Scale bar = 1 cm, C-E: Scale bars = 1 mm. Abbreviations: ae, anterior end; dm, dorsal margin; lb, labial margin; lg, lingual margin; ms, mesial margin; p, pegs; pa, prearticular bone; pe, posterior end; vm, ventral margin; y, mesiolingual junction; α, inter angle.

Tetrapoda

Coprolite BP/21/263 contains a left mandibular fragment (Fig. 13E), which is oriented based on the smooth, convex surface being the labial surface. The lingual surface (Fig. 13E2) is concave medially with two ridges along the ventral and occlusal margins. The ventral ridge contains a posterior-anterior channel, and the occlusal ridge contains the teeth. Although no teeth are preserved in this fragment there are at least eight oval tooth sockets (Fig. 13E1).

Coprolite BP/21/421 (Fig. 14A, B) contains a tooth-bearing right-maxillary fragment (Fig. 14D) which is oriented based on the convex, highly weathered surface being the labial surface. The fragment measures 4.24 mm in length and 1.26 mm in width and contains 14 teeth. The teeth are conical decrease in size posteriorly (0.67 - 0.44 mm) and are arranged in into two rows that are oriented diagonally, distolingually across the jaw (Fig. 14D_2). The rows overlap such that the most mesial tooth from one row is never directly labial to the most mesial tooth of the adjacent row. The mode of implantation is unclear based on the digital reconstructions of the maxilla. Significant wear on the labial surface of the specimen provides a cross-section of the teeth in the outer tooth row and exposed the posterior-anterior channels that run above the tooth rows.

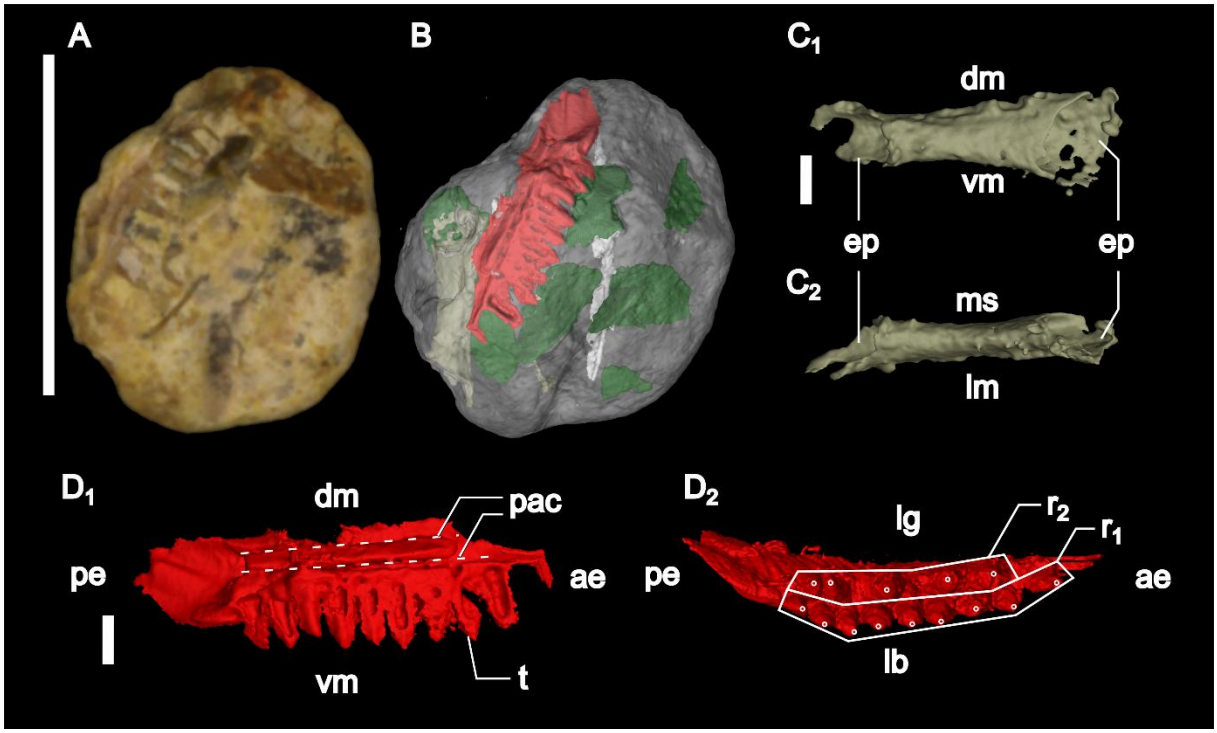

Figure 14: Contents of coprolite BP/21/421, assigned to morphotype 4. (A) Dorsal view of BP/21/421, (B) Semi-transparent rendering of coprolite with a tetrapod jaw fragment, a long bone, ribs and fish scales, (C) a long bone in medial (C_1) and ventral (C_2) view, (D) a tooth-bearing right-maxilla fragment in labial (D_1) and occlusal (D_2) view. A-B: Scale bar = 0.5 cm, C-D: Scale bars = 0.5 mm. Abbreviations: ae, anterior end; dm, dorsal margin; lb, labial margin; lg, lingual margin; lm, lateral margin; ms, mesial margin; pac, posterior-anterior channels; pe, posterior end; r_1, tooth row one; r_2, tooth row two; t, tooth; vm, ventral margin.

11.3. Coprolite Ordination

In total, 14 coprolite specimens, of varying coprofabrics and morphotypes, did not contain any microfossil inclusions and were thus excluded from this NMDS analysis. Two NMDS plots were generated from the same analyses, one highlighting the potential groupings based on coprofabrics (Fig. 15) and the other based on morphotypes (Fig. 16). The NMDS has a stress of 0.012 and is therefore reliable for describing the relationships among the coprolite specimens. Only coprolites with heterogenous massive or heterogenous zoned coprofabrics were included in the NMDS analysis. The resulting plot (Fig. 15) shows that coprolites with these aforementioned coprofabrics occupy the same dimensional space, with heterogenous massive coprolites occupying a smaller amount of dimensional space. The NMDS analysis shows that the majority of the coprolite specimens show no marked variation in inclusion types (Fig. 15; 16, point A). This is expected since most of the coprolites (58%) contain inclusions that are unidentifiable.

All of the coprolite specimens from the *Eucoprus cylindratus* and *Hyronocoprus amphipola* ichnotaxa as well as morphotypes 7 and 8 show no marked variation in inclusion types (Fig. 16, point A). Coprolite specimens that are unassigned or assigned to the *Alococoprus triassicus* ichnotaxon and morphotype 1, morphotype 4, morphotype 5 and morphotype 6 show both intramorphotype and intermorphotype variations (Fig. 16). One unassigned coprolite (BP/21/424) plots with the coprolite morphotypes that contain unidentifiable inclusions (Fig. 16, point A) and another (BP/21/423) plots in the upper left-hand quadrant. Alococoprus triassicus has two coprolites (BP/21/12, BP/21/96) that plot with the coprolite morphotypes that contain unidentifiable inclusions (Fig. 16, point A) and one specimen (BP/21/2) that plots in the lower left-hand quadrant (Fig. 16). Morphotype 1 has two coprolites (BP/21/109, BP/21/147) that plot with the coprolite morphotypes that contain unidentifiable inclusions (Fig. 16, point A), one coprolite (BP/21/422) that plots in the upper left-hand quadrant (Fig. 16) and one coprolite (BP/21/ 428) that plot in the lower right-hand quadrant (Fig. 16). Morphotype 4 has no coprolites that plot at point A, three coprolites (BP/21/262, BP/21/263, BP/21/421) plot in the lower right-hand quadrant, with coprolites BP/21/263 and BP/21/421 plotting together, and one coprolite

(BP/21/431) that plots in the upper right-hand quadrant (Fig. 16). Morphotype 5 has two coprolites (BP/21/55, BP/21/186) that plot with the coprolite morphotypes that contain unidentifiable inclusions (Fig. 16, point A) and one specimen (BP/21/54) that plots in the upper left-hand quadrant (Fig. 16); close to the unassigned coprolite BP/21/423. Morphotype 6 has three coprolites (BP/21/289, BP/21/316, BP/21/430) that plot with the coprolite morphotypes that contain unidentifiable inclusions (Fig. 16, point A) and two coprolites (BP/21/330, BP/21/429) that plot close together in the upper right-hand quadrant (Fig. 16).

Only one irregular (BP/21/426) coprolite and one of each coprolite specimen assigned to morphotype 2 and morphotype 3 (BP/21/ 161 and BP/21/326 respectively) were included in the NMDS analysis (Fig. 16). The irregular coprolite (BP/21/426) plots in the lower right-hand quadrant (Fig. 16), close to coprolite BP/21/428 (morphotype 1). Coprolite BP/21/161 (Morphotype 2) plots in the lower left-hand corner and coprolite BP/21/326 (Morphotype 2) plots in the lower right-hand quadrant with coprolites BP/21/263 and BP/21/421 (both morphotype 4, Fig. 16). Due to the small sample size for these (n=1 each) no intramorphotype or intermorphotype patterns for these morphotypes can be assessed.

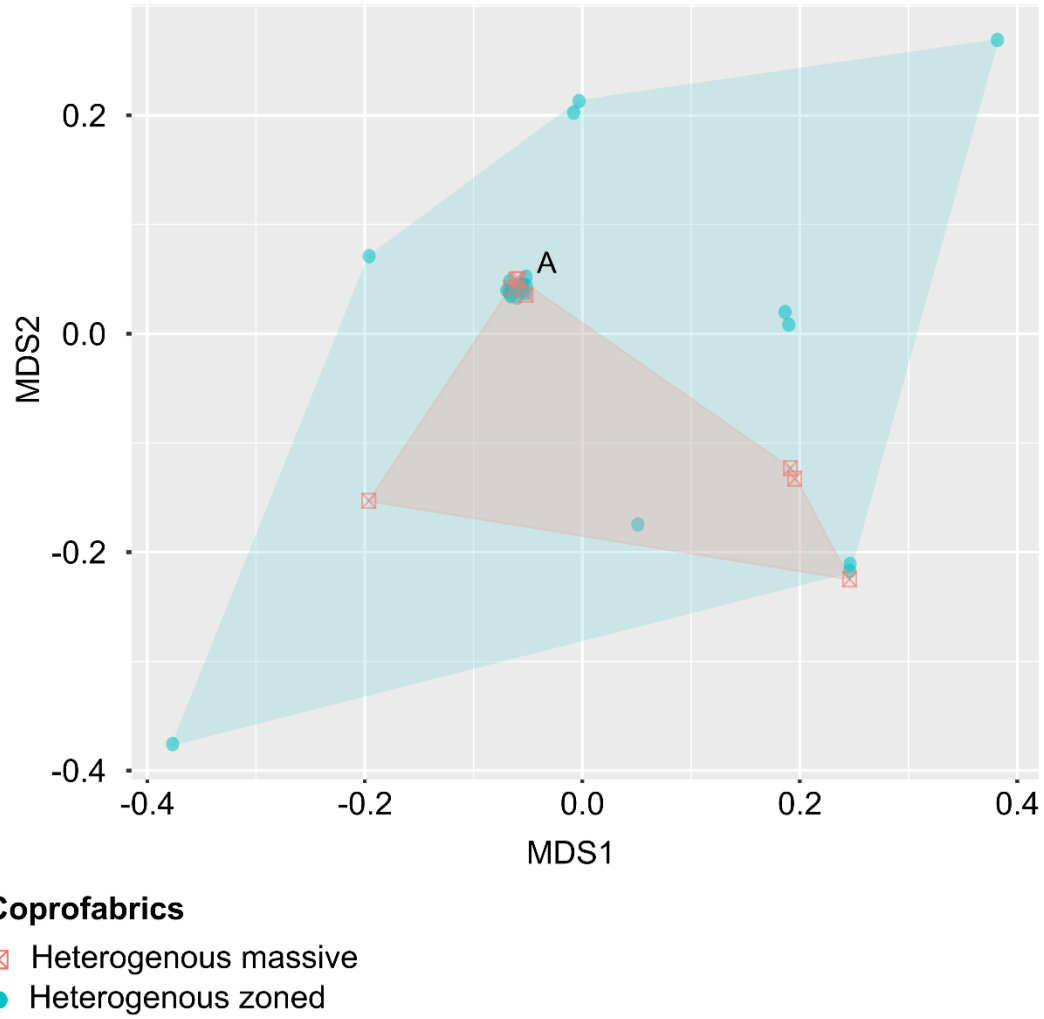

Figure 15: Non-metric Multidimensional Scaling (NMDS) ordination. The graph represents the relationships among coprolite heterogenous coprofabrics according to the coprolite inclusions per specimen. The convex hulls indicate the dimensional space occupied by coprolite specimens with either heterogenous massive or heterogenous zoned coprofabrics.

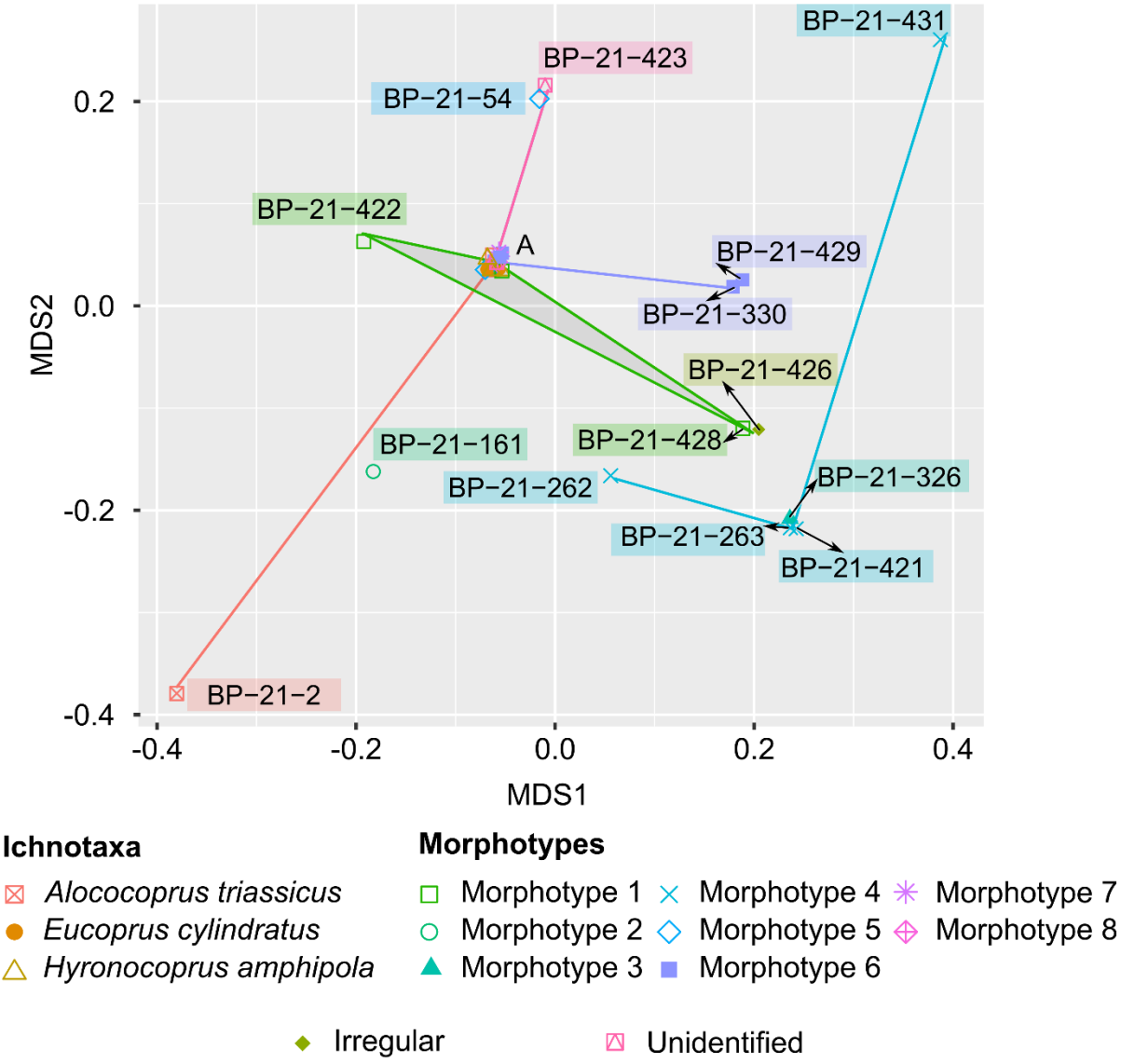

Figure 16: Non-metric Multidimensional Scaling (NMDS) ordination. The graph represents the relationships among coprolite morphotypes according to the coprolite inclusions per specimen. The lines indicate the Minimum Spanning Network connecting coprolites of the same morphotype together.

12. DISCUSSION

This study was designed to characterise a representative sample of the Driefontein 11 coprolite assemblage in terms of coprofabrics and inclusions and assessing how well these variables correspond to previous morphological observations (Montgomery, 2019). To ensure that the sample is representative, more than one specimen from each morphotype was included, as well as specimens with irregular shapes or that do not fit into the already identified morphotypes (unidentified). Overall, the Driefontein 11 coprolite assemblage is a freshwater association characterised by a high relative abundance of specimens with good preservation, that can be assigned to various morphotypes, and contain a wide taxonomic range of microfossil inclusions.

12.1. Coprofabrics

Defining coprofabric (microfabric in some studies) is an integral part of characterising a coprolite assemblage as coprofabrics may in part reflect the diets and digestive processes of the coprolite perpetrators (Eriksson et al., 2011, Owocki et al., 2012, Bajdek et al., 2015, Niedźwiedzki et al., 2016b, Qvarnström et al., 2019b, Barrios-de Pedro et al., 2020). Characterising coprofabrics based on CT-slice images is a novel technique explored in this study, compared to classic methods using SEM and petrographic thin section analyses (Eriksson et al., 2011, Qvarnström et al., 2019b, Barrios-de Pedro et al., 2020). Classic methods define coprofabrics based on mineral composition and grain size of the ground mass, along with the presence/absence of inclusions and the type of inclusions. Investigating the mineral composition and grain size of the ground mass from single-slice CT images is impossible. Instead, this study made use of differences in the spatial arrangement of the coprolite ground mass, indicated by density differences or lack thereof (Figs. 4-9). By using the CT-slice images, I made 3D reconstructions of the coprolite material inclusions (Figs. 10-14). This made identifying the presence/absence of inclusions easy and allowed me to visualise their 3D geometric distributions. Identifying the type of inclusion was often impossible however due to the limited resolution of the micro-CT scans. This meant that there was little correlation between coprofabric and inclusion type (Fig.

15) and therefore I did not use inclusion types as a defining character of the coprofabrics. In summary, this study defined coprofabrics based on the differences in the spatial arrangement of the coprolite ground mass and the presence/absence of inclusions. This made a one-to-one comparison between the coprofabrics characterised in this study and known coprofabrics from literature difficult.

It is also important to note that it is possible to distinguish between some of the fabric attributed to primary and secondary mineralisation using the single-slice CT images (Figs. 4-9) even though the mineral composition cannot be identified. Primary mineralisation (ground mass) occurs when the coprolites are initially lithified, a process often aided by microbial activity (Eriksson et al., 2011, Luo et al., 2018), whereas secondary mineralisation replaces or overprints this original mineralisation. Specimens from the Driefontein 11 coprolite assemblage have good preservation evidenced by the minimal presence of secondary mineralisation (manifesting as extremely bright areas on CT cross sections, see Figs. 4-9), never obscuring the textures of the primary coprofabric. Primary mineralisation is thus most likely to result in coprofabrics that reflect the diets and digestive processes of the perpetrators from the Driefontein 11 coprolite assemblage. Differentiating between more subtle secondary geochemical infilling in the coprofabrics is currently impossible at the resolution of lab-based CT-scans and will require thin sectioning specimens in future studies and the use of Raman spectroscopy or similar analytical methods.

In total, this study identified three distinct coprofabrics: homogenous massive, heterogenous massive, and heterogenous zoned (Figs. 4-9). The homogenous massive coprofabric is characterised by no internal structure, habit or layering, no density differences in the ground mass, and a lack of microfossil inclusions (Fig. 4). This coprofabric can be likened to the ‘nondescript’ coprofabric identified by Barrios-de Pedro et al (2020). The heterogenous massive coprofabric is characterised by density differences in the ground mass that show no distinct internal structure, habit or layering, and a variety of microfossil inclusions of various sizes and states of preservation (Fig. 4). Similarly, the heterogenous zoned coprofabric is characterised by density differences in the ground mass and a variety of microfossil inclusions of various sizes and states of preservation but the density differences are arranged as

concentric layers (Figs. 5-9). No clear comparison for either of these heterogeneous coprofabrics can be found in existing literature. It is possible that some of the concentric heterogenous zoned coprofabrics (Figs. 6A, B, D; 8A-F) can be attributed to secondary geochemical mineral infill, but this can only be confirmed through petrographic thin sectioning of specimens.

12.2. Inclusions

Microfossil coprolite inclusions are useful for identifying diets and digestive processes of the coprolite perpetrators (Thulborn, 1991, Hunt et al., 1994, Rodriguez-de la Rosa et al., 1998, Qvarnström et al., 2017, Zatoń et al., 2017, Qvarnström et al., 2019a, 2021), and prey selection patterns (Chin, 2002, Eriksson et al., 2011, Qvarnström et al., 2019b, Barrios-de Pedro et al., 2020). It is important to mention that any dietary information obtained from coprolites is likely biased by (1) what was eaten, (2) the chewing mechanism of the perpetrator, (3) the gut retention length, and (4) the strength of the perpetrator's digestive acids (Thulborn, 1991, Owocki et al., 2012). Overall, 72% of the sampled coprolite specimens from Driefontein 11 contain microfossil remains (Fig. 10-14). Reliably assigning microfossil remains to higher taxonomic ranks was a challenge due to the limited resolution of the scans therefore most of the microfossil remains are currently unidentifiable. For the coprolite specimens with identifiable microfossil remains, fish scales are the dominant inclusion (24%), and noteworthy microfossil remains include bivalves (Fig. 10), arthropods (Fig. 11, 12), dipnoans (Fig. 13) and tetrapods (Fig. 13, 14). The following sections will explore the significance of the microfossil remains.

12.2.1. Bivalves

Coprolite BP/21/422 (Fig. 10) is filled with fully articulated bivalves. Due to the limited resolution of the reconstructions narrowing down the taxonomic level further is not currently possible. These are the second documented instance of bivalve inclusions in coprolites from Driefontein 11 (Yates et al., 2012). Yates and his colleagues (2012)

studied one articulated specimen and two single fragments of the shell preserved in three different coprolites and tentatively assigned them to the freshwater clade Unionoida. The bivalves in BP/21/422 (Fig. 10) are not strictly comparable to those identified by Yates *et al* (2012) due to the different visualisation methods used. Following the PT-extinction event, bivalves successfully invade both marine and terrestrial Mesozoic habitats (Cox, 1969, Mondal, 2017). Due to the abundance of Early Triassic marine deposits, extensive work has been done on marine bivalves and how they recovered from the PT-extinction (e.g., Wasmer et al., 2012, Hautmanna et al., 2013, Pan et al., 2014) but the recovery of freshwater bivalves is poorly understood. Triassic freshwater bivalves have previously been documented in one Early Triassic locality (Driefontein 11, Yates et al., 2012) and several Middle and Late Triassic localities (Cox, 1932, Dixey, 1937, Good, 1989, Kondo and Sano, 2009). This highlights the importance of the Driefontein 11 coprolite assemblage in understanding how the P-T extinction event affected freshwater bivalve communities and their subsequent radiation.

12.2.2. Arthropods

Arthropod remains are present in two Driefontein 11 coprolites. Coprolite BP/21/161 (Fig. 11) contains small arthropod body parts (segmented thorax/abdomen, see Fig. 11C) and isolated fragments of larger species (articulated leg, see Fig. 11E.) No diagnostic features are present that would allow for a more comprehensive identification. Qvarnström et al. (2021) noted similar associations with coprolite specimens containing elements from both small and large species. The beetle fossils present in BP/21/2 (Fig. 12) bear some morphological synapomorphies of modern beetles and thus are tentatively assigned to Coleoptera. Currently, there are four recognised suborders of beetles in the literature namely, Adephaga, Archostemata, Myxophaga and Polyphaga. Morphologically, these can be differentiated based on the prothorax morphology (Qvarnström et al., 2021). Due to the limited resolution of the micro-CT reconstructions, the isolation and study of prothorax morphology is not possible for the beetles in coprolite BP/21/2 and thus they cannot be assigned to any lower taxonomic rank.

Documentation of Permian and early Mesozoic beetle remains is rare (Northwood, 2005, Ponomarenko and Mostovski, 2005, Kirejtshuk et al., 2014, Yan et al., 2017, Qvarnström et al., 2017, Yan et al., 2018, Fikáček et al., 2019, Qvarnström et al., 2019c, 2021). These are described for the most part purely based on individual elytra or elytron specimens with few body specimens, usually preserved in sedimentary rocks. Beetles are preserved in coprolites from the Early Triassic Arcadia Formation of Australia (Northwood, 2005) and from the Late Triassic Krasiejów locality of Poland (Qvarnström et al., 2019c, 2021). The Australian beetle is an impression of an insect head preserved on the external surface (Northwood, 2005). The Late Triassic beetles from Poland were reconstructed in 3D by making use of high-resolution imaging (Qvarnström et al., 2019c, 2021). The Driefontein 11 locality is therefore the third Triassic locality with coprolites that preserve beetles and is the second to document beetles in the Early Triassic.

12.2.3. Pisces

Pisces are the dominant prey inclusion in the Driefontein 11 coprolite assemblage. This is indicated by the large abundance of fish scale inclusions (Fig. 4E, F; 5A, 6D, E; 7G, I; 8B-D; 13D) in the assemblage and one dipnoan lungfish tooth plate (Fig. 13C). The scales are rhomboidal and vary in size, some with posterior pegs (Fig. 13D$_{1,3}$) and some lacking such pegs (Fig. 13D$_2$). Even though they lack surface sculpture, their morphology is indicative of ganoid scales, but further taxonomic attribution of the prey cannot be determined. Other studies have commonly found fish scales in coprolites with cylindrical morphotypes and irregular shapes (Zangerl and Richardson, 1963, Owocki et al., 2012, Bajdek et al., 2015, Qvarnström et al., 2017, Segesdi et al., 2017). This study found fish scales in five different morphotypes (see Table 1 and Appendix B, Table 4): irregular, Morphotype 1 (oval, anisopolar), Morphotype 3 (arcuate, hook-shaped), Morphotype 4 (small, spherical) and Morphotype 6 (anisopolar, amphipolar).

Coprolite BP/21/263 (Fig. 13) contains a positively identified dipnoan lungfish tooth plate (Fig. 13C). Many isolated lungfish tooth plates have been collected from

Driefontein 11, some of which have been documented formally in literature (Bender and Hancox, 2004). These have distinct tooth ridges, five in the upper tooth plates and four in the lower tooth plates (Bender and Hancox, 2004). The tooth rows are deeply-ridged, radiate form a point anterior on the plate and are slightly ovate in shape with the last ridge being almost parallel to the lingual surface (Bender and Hancox, 2004). Bender and Hancox (2004) tentatively assigned these tooth plates to *Ptychoceratodus*. The tooth plate identified in this study shares many morphological features with the specimens already described but preserves only three distinct tooth rows (Fig. 13C) with is a feature exclusive to Lepidosirenid lungfishes. If this is accurate it would be the first documented Lepidosirenid lungfishes from Driefontein 11.

12.2.4. Tetrapods

Two coprolites in the Driefontein collection contain microfossil remains of tetrapod individuals. Coprolite BP/21/263 (Fig. 13) contains a left mandibular fragment (Fig. 13E), with at least eight oval tooth sockets (Fig. 13E_1) of thecodont type implantation (Zaher and Rieppel, 1999, Heckert, 2004). In this study, I tentatively assign this left mandibular fragment (Fig. 13E) to an archosauriform since thecodont implantation is restricted to the archosaurs (Edmund, 1969, Romer, 1956). Without the teeth, no further analyses can be done to assign the jaw fragment to a lower taxonomic rank. Coprolite BP/21/421 (Fig. 14) contains a tooth-bearing right-maxillary fragment with conical teeth that decrease in size posteriorly and are arranged in into two rows that are oriented diagonally, distolingually across the jaw (Fig. 14D). The identity of this specimen rests on the tooth implantation which is not resolvable at this resolution. If it is acrodont it most likely represents the marginal dentition of a temnospondyl amphibian and if it is sub-thecodont the most likely potential candidate is a late surviving captorhinid, a group that is currently hypothesized to go extinct at the end of the Permian (Olson, 1962, 1965, Romer, 1966).

12.3. Digestive Strategies

Any dietary information obtained from coprolites is biased by preservation factors, the digestibility of the prey items, prey items accidentally ingested, perpetrators that are specialist feeders, the digestive capabilities of the perpetrator, and perpetrators that regurgitate indigestible food residues (Thulborn, 1991). Digestive strategies inferred from coprolites will thus likely be biased and will not allow us to account for certain nuances. The homogenous massive coprofabric (Fig. 4) can be indicative of either perpetrators that fed on soft-bodied prey items (Thulborn, 1991), had an emetic digestive mechanism (Andrews et al., 2000, Wallace, 2006), had the ability to corrode enamel and ganoine, and decalcify bone (Fisher, 1981, Milàn, 2012, Milàn et al., 2012), retained food until everything was almost digested (Fernández-Jalvo and Andrews, 2016) or a combination of all of these. Regardless, these perpetrators have a high digestive efficacy. The NMDS analyses (Fig. 15) provided no basis for outlining the different digestive strategies of the Driefontein 11 ecosystem, as there is no unambiguous correspondence between the heterogenous massive and zoned coprofabrics. The perpetrators of both types of heterogenous coprofabrics probably had some combination of the digestive strategies employed by the perpetrators of the homogenous massive coprofabrics. There is no clear evidence of dietary specialisation, as many of the coprolites contain more than one prey type or prey of indeterminate origins (see Appendix B, Table 5). The NMDS analysis (Fig. 16) shows that there is no unambiguous correspondence between coprolite inclusions and the coprolite morphotypes. The following paragraphs will explore the digestive strategies employed by the perpetrators of individual coprolites based of their microfossil inclusions.

Coprolite BP/21/422 (Fig. 9) presents an interesting case. It has a high relative abundance of bivalves from one specimen (at least twelve), considering Yates et al. (2012) identified one bivalve specimen in each of the three coprolite specimens they studied. The bivalves are exceptionally well preserved, with no visible evidence of digestion, and they are fully articulated. This means that they were potentially accidentally ingested with no mechanical action and that the perpetrator was not capable of decalcifying the shells. Coprolite BP/21/161 (Fig. 11) contains a small

number of disarticulated arthropod inclusions and this either means that the elements were accidentally ingested, or few beetles were present where the perpetrator who produced the coprolite was foraging. Coprolite BP/21/2 (Fig. 12) contains beetles in various degrees of disarticulation, with missing abdomens and no surface traces or burrows in association with the beetle body fossils. This clearly showing that they were ingested rather than having colonized the faeces for feeding or laying eggs, similar to the beetles studied by Qvarnström et al. (2021). Even though beetles were found in large numbers, the coprolite contains several unidentifiable inclusions and thus it cannot be concluded the perpetrator is strictly insectivorous. Coprolites BP/21/263 (Fig. 13) and BP/21/421 (Fig. 14) contain fish and tetrapod inclusions, indicating that the perpetrators ate both aquatic and terrestrial prey. Only a few elements of each prey item have been preserved in the coprolite. This could either be because (1) all non-digestive elements that pass through the entire digestive system did not get expelled in the same faeces; (2) different elements of an organism might withstand digestion differently and (3) larger undigestible elements may be regurgitated and thus never pass through the entire digestive system.

12.4. Comparison of classic and non-destructive methods

Classic methods have allowed for the characterisation of coprolite assemblages with great success (Eriksson et al., 2011, Fiorelli et al., 2013, Bajdek et al., 2014, 2015, Niedźwiedzki et al., 2016a, 2016b, Bajdek et al., 2017, Barrios-de Pedro and Buscalioni, 2018, Barrios-de Pedro et al., 2018, Dentzien-Dias et al., 2018, Barrios-de Pedro et al., 2020, Qvarnström et al., 2019b, Rakshit et al., 2019, Cueille et al., 2020, Dentzien-Dias et al., 2020, Rakshit and Ray, 2021). However, there are limits to classical destructive methods, including the lack of 3D visualisation of the spatial arrangement of the coprolite ground mass and geometric arrangement of the material inclusions, and the inability to identify microfossil inclusions to lower taxonomic levels.

CT-imaging addresses many of the limitations that are inherent in classical techniques. Through carefully scrutinising the single-slice CT-images, density

differences (or the lack thereof) in the coprolite ground mass allow for the visualisation of spatial arrangement of the groundmass in 3D. As long as they produce a difference in contrast, the CT-slice images also make it possible to reconstruct microfossil inclusions, which we can then use to visualise the geometric arrangement and morphology of the inclusions in 3D. Being able to study the morphology of the inclusion in 3D allows us to classify the types of inclusions beyond simply vertebrate indeterminate (e.g., Rakshit et al., 2019; Fig.7; Rakshit & Ray, 2021; Fig. 5, Fig. 10) to lower taxonomic levels (e.g., tooth-bearing right-maxillary fragment; Fig. 14D).

Even though a representative subsample of the Driefontein 11 coprolite assemblage was selected for this study there is a lot of uncertainty in the current coprolite dataset (Fig. 15, 16). Further scanning of the Driefontein 11 coprolites is necessary to increase the sample size in order to improve the precision of our ordinations along with allowing for the identification of more Early Triassic recovery fauna. High-resolution synchrotron images in particular will allow for the identification of diagnostic features for inclusions whose reconstructions are currently limited by the resolution of the micro-CT scans (e.g., bivalve and beetles, Fig. 10 and Fig. 11, 12).

Going forward it is also important to assemble a representative database for modern faecal material that can be used to test assumptions made for corprolites in extant taxa where digestive strategies are known.

13. CONCLUSION

This study used micro-CT to non-destructively characterise 47 coprolites from the Driefontein 11 locality in terms of their internal microstructures (coprofabrics) and to produce three-dimensional (3D) reconstructions of material inclusions. NMDS ordination was then used to assess how well coprofabrics and inclusion type correlate with their morphotypes. Characterisation of the coprofabrics and inclusions provided information on the prey consumed by the coprolite perpetrators and their digestive processes. This is important because direct evidence of animal behaviour and interaction is rare in the fossil record.

The differences in ground mass density or lack thereof and the internal structure, habit, or layering, allowed for the characterisation of three distinct coprofabrics: homogenous massive, heterogenous massive, heterogenous zoned. The coprolite ordination showed no unambiguous correspondence between the heterogenous massive and zoned coprofabrics. The homogenous massive coprofabric is considered indicative of perpetrators that have long retention time and high digestive efficacy in the gut/alimentary canal.

The microfossil inclusions are important on several grounds as they provide the first definitive record of Early Triassic beetles in the South African rock record, and only the second instance of bivalves. The coprolites also likely preserve some of the earliest archosauriforms and if the jaw in BP/21/422 is shown to belong to a captorhinid this would mean that some individuals survived past the P-T boundary. This reaffirms the importance of coprolites as a micro-lagerstätte and highlights their pivotal role in understanding these Early Triassic recovery fauna.

Coprolite perpetrators identified previously at Driefontein 11 include erythrosuchid archosaurs, the dipnoan species *Ptychoceratodus phillipsi*, actinopterrrygian genus *Saurichthys* sp., and indeterminate vertebrates. Many of these animals based their diets on fish but also fed on indeterminate tetrapods and beetles.

14. APPENDIX.

14.1. Appendix A

Table 3: Species found in the lowest most subzone of Cynognathus Assemblage Zone (*Langbergia-Garjainia* subzone) at Driefontein, adapted from Hancox et al. (2020).

Vertebrates	Pisces	*Lissodus tumidoclavus, Polyacrodus* sp., *Ptychoceratodus phillipsi, Saurichthys* sp.	
	Amphibia	*Bathignathus poikilops, Kestrosaurus dreyeri, Kestrosaurus kitchingi, Paratosuchus haughtoni, Trematosuchus sobeyi*	
	Reptillia	**Parareptilia** **Eureptilia** **Archosauriformes**	Procolophinid indet. *Palacrodon browni* *Garjainia madiba*
	Synapsida	**Therocephalia** **Cynodontia**	*Microgomphodon oligocynus* *Cynognathus crateronotus* *Eucynodont* sp. *Langbergia modisei*
Invertebrates	Mollusca	*Unio karooensis*	
Trace Fossils		Arthropod trails (*Diplichnites*), crayfish burrows, *Lockeia* sp., vertebrate burrows (*trirachodontids*), worm burrows (*Planolites*)	

14.2. Appendix B

Table 4: Coprolites from the farm Driefontein 11 coprolite collection with their corresponding inchnotaxa/morphotypes (Montgomery, 2019), their maximum length and diameter (cm), their primary and sub-coprofabric, the absence (0) or presence (1) of scales, shells, bones, teeth, plants, arthropods, gastroliths, unknown inclusions, microvesicles, cracks, secondary precipitation, invertebrate burrows and the results from the NMDS analyses (MDS1 and MDS2).

Specimen #	Ichnotaxa/ morphotypes	Maximum Length (cm)	Maximum Diameter (cm)	Primary Coprofabric	Sub-coprofarbic	Scales	Shells	Bones	Teeth	Bacteria	Plants	Arthropods	Gastroliths	Unknown inclusions	Microvesicles	Cracks	Secondary Precipitation	Invertebrate Burrow	MDS1	MDS2
BP/21/1	Alococoprus triassicus	4.45	2.3	Homogenous	Massive	0	0	0	0	0	0	0	0	0	0	1	1	0	-0.11289334	-0.286778144
BP/21/302	Morphotype 4	0.42	0.42	Homogenous	Massive	0	0	0	0	0	0	0	0	0	1	0	1	1	0.218336946	-0.118289553

BP/21/31	BP/21/12	BP/21/314	Specimen #
Eucoprus cylindratus	Alococoprus triassicus	Morphotype 4	**Ichnotaxa/ morphotypes**
4.87	2.49	0.73	**Maximum Length (cm)**
2.48	1.76	0.52	**Maximum Diameter (cm)**
Homogenous	Heterogenous	Homogenous	**Primary Coprofabric**
Massive	Zoned Muddled	Massive	**Sub-coprofarbic**
0	0	0	**Scales**
0	0	0	**Shells**
0	0	0	**Bones**
0	0	0	**Teeth**
0	0	0	**Bacteria**
0	0	0	**Plants**
0	0	0	**Arthropods**
0	0	0	**Gastroliths**
0	1	0	**Unknown inclusions**
0	1	1	**Microvesicles**
1	1	0	**Cracks**
1	1	1	**Secondary Precipitation**
0	0	1	**Invertebrate Burrow**
0.061867618	0.061867618	-0.240021833	**MDS1**
0.039433986	0.039433986	-0.187286859	**MDS2**

BP/21/427	BP/21/56	BP/21/329	Specimen #
Irregular	Morphotype 5	Unidentified	**Ichnotaxa/ morphotypes**
1.25	2.71	5.41	**Maximum Length (cm)**
0.83	2.58	2.39	**Maximum Diameter (cm)**
Heterogenous	Homogenous	Homogenous	**Primary Coprofabric**
Massive	Massive	Massive	**Sub-coprofarbic**
0	0	0	**Scales**
0	0	0	**Shells**
0	0	0	**Bones**
0	0	0	**Teeth**
0	0	0	**Bacteria**
0	0	0	**Plants**
0	0	0	**Arthropods**
0	0	0	**Gastroliths**
0	0	0	**Unknown inclusions**
1	0	1	**Microvesicles**
0	1	1	**Cracks**
1	1	1	**Secondary Precipitation**
0	0	0	**Invertebrate Burrow**
0.061867618	-0.207124633	-0.207124633	**MDS1**
0.039433986	-0.098959404	-0.098959404	**MDS2**

BP/21/243	BP/21/96	BP/21/2	Specimen #
Eucoprus cylindratus	Alococoprus triassicus	Alococoprus triassicus	**Ichnotaxa/ morphotypes**
2.48	2.27	4.69	**Maximum Length (cm)**
2.17	1.23	1.4	**Maximum Diameter (cm)**
Heterogenous	Heterogenous	Heterogenous	**Primary Coprofabric**
Zoned Muddled	Massive	Zoned Folded	**Sub-coprofarbic**
0	0	0	**Scales**
0	0	0	**Shells**
0	0	0	**Bones**
0	0	0	**Teeth**
0	0	0	**Bacteria**
0	0	0	**Plants**
0	0	1	**Arthropods**
0	0	0	**Gastroliths**
1	1	0	**Unknown inclusions**
1	0	1	**Microvesicles**
1	1	0	**Cracks**
1	1	1	**Secondary Precipitation**
0	0	0	**Invertebrate Burrow**
-0.067135939	0.061867618	0.061867618	**MDS1**
-0.161046292	0.039433986	0.039433986	**MDS2**

BP/21/272	BP/21/379	BP/21/33	Specimen #
Hyranocoprus amphipola	Irregular	Eucoprus cylindratus	**Ichnotaxa/ morphotypes**
2.71	1.97	4.25	**Maximum Length (cm)**
0.83	1.87	2.6	**Maximum Diameter (cm)**
Heterogenous	Heterogenous	Heterogenous	**Primary Coprofabric**
Zoned Muddled	Massive	Zoned	**Sub-coprofarbic**
0	0	0	**Scales**
0	0	0	**Shells**
0	0	0	**Bones**
0	0	0	**Teeth**
0	0	0	**Bacteria**
0	0	0	**Plants**
0	0	0	**Arthropods**
0	0	0	**Gastroliths**
1	0	1	**Unknown inclusions**
1	1	1	**Microvesicles**
0	1	1	**Cracks**
1	1	1	**Secondary Precipitation**
0	0	0	**Invertebrate Burrow**
0.006322342	0.061867618	0.061867618	**MDS1**
0.210274402	0.039433986	0.039433986	**MDS2**

BP/21/426	BP/21/275	BP/21/273	Specimen #
Irregular	Hyranocoprus amphipola	Hyranocoprus amphipola	**Ichnotaxa/ morphotypes**
1.97	1.88	2.49	**Maximum Length (cm)**
1.04	0.73	0.62	**Maximum Diameter (cm)**
Heterogenous	Heterogenous	Heterogenous	**Primary Coprofabric**
Massive	Zoned Folded	Zoned Muddled	**Sub-coprofarbic**
1	0	0	**Scales**
0	0	0	**Shells**
1	0	0	**Bones**
0	0	0	**Teeth**
0	0	0	**Bacteria**
0	0	0	**Plants**
0	0	0	**Arthropods**
0	0	0	**Gastroliths**
1	1	1	**Unknown inclusions**
1	1	1	**Microvesicles**
1	0	0	**Cracks**
1	1	1	**Secondary Precipitation**
0	0	0	**Invertebrate Burrow**
-0.240023617	0.061867618	0.395928098	**MDS1**
-0.187288359	0.039433986	-0.340241411	**MDS2**

BP/21/109	BP/21/108	BP/21/432	Specimen #
Morphotype 1	Morphotype 1	Irregular	**Ichnotaxa/ morphotypes**
2.17	1.96	1.04	**Maximum Length (cm)**
0.73	1.04	1.24	**Maximum Diameter (cm)**
Heterogenous	Homogenous	Heterogenous	**Primary Coprofabric**
Zoned Mottled	Massive	Massive	**Sub-coprofarbic**
0	0	0	**Scales**
0	0	0	**Shells**
0	1	0	**Bones**
0	1	0	**Teeth**
0	0	0	**Bacteria**
0	0	0	**Plants**
0	0	0	**Arthropods**
0	0	0	**Gastroliths**
1	1	1	**Unknown inclusions**
1	0	0	**Microvesicles**
0	1	0	**Cracks**
1	1	1	**Secondary Precipitation**
1	1	1	**Invertebrate Burrow**
0.061867618	0.061867618	0.061867618	**MDS1**
0.039433986	0.039433986	0.039433986	**MDS2**

BP/21/428	BP/21/422	BP/21/147	Specimen #
Morphotype 1	Morphotype 1	Morphotype 1	**Ichnotaxa/ morphotypes**
2.08	1	4.37	**Maximum Length (cm)**
0.83	0.6	1.98	**Maximum Diameter (cm)**
Heterogenous	Heterogenous	Heterogenous	**Primary Coprofabric**
Massive	Zoned Muddled	Zoned	**Sub-coprofarbic**
1	0	0	**Scales**
0	1	0	**Shells**
1	0	0	**Bones**
0	0	0	**Teeth**
0	0	0	**Bacteria**
0	0	0	**Plants**
0	0	0	**Arthropods**
0	0	0	**Gastroliths**
1	1	1	**Unknown inclusions**
1	0	1	**Microvesicles**
0	0	0	**Cracks**
1	1	1	**Secondary Precipitation**
0	1	0	**Invertebrate Burrow**
0.061867618	0.061867618	0.061867618	**MDS1**
0.039433986	0.039433986	0.039433986	**MDS2**

BP/21/170	BP/21/326	BP/21/161	Specimen #
Morphotype 2	Morphotype 3	Morphotype 2	**Ichnotaxa/ morphotypes**
5.02	1.98	5.31	**Maximum Length (cm)**
2.39	0.73	2.41	**Maximum Diameter (cm)**
Heterogenous	Heterogenous	Heterogenous	**Primary Coprofabric**
Zoned Mottled	Zoned Folded	Massive	**Sub-coprofarbic**
0	1	0	**Scales**
0	0	0	**Shells**
0	1	0	**Bones**
0	1	0	**Teeth**
0	0	0	**Bacteria**
0	0	0	**Plants**
0	0	1	**Arthropods**
0	0	0	**Gastroliths**
0	1	1	**Unknown inclusions**
1	0	1	**Microvesicles**
1	0	1	**Cracks**
1	1	1	**Secondary Precipitation**
0	0	0	**Invertebrate Burrow**
-0.158882677	0.061867618	0.061867618	**MDS1**
0.046275009	0.039433986	0.039433986	**MDS2**

BP/21/421	BP/21/263	BP/21/262	Specimen #
Morphotype 4	Morphotype 4	Morphotype 4	**Ichnotaxa/ morphotypes**
0.4	1.46	1.66	**Maximum Length (cm)**
0.6	0.63	1.35	**Maximum Diameter (cm)**
Heterogenous	Heterogenous	Heterogenous	**Primary Coprofabric**
Zoned Muddled	Massive	Zoned	**Sub-coprofarbic**
1	1	0	**Scales**
0	0	0	**Shells**
1	1	1	**Bones**
1	1	0	**Teeth**
0	0	0	**Bacteria**
0	0	0	**Plants**
0	0	0	**Arthropods**
0	0	0	**Gastroliths**
1	1	1	**Unknown inclusions**
1	1	1	**Microvesicles**
0	1	0	**Cracks**
1	1	1	**Secondary Precipitation**
0	1	0	**Invertebrate Burrow**
0.061867618	0.197565941	-0.240022058	**MDS1**
0.039433986	0.098553247	-0.187287048	**MDS2**

BP/21/186	BP/21/431	BP/21/191	Specimen #
Morphotype 5	Morphotype 4	Morphotype 8	**Ichnotaxa/ morphotypes**
4.16	1.56	3.54	**Maximum Length (cm)**
2.59	1.24	2.81	**Maximum Diameter (cm)**
Heterogenous	Heterogenous	Heterogenous	**Primary Coprofabric**
Zoned Mottled	Zoned Muddled	Zoned Muddled	**Sub-coprofarbic**
0	1	0	**Scales**
0	0	0	**Shells**
0	0	0	**Bones**
0	0	0	**Teeth**
0	0	0	**Bacteria**
0	0	0	**Plants**
0	0	0	**Arthropods**
0	1	0	**Gastroliths**
1	0	0	**Unknown inclusions**
1	0	1	**Microvesicles**
0	0	1	**Cracks**
1	1	1	**Secondary Precipitation**
1	0	0	**Invertebrate Burrow**
-0.367849	0.061867618	-0.158882677	**MDS1**
0.305238678	0.039433986	0.046275009	**MDS2**

BP/21/289	BP/21/55	BP/21/54	Specimen #
Morphotype 6	Morphotype 5	Morphotype 5	**Ichnotaxa/ morphotypes**
1.98	3.95	4.37	**Maximum Length (cm)**
1.94	1.87	2.39	**Maximum Diameter (cm)**
Heterogenous	Heterogenous	Heterogenous	**Primary Coprofabric**
Zoned Mottled	Zoned	Zoned Muddled	**Sub-coprofarbic**
0	0	0	**Scales**
0	0	0	**Shells**
0	0	0	**Bones**
0	0	0	**Teeth**
0	0	0	**Bacteria**
0	0	0	**Plants**
0	0	0	**Arthropods**
0	0	1	**Gastroliths**
1	1	1	**Unknown inclusions**
1	1	1	**Microvesicles**
0	0	1	**Cracks**
1	1	1	**Secondary Precipitation**
0	0	1	**Invertebrate Burrow**
-0.11289334	0.061867618	0.006322342	**MDS1**
-0.286778144	0.039433986	0.210274402	**MDS2**

BP/21/316	BP/21/325	BP/21/322	Specimen #
Morphotype 6	Morphotype 3	Morphotype 3	**Ichnotaxa/ morphotypes**
1.77	4.89	0.94	**Maximum Length (cm)**
0.83	2.18	0.52	**Maximum Diameter (cm)**
Heterogenous	Heterogenous	Heterogenous	**Primary Coprofabric**
Massive	Zoned Muddled	Zoned Muddled	**Sub-coprofarbic**
0	0	0	**Scales**
0	0	0	**Shells**
0	0	0	**Bones**
0	0	0	**Teeth**
0	0	0	**Bacteria**
0	0	0	**Plants**
0	0	0	**Arthropods**
0	0	0	**Gastroliths**
1	0	0	**Unknown inclusions**
1	1	0	**Microvesicles**
0	1	0	**Cracks**
1	1	1	**Secondary Precipitation**
0	0	0	**Invertebrate Burrow**
0.061867618	-0.240021833	0.218336946	**MDS1**
0.039433986	-0.187286859	-0.118289553	**MDS2**

BP/21/429	BP/21/330	BP/21/353	Specimen #
Morphotype 6	Morphotype 6	Morphotype 2	**Ichnotaxa/ morphotypes**
1.14	1.87	5.62	**Maximum Length (cm)**
0.52	0.62	2.51	**Maximum Diameter (cm)**
Heterogenous	Heterogenous	Heterogenous	**Primary Coprofabric**
Zoned Muddled	Zoned Muddled	Zoned Muddled	**Sub-coprofarbic**
1	1	0	**Scales**
0	0	0	**Shells**
0	0	0	**Bones**
0	0	0	**Teeth**
0	0	0	**Bacteria**
0	0	0	**Plants**
0	0	0	**Arthropods**
0	0	0	**Gastroliths**
1	1	0	**Unknown inclusions**
0	0	1	**Microvesicles**
0	0	1	**Cracks**
1	1	1	**Secondary Precipitation**
1	0	0	**Invertebrate Burrow**
-0.207124633	-0.207124633	0.061867618	**MDS1**
-0.098959404	-0.098959404	0.039433986	**MDS2**

BP/21/320	BP/21/319	BP/21/430	Specimen #
Morphotype 7	Morphotype 7	Morphotype 6	**Ichnotaxa/ morphotypes**
1.25	1.35	1.03	**Maximum Length (cm)**
0.62	0.42	0.2	**Maximum Diameter (cm)**
Heterogenous	Heterogenous	Heterogenous	**Primary Coprofabric**
Massive	Zoned Muddled	Zoned Muddled	**Sub-coprofarbic**
0	0	0	**Scales**
0	0	0	**Shells**
0	0	0	**Bones**
0	0	0	**Teeth**
0	0	0	**Bacteria**
0	0	0	**Plants**
0	0	0	**Arthropods**
0	0	0	**Gastroliths**
1	1	1	**Unknown inclusions**
1	1	1	**Microvesicles**
0	0	0	**Cracks**
1	1	1	**Secondary Precipitation**
0	0	1	**Invertebrate Burrow**
0.061867618	0.061867618	0.061867618	**MDS1**
0.039433986	0.039433986	0.039433986	**MDS2**

BP/21/424	BP/21/423	BP/21/190	Specimen #
Unidentified	Unidentified	Morphotype 8	**Ichnotaxa/ morphotypes**
1.87	6.86	4.79	**Maximum Length (cm)**
0.72	3.12	2.29	**Maximum Diameter (cm)**
Heterogenous	Heterogenous	Heterogenous	**Primary Coprofabric**
Zoned Muddled	Zoned	Zoned Muddled	**Sub-coprofarbic**
0	0	0	**Scales**
0	0	0	**Shells**
0	0	0	**Bones**
0	0	0	**Teeth**
0	0	0	**Bacteria**
0	0	0	**Plants**
0	0	0	**Arthropods**
0	1	0	**Gastroliths**
1	1	1	**Unknown inclusions**
1	1	1	**Microvesicles**
0	1	0	**Cracks**
1	1	1	**Secondary Precipitation**
1	0	1	**Invertebrate Burrow**
0.061867618	0.061867618	-0.067135939	**MDS1**
0.039433986	0.039433986	-0.161046292	**MDS2**

14.3. Appendix C

```
# Loading necessary packages
library (vegan)
library (ggplot2)
library (ggrepel)
options(ggrepel.max.overlaps = Inf)

# Setting working directory
setwd("~/Academics/HET/University of the Witwatersrand/Postgraduate degrees/Masters degree/Figures/Ordination/NMDS")

# Reading in your data
Copro.matrix <-
  read.csv("MSc_Coprolites_matrix.csv", row.names = 1)
str(Copro.matrix)

# Subsetting binary variables for the coprolite inclusion types
Copro.spec <- cbind(Copro.matrix$Scales, Copro.matrix$Shells, Copro.matrix$Bones, Copro.matrix$Teeth, Copro.matrix$Bacteria, Copro.matrix$Plants, Copro.matrix$Arthropods, Copro.matrix$Gastroliths, Copro.matrix$Unknown)
str(Copro.spec)

# Running an NMDS analyses using the metaMDS function
dist.copro.spec<-dist(Copro.spec, method ="binary")
str(dist.copro.spec)
meta.copro.spec<-metaMDS(dist.copro.spec, trymax=100)
plot(meta.copro.spec, "sites")
str(meta.copro.spec)

# Creating a subset of you NMDS results (MDS1 and MDS2)
meta.copro.spec$points
meta.scores <- meta.copro.spec$points
str(meta.scores)
```

```
meta.scores.v <- meta.scores[,1:2]
str(meta.scores.v)

# Combining the raw dataset with the NMDS results
Copro.data.full<-cbind(Copro.matrix, meta.scores.v)
str(Copro.data.full)
write.csv(Copro.data.full, "~/Academics/HET/University of the
Witwatersrand/Postgraduate degrees/Masters
degree/Figures/Ordination/NMDS/MDS.csv")

# Plotting NMDS results with the coprofabrics (Subfabric) highlighted
ggplot(Copro.data.full, aes(x=MDS1, y=MDS2)) +
  scale_shape_manual(values = c(7, 16)) +
  geom_jitter(width=0.01, height=0.01, aes(shape=Subfabric, colour=Subfabric,
alpha=0.1, size=2))

# Plotting NMDS results with the ichnotaxa/morphotypes (Taxon) highlighted
and  showing the minimum spanning network
ggplot(Copro.data.full, aes(x=MDS1, y=MDS2, label = rownames(Copro.data.full))) +
  geom_polygon(aes(group=Taxon, colour=Taxon, alpha = 0.05)) +
  scale_shape_manual(values = c(7, 16, 2, 18, 0, 1, 17, 4, 5, 15, 8, 9, 14)) +
  geom_jitter(width=0.01, height=0.01, aes(shape=Taxon, colour=Taxon, alpha=0.1,
size=2)) + geom_text_repel()
```

15. REFERENCES

ALDRIDGE, R. J., GABBOTT, S. E., SIVETER, L. J. & THERON, J. N. 2006. Bromalites from the Soom Shale Lagerstätte (Upper Ordovician) of South Africa: Palaeoecological and palaeobiological implications. *Palaeontology,* 49**,** 857-871.

ALVES, Y. M. 2010. Report on the Upper Permian and Lower Cretaceous fossiliferous localities vertebrates-bearing in the central north of Tocantins State, Brazil. *Brazilian Geographical Journal: Geosciences and Humanities research medium, Uberlândia,* 1**,** 372-386.

BAJDEK, P. 2013. Coprolite of a durophagous carnivore from the Upper Cretaceous Godula Beds, Outer Western Carpathians, Poland. *Geological Quarterly,* 57.

BAJDEK, P. & BIENKOWSKA-WASILUK, M. 2020. Deep-sea ecosystem revealed by teleost fish coprolites from the Oligocene of Poland. *Palaeogeography, Palaeoclimatology, Palaeoecology,* 540.

BAJDEK, P., OWOCKI, K. & NIEDŹWIEDZKI, G. 2014. Putative dicynodont coprolites from the Upper Triassic of Poland. *Palaeogeography, Palaeoclimatology, Palaeoecology,* 411**,** 1-17.

BAJDEK, P., OWOCKI, K., SENNIKOV, A. G., GOLUBEV, V. K. & NIEDŹWIEDZKI, G. 2017. Residues from the Upper Permian carnivore coprolites from Vyazniki in Russia - key questions in reconstruction of feeding habits. *Palaeogeography, Palaeoclimatology, Palaeoecology,* 482**,** 70-82.

BAJDEK, P., QVARNSTRÖM, M., OWOCKI, K., SULEJ, T., SENNIKOV, A. G., GOLUBEV, V. K. & NIEDŹWIEDZKI, G. 2015. Microbiota and food residues including possible evidence of pre-mammalian hair in Upper Permian coprolites from Russia. *Lethaia,* 49**,** 455-477.

BAJDEK, P., SZCZYGIELSKI, T., KAPUŚCIŃSKA, A. & SULEJ, T. 2019. Bromalites from a turtle-dominated fossil assemblage from the Triassic of Poland. *Palaeogeography, Palaeoclimatology, Palaeoecology,* 520**,** 214-228.

BARRIOS-DE PEDRO, S. & BUSCALIONI, Á. D. 2018. Scrutinizing Barremian coprolite inclusions to record digestive strategies. *Annales Societatis Geologorum Poloniae*.

BARRIOS-DE PEDRO, S., CHIN, K. & BUSCALIONI, Á. D. 2020. The late Barremian ecosystem of Las Hoyas sustained by fishes and shrimps as inferred from coprofabrics. *Cretaceous Research,* 110**,** 1-17.

BARRIOS-DE PEDRO, S., POYATO-ARIZA, F. J., MORATALLA, J. J. & BUSCALIONI, A. D. 2018. Exceptional coprolite association from the Early Cretaceous continental Lagerstatte of Las Hoyas, Cuenca, Spain. *PLoS One,* 13**,** e0196982.

BARTELS, C., BRIGGS, D. E. G. & BRASSEL, G. 1998. *The fossils of the Hunsrück Slate: Marine life in the Devonian,* Cambridge, Cambridge University Press.

BAYER, B. 1934. Koprolity z kounovských vrestev na Plzensku. *Príroda Brno,* 27**,** 21-22.

BENDER, P. A. & HANCOX, P. J. 2003. Fossil fishs of the *Lystrosaurus* and *Cynognathus* assemblage zones, Beaufort Group, South Africa: Correlative implications. *Bouncil for Geoscience Research South Africa Bulletin,* 136**,** 1-27.

BENDER, P. A. & HANCOX, P. J. 2004. Newly discovered fish faunas from the Early Triassic, Karoo Basin, South Africa, and their correlative implications. *Gondwana Research,* 7**,** 185-192.

BENTON, M. J. 2010. Studying Function and Behaviour in the Fossil Record. *PloS Biology* 8**,** e1000321.

BINGHAM-KOSLOWSKI, N., GREY, M., EHRMAN, J. M. & PUFAHL, P. 2021. Investigating the relationship between the elemental composition of coprolites and trophic level: A brief digest of late Carboniferous coprolites from the Joggins Formation, Nova Scotia, Canada. *Atlantic Geology,* 57**,** 107-108.

BOLT, J. R. & DEMAR, R. E. 1975. An explanatory model of the evolution of multiple rows of teeth in Captorhinus aguti. . *Journal of Palaeontology,* 49**,** 814–832

BOOS, A. D. S., SCHULTZ, C. L., VEGA, C. S. & AUMOND, J. J. 2013. On the presence of the Late Permian dicynodont *Endothiodon* in Brazil. *Palaeontology,* 56**,** 837-848.

BORDY, E. M., ABRAHAMS, M., SHARMAN, G. R., VIGLIETTI, P. A., BENSON, R. B. J., MCPHEE, B. W., BARRETT, P. M., SCISCIO, L., CONDON, D., MUNDIL, R., RADEMAN, Z., JINNAH, Z., CLARK, J. M., SUAREZ, C. A., CHAPELLE, K. E. J. & CHOINIERE, J. N. 2020. A chronostratigraphic framework for the upper Stormberg Group: Implications for the Triassic-Jurassic boundary in southern Africa. *Earth-Science Reviews***,** 103120.

BOTHA, J., HUTTENLOCKER, A. K., SMITH, R. M. H., PREVEC, R., VIGLIETTI, P. & MODESTO, S. P. 2020. New geochemical and palaeontological data from the Permian-Triassic boundary in the South African Karoo Basin test the synchronicity of terrestrial and marine extinctions. *Palaeogeography, Palaeoclimatology, Palaeoecology,* 540.

BRAMBLE, K., LEBLANC, A. R. H., LAMOUREUX, D. O., WOSIK, M. & CURRIE, P. J. 2017. Histological evidence for a dynamic dental battery in hadrosaurid dinosaurs. . *Scientific Reports,* 7**,** 1-3.

BRANSON, E. B. 1914. The Devonian fishes of Missouri. *The University of Missouri Bulletin,,* 2**,** 59-74.

BRIGGS, D. E. G., LIU, H. P., MCKAY, R. M. & WITZKE, B. J. 2015. Bivalved arthropods from the Middle Ordovician Winneshiek Lagerstätte, Iowa, USA. *Journal of Paleontology,* 89**,** 991-1006.

BUCKLAND, W. 1829. On the Discovery of Coprolites, or Fossil Faeces, in the Lias at Lyme Regis, and in other Formations. *Transactions of the Geological Society of London,* 2**,** 223-238.

BUCKLAND, W. 1836. *Geology and mineralogy considered with reference to natural theology. The Bridgewater Treatises on the power, wisdom and goodness of God as manifested in the Creation,* London, Pickering.

BURTIN, F.-X. 1784. *Oryctographie de Bruxelles ou Déscription des fossiles tant naturels qu'accidentels découverts jusqu'à ce jour dans les environs de cette ville. ,* Bruxelles.

CANTRELL, A. K., SUAZO, T. L., SPIELMANN, J. A. & LUCAS, S. G. 2012. Vertebrate coprolites from the Lower Permian (middle Wolfcampian) Gallina Well locality, Joyita Hills, Socorro County, New Mexico. *New Mexico Museum of Natural History and Science Bulletin,* 57**,** 197-202.

CASTER, K. E. & KJELLESYIG-WAERING, E. N. 1964. Upper Ordovician eurypterids from Ohio. *Palaeontographica Americana,* 4**,** 297-358.

CATUNEANU, O., HANCOX, P. J. & RUBIDGE, B. S. 1998. Reciprocal flexural behaviour and contrasting stratigraphies: A new basin development model for the Karoo retroarc foreland system, South Africa. *Basin Research,* 10**,** 417–439.

CATUNEANU, O., WOPFNER, H., ERIKSSON, P. G., CAIRNCROSS, B., RUBIDGE, B. S., SMITH, R. M. H. & HANCOX, P. J. 2005. The Karoo basins of south-central Africa. *Journal of African Earth Sciences,* 43**,** 211-253.

CHIN, K. 2002. Analyses of coprolites produced by carnivorous vertebrates. *The Paleontological Society Papers,* 8**,** 43-50.

CHIN, K. 2007. Thin section analysis of lithified coprolites (fossil feces). *Microsc Microanalysis,* 13**,** 504-505.

CHIN, K., EBERTH, D. A., SCHWEITZER, M. H., RANDO, T. A., SLOBODA, W. J. & HORNER, J. R. 2003. Remarkable preservation of undigested muscle tissue within a Late Cretaceous tyrranosaurid coprolite from Alberta, Canada. *PALAIOS,* 18**,** 286-294.

CHIN, K., HARTMAN, J. H. & ROTH, B. 2009. Opportunistic exploitation of dinosaur dung: fossil snails in coprolites from the Upper Cretaceous Two Medicine Formation of Montana. *Lethaia,* 42**,** 185-198.

CHIN, K. & KIRKLAND, J. L. 1998. Probable herbivore coprolites from the Upper Jurassic Mygatt-Moore Quarry, Western Colorado. *Modern Geology,* 23**,** 249-275.

CHIPMAN, M., GREY, M. & PUFAHL, P. K. 2020. Coprolites from a brackish ecosystem in the Pennsylvanian Joggins Formation, Nova Scotia, Canada and their palaeoecological implications. *Palaeogeography, Palaeoclimatology, Palaeoecology,* 538.

CONWAY MORRIS, S. & ROBISON, R. A. 1986. Middle Cambrian priapulids and other softbodied fossils from Utah and Spain. *The University of Kansas Paleontological Contributions,* Paper 117**,** 22.

COX, L. R. 1932. Lamellibranchia from the Karroo Beds of the Ruhuhu Coalfields, Tanganyika Territory. *Quarterly Journal of the Geological Society of London,* 88**,** 623-633.

COX, L. R. 1969. General features of Bivalvia. . *In:* MOORE, R. C. (ed.) *Treatise on invertebrate paleontology.* Lawrence: Geological Society of America and University of Kansas Press.

CUEILLE, M., GREEN, E., DUFFIN, C. J., HILDEBRANDT, C. & BENTON, M. J. 2020. Fish and crab coprolites from the latest Triassic of the UK: From Buckland to the Mesozoic Marine Revolution. *Proceedings of the Geologists' Association*.

DAMIANI, R. J. & WELMAN, J. 2001. A long-snouted trematosaurid amphibian from the Early Triassic of South Africa. *South African Journal of Science,* 97**,** 318-319.

DAY, M. O., RAMEZANI, J., BOWRING, S. A., SADLER, P. M., ERWIN, D. H., ABDALA, F. & RUBIDGE, B. S. 2015. When and how did the terrestrial mid-Permian mass extinction occur. Evidence from the tetrapod record of the Karoo Basin, South Africa. . *Proceedings of the Royal Society B: Biological Sciences,* 282**,** 20150834.

DE RICQLES, A. & BOLT, J. R. 1983. Jaw growth and tooth replacement in Captorhinus aguti (Reptilia: Captorhinomorpha): A morphological and histological analysis. *Journal of Vertabrate Paleontology,* 3**,** 7–24.

DENTZIEN-DIAS, P., CARRILLO-BRICEÑO, J. D., FRANCISCHINI, H. & SÁNCHEZ, R. 2018. Paleoecological and taphonomical aspects of the Late Miocene vertebrate coprolites (Urumaco Formation) of Venezuela. *Palaeogeography, Palaeoclimatology, Palaeoecology,* 490**,** 590-603.

DENTZIEN-DIAS, P., HUNT, A. P., LUCAS, S. G., FRANCISCHINI, H. & GULOTTA, M. 2020. Coprolites from shallow marine deposits of the Nanjemoy Formation, Lower Eocene of Virginia, USA. *Lethaia*.

DENTZIEN-DIAS, P., HUNT, A. P., LUCAS, S. G., FRANCISCHINI, H. & GULOTTA, M. 2021. Coprolites from shallow marine deposits of the Nanjemoy Formation, Lower Eocene of Virginia, USA. *Lethaia,* 54**,** 26-39.

DENTZIEN-DIAS, P., POINAR, G. & FRANCISCHINI, H. 2017. A new actinomycete from a Guadalupian vertebrate coprolite from Brazil. *Historical Biology,* 29**,** 770-776.

DENTZIEN-DIAS, P. C., DE FIGUEIREDO, A. E. Q., HORN, B., CISNEROS, J. C. & SCHULTZ, C. L. 2012. Paleobiology of a unique vertebrate coprolites concentration from Rio do Rasto Formation (Middle/Upper Permian), Paraná Basin, Brazil. *Journal of South American Earth Sciences,* 40**,** 53-62.

DENTZIEN-DIAS, P. C., POINAR, G., JR., DE FIGUEIREDO, A. E. Q., PACHECO, A. C. L., HORN, B. L. D. & SCHULTZ, C. L. 2013. Tapeworm Eggs in a 270 Million-Year-Old Shark Coprolite. *PLOS One,* 8**,** e55007.

DEXTER, E., ROLLWAGEN-BOLLENS, G. & BOLLENS, S. M. 2018. The trouble with stress: A flexible method for the evaluation of nonmetric multidimensional scaling. *Limnology and Oceanography: Methods,* 16**,** 434-443.

DIEDRICH, C. G. 2009. A coelacanthid-rich site at Hasbergen (NW Germany): Taphonomy and palaeoenvironment of a first systematic excavation in the Kupferschiefer (Upper Permian, Lopingian). *Palaeobiodiversity and Palaeoenvironments,* 89**,** 67–94.

DIXEY, F. 1937. The geology of part of the upper Luangwa Valley, north-eastern Rhodesia. *Quaterly Journal of the Geological Society* 93**,** 52–76.

DUFFIN, C. J. 2010. Coprolites. *In:* LORD, A. R. & DAVIS, P. G. (eds.) *Fossils from the Lower Lias of the Dorset Coast: Palaeontological Association.* Field Guides to Fossils.

DUFFIN, C. J. 2012. The earliest published records of coprolites. *New Mexico Museum of Natural History and Science Bulletin,* 57**,** 25-28.

DUFFIN, C. J. & WARD, D. J. 2020. Coprolites in an Early Carboniferous microvertebrate fauna from Dervyshire, UK. *Neues Jahrbuch für Geologie und Paläontologie,* 297**,** 1-10.

DUNCAN, R. A., HOOPER, P. R., REHACEK, J., MARSH, J. S. & DUNCAN, A. R. 1997. The timing and duration of the Karoo igneous event, southern Gondwana. *Journal of Geophysical Research: Solid Earth,* 102**,** 18127-18138.

EDMUND, A. G. 1960. Tooth replacement phenomena in the lower vertebrates. *Life Sciences Museum Royal Ontario Museum Contributions,* 52**,** 1-190.

EDMUND, A. G. 1969. Dentition. *In:* GANS, C., BELLAIRS, A. A. & PARSONS, T. S. (eds.) *Biology of the Reptilia.* London: Academic Press.

ERIKSSON, M. E., LINDGREN, J., CHIN, K. & MÅNSBY, U. 2011. Coprolite morphotypes from the Upper Cretaceous of Sweden: novel views on an ancient ecosystem and implications for coprolite taphonomy. *Lethaia,* 44**,** 455-468.

FIKÁČEK, M., BEUTEL, R. G., CAI, C., LAWRENCE, J. F., NEWTON, A. F., SOLODOVNIKOV, A., ŚLIPIŃSKI, A., THAYER, M. K. & YAMAMOTO, S. 2019. Reliable placement of beetle fossils via phylogenetic analyses – Triassic Leehermania as a case study (Staphylinidae or Myxophaga?). *Systematic Entomology,* 45**,** 175-187.

FIORELLI, L. E., EZCURRA, M. D., HECHENLEITNER, E. M., ARGANARAZ, E., TABORDA, J. R., TROTTEYN, M. J., VON BACZKO, M. B. & DESOJO, J. B. 2013. The oldest known communal latrines provide evidence of gregarism in Triassic megaherbivores. *Sci Rep,* 3**,** 3348.

FRANCISCHINI, H., PAES NETO, V. D., MARTINELLI, A. G., PEREIRA, V. P., MARINHO, T. S., TEIXEIRA, V. P. A., FERRAZ, M. L. F., SOARES, M. B. & SCHULTZ, C. L. 2016. Invertebrate traces in pseudo–coprolites from the upper Cretaceous Marília Formation (Bauru Group), Minas Gerais State, Brazil. *Cretaceous Research,* 57**,** 29-39.

FRÖBISCH, J. 2013. Vertebrate diversity across the end-Permian mass extinction — Separating biological and geological signals. *Palaeogeography, Palaeoclimatology, Palaeoecology,* 372**,** 50-61.

GASTALDO, R. A., KAMO, S. L., NEVELING, J., GEISSMAN, J., LOOY, C. V. & MARTINI, A. M. 2020. The base of the Lystrosaurus Assemblage Zone, Karoo Basin, predates the end-Permian marine extinction. *Nature Communications,* 11**,** 1428.

GASTALDO, R. A., KAMO, S. L., NEVELING, J., GEISSMAN, J. W., BAMFORD, M. & LOOY, C. V. 2015. Is the vertebrate-defined Permian-Triassic boundary in the Karoo Basin, South Africa, the terrestrial expression of the end-Permian marine event? *Geology,* 43**,** 939-942.

GAUDY, A. 1887. L'Actinodon. *Mémoire extrait des Nouvelles Archives du Muséum National d'Histoire naturelle,* v. 10 (Serie 2)**,** 30.

GILMORE, B. 1992. Scroll coprolites from the Silurian of Ireland and the feeding of early vertebrates *Palaeontology,* 35**,** 319-333.

GILPIN, E. 1886. The Geology of Cape Breton Island, Nova Scotia. *Quarterly Journal of the Geological Society,* 42**,** 515-526.

GOOD, S. C. 1989. Nonmarine Mollusca in the Upper Triassic Chinle Formation and related strata of the Western Interior. *In:* LUCAS, S. G. & HUNT, A. P. (eds.) *Dawn of the Age of Dinosaurs in the American Southwest.* Albuquerque: New Mexico Museum of Natural History.

HANCOX, P. J. 1998a. *A stratigraphic, sedimentological and palaeoenvironmental synthesis of the Beaufort-Molteno contact, in the Karoo Basin. .* Philosophiae Doctor in the Faculty of Science, University of the Witwatersrand.

HANCOX, P. J. 1998b. *A stratigraphic, sedimentological and paleoenvironmental synthesis of the Beaufort-Molteno contact in the Karoo basin.* Ph.D., University of the Witwatersrand.

HANCOX, P. J., NEVELING, J. & RUBIDGE, B. S. 2020. Biostratigraphy of the Cynognathus Assemblage Zone (Beaufort Group, Karoo Supergroup), South Africa. *South African Journal of Geology,* 123**,** 217-238.

HANCOX, P. J. & RUBIDGE, B. S. 1997. The role of fossils in interpreting the development of the Karoo Basin. *Palaeontologia africana,* 33**,** 41-54.

HANCOX, P. J. & RUBIDGE, B. S. 2001. Breakthroughs in the biodiversity, biogeography, biostratigraphy, and basin analysis of the Beaufort group. *Journal of African Earth Sciences,* 33**,** 563-577.

HANCOX, P. J., SHISHKIN, M. A., RUBIDGE, B. S. & KITCHING, J. W. 1995. A threefold subdivision of the *Cynognathus* Assemblage Zone (Beaufort Group, South Africa) and its palaeogeographical implications. . *South African Journal of Science,* 91**,** 143-144.

HANSEN, B. B., MILÀN, J., CLEMMENSEN, L. B., ADOLFSSEN, J. S., ESTRUP, E. J., KLEIN, N., MATEUS, O. & WINGS, O. 2016. Coprolites from the Late Triassic Kap Stewart Formation, Jameson Land, East Greenland: morphology, classification and prey inclusions. *Geological Society, London, Special Publications,* 434**,** 49-69.

HAUTMANNA, M., SMITH, A. B., MCGOWAN, A. J. & BUCHER, H. 2013. Bivalves from the Olenekian (Early Triassic) of southwestern Utah: Systematics and evolutionary significance. Journal of Systematic Palaeontology. *Journal ofSystematic Palaeontology,* 11**,** 263-293.

HAWKINS, A. D., LIU, H. P., BRIGGS, D. E. G., MUSCENTE, A. D., MCKAY, R. M., WITZKE, B. J. & XIAO, S. 2018. Taphonomy and Biological Affinity of Three-Dimensionally Phosphatized Bromalites from the Middle Ordovician Winneshiek LagerstÄtte, Northeastern Iowa, USA. *Palaios,* 33**,** 1-15.

HECKERT, A. B. 2004. Late Triassic microvertebrates from the Lower Chinle Group (Otischalkian-Adamanian: Carnian), southwestern U.S.A. *New Mexico Museum of Natural History and Science Bulletin,* 27**,** 1-170.

HOLLOCHER, K. & HOLLOCHER, T. C. 2012. Early processes in the fossilization of terrestrial feces to coprolites, and microstructure preservation. *New Mexico Museum of Natural History and Science Bulletin,* 57**,** 79-92.

HOLLOCHER, T. C., CHIN, K., HOLLOCHER, K. T. & KRUGE, M. A. 2001. Bacterial residues in coprolite of herbivorous dinosaurs: role of bacteria in mineralization of feces. *Palaios,* 16**,** 547–565.

HORNER, J. R., WEISHAMPEL, D. B. & FORSTER, C. A. 2004. Hadrosauridae. *In:* WEISHAMPEL, D. B., DODSON, P. & OSMÓLSKA, H. (eds.) *The Dinosauria, Second Edition.* Berkeley: University of California Press.

HSIEH, S. & PLOTNICK, R. E. 2020. The representation of animal behaviour in the fossil record. *Animal Behaviour,* 169**,** 65-80.

HUNT, A. P. 1992. Late Pennsylvanian coprolites from the Kinney Brick Quarry, central New Mexico, with notes on the classification and utility of coprolites. *New Mexico Bureau of Mines and Mineral Resources Bulletin,* 138**,** 221-229.

HUNT, A. P., CHIN, K. & LOCKLEY, M. G. 1994. The paleobiology of vertebrate coprolites. *In:* DONOVAN, S. K. (ed.) *The Paleobiology of Trace Fossils.* London: John Wiley & Sons.

HUNT, A. P., LOCKLEY, M. G., CONRAD, K. L., PAQUETTE, M. & CHURE, D. J. 1993. Late Triassic vertebrates from the Dinosaur National Monument Area (Utah, USA) with an example of the utility of coprolites for correlation. *New Mexico Museum of Natural History and Science Bulletin,* 3**,** 197-198.

HUNT, A. P. & LUCAS, S. G. 2005a. A new coprolite ichnotaxon from the Early Permian of Texas. *New Mexico Museum of Natural History and Science Bulletin,* 30**,** 121-122.

HUNT, A. P. & LUCAS, S. G. 2005b. The origin of large vertebrate coprolites from the Early Permian of Texas. *New Mexico Museum of Natural History and Science Bulletin,* 30**,** 125-126.

HUNT, A. P. & LUCAS, S. G. 2012. Descriptive terminology of coprolites and recent feces. *New Mexico Museum of Natural History and Science Bulletin,* 57**,** 153-160.

HUNT, A. P. & LUCAS, S. G. 2013. The fossil record of Carboniferous and Permian vertebrate coprolites. *New Mexico Museum of Natural History and Science Bulletin,* 60**,** 121-127.

HUNT, A. P. & LUCAS, S. G. 2017. A new vertebrate coprolite locality from the Late Pennsylvanian of central New Mexico, USA, and the environmental context of Carboniferous bromalites. *New Mexico Museum of Natural History and Science Bulletin* 77**,** 139-150.

HUNT, A. P. & LUCAS, S. G. 2020 Hyena hegemony: Biogeography and taphonomy of Pleistocene vertebrate coprolites with description of a new mammoth coprolite ichnotaxon. *Ichnos,* 27**,** 111-121.

HUNT, A. P. & LUCAS, S. G. 2021. *The ichnology of vertebrate consumption: Dentalites, gastroliths and bromlites*.

HUNT, A. P., LUCAS, S. G. & KLEIN, H. 2018. Late Triassic nonmarine vertebrate and invertebrate trace fossils and the pattern of the Phanerozoic record of vertebrate trace fossils. *In:* TANNER, L. H. (ed.) *The Late Triassic world.* New York: Springer Verlag.

HUNT, A. P., LUCAS, S. G. & LOCKLEY, M. G. 1998. Taxonomy and Stratigraphic and Fades Significance of Vertebrate Coprolites of the Upper Triassic Chinle Group, Western United States. *Ichnos,* 5**,** 225-234.

HUNT, A. P., LUCAS, S. G., MILÀN, J. & SPIELMANN, J. A. 2012a. Vertebrate coprolite studies: Status and prospectus. *New Mexico Museum of Natural History and Science Bulletin,* 57**,** 5-24.

HUNT, A. P., LUCAS, S. G. & SPIELMANN, J. A. 2005a. Biochronology of the Early Permian vertebrate coprolites of the American southwest. *New Mexico Museum of Natural History and Science Bulletin,* 31**,** 43-45.

HUNT, A. P., LUCAS, S. G. & SPIELMANN, J. A. 2005b. Early Permian vertebrate coprolites from the North-Central New Mexico with descriptions of a new ichnogenus. *New Mexico Museum of Natural History and Science Bulletin,* 31**,** 39-42.

HUNT, A. P., LUCAS, S. G. & SPIELMANN, J. A. 2012b. The bromalite collection at the National Museum of Natural History (Smithsonian Institution), with the descriptions of new inchnotaxa and notes on other significant coprolite collections. *New Mexico Museum of Natural History and Science Bulletin,* 57**,** 105-114.

HUNT, A. P., LUCAS, S. G. & SPIELMANN, J. A. 2012c. New coprolite ichnotaxa from the Buckland Collection at the Oxford University Museum of Natural History. *New Mexico Museum of Natural History and Science Bulletin,* 57**,** 115-124.

HUNT, A. P., LUCAS, S. G. & SPIELMANN, J. A. 2012d. The vertebrate coprolite collection at the Natural History Museum (London). *New Mexico Museum of Natural History and Science Bulletin,* 57**,** 125-130.

HUNT, A. P., LUCAS, S. G. & SPIELMANN, J. A. 2013a. A large heteropolar coprolite from the early Permian of New Mexico. *New Mexico Museum of Natural History and Science,* Bulletin 59**,** 327-329.

HUNT, A. P., LUCAS, S. G. & SPIELMANN, J. A. 2013b. Triassic vertebrate coprolite ichnofaunas. *New Mexico Museum of Natural History and Science Bulletin,* 61**,** 237-258.

HUNT, A. P., LUCAS, S. G., SPIELMANN, J. A., CANTRELL, A. K. & SUAZO, T. L. 2012e. A new marine coprofauna from the Beeman Formation (Late

Pennsylvanian: Late Missourian), Sacremento Mountains, New Mexico, USA. *New Mexico Museum of Natural History and Science Bulletin,* 57**,** 193-196.

HUNT, A. P., LUCAS, S. G., SPIELMANN, J. A., CANTRELL, A. K., SUAZO, T. L. & LERNER, A. J. 2012f. Bromalites from the Tinajas Lagerstätte (Late Pennsylvanian: Late Missourian), Central New Mexico, USA. *New Mexico Museum of Natural History and Science Bulletin,* 57**,** 175-184.

HUNT, A. P., LUCAS, S. G., SPIELMANN, J. A. & LERNER, A. J. 2007. A review of vertebrate coprolites of the Triassic with descriptions of new Mesozoic ichnotaxa. *New Mexico Museum of Natural History and Science Bulletin,* 41**,** 88-107.

HUNT, A. P., LUCAS, S. G., SPIELMANN, J. A. & LOCKLEY, M. G. 2012g. Bromalites from the Mississippian Bear Gulch Lagerstätte of Central Montana, USA. *New Mexico Museum of Natural History and Science Bulletin,* 57**,** 171-174.

HUNT, A. P., LUCAS, S. G., SPIELMANN, J. A., SUAZO, T. L. & CANTRELL, A. K. 2012h. A re-evaluation of Late Pennsylvanian bromalites from the Kinney Brick Quarry Lagerstätte, New Mexico, USA. *New Mexico Museum of Natural History and Science Bulletin,* 57**,** 185-192.

HUNT, A. P., SANTUCCI, V. L., TWEET, J. S. & LUCAS, S. G. 2012i. Vertebrate coprolites and other bromalites in National Park Service areas. *New Mexico Museum of Natural History and Science Bulletin,* 57**,** 343-354.

IRMIS, R. B. & WHITESIDE, J. H. 2012. Delayed recovery of non-marine tetrapods after the end-Permian mass extinction tracks global carbon cycle. *Proc Biol Sci,* 279**,** 1310-8.

IRMIS, R. B., WHITESIDE, J. H. & KAMMERER, C. F. 2013. Non-biotic controls of observed diversity in the paleontologic record: An example from the Permo-Triassic Karoo Basin of South Africa. *Palaeogeography, Palaeoclimatology, Palaeoecology,* 372**,** 62-77.

JOHNSON, J. H. 1934. A coprolite horizon in the Pennsylvanian of Chafee and Park Counties, Colorado. *Journal of Paleontology,* 8**,** 477-479.

JOHNSON, M. R. 1991. Sandstone petrography, provenance and plate tectonic setting in Gondwana of the south-eastern Cape Karoo Basin. *South African Journal of Geology,* 94**,** 137-154.

KEYSER, A. W. & SMITH, R. M. H. 1978. Vertebrate biozonation of the Beaufort Group with special reference to the Western Karoo Basin. *Ann. Geol. Survey S. Afr. ,* 12**,** 1-36.

KIREJTSHUK, A. G., POSCHMANN, M., PROKOP, J., GARROUSTE, R. & NEL, A. 2014. Evolution of the elytral venation and structural adaptations in the oldest

Palaeozoic beetles (Insecta: Coleoptera: Tshekardocoleidae). *Journal of Systematic Palaeontology,* 12**,** 575-600.

KITCHING, J. W. 1977. The distribution of the Karroo vertebrate fauna: with special reference to certain genera and the bearing of this distribution on the zoning of the Beaufort Beds. *Memoir Bernard Price Institute Palaeontological Research,* 1**,** 131.

KNAUST, D. 2020. Invertebrate coprolites and cololites revised *Papers in Palaeontology,* 6**,** 385-423.

KONDO, Y. & SANO, S.-I. 2009. Origination of extant heteroconch families: ecological and environmental patterns in post-Paleozoic bivalve diversification. *Paleontological Research* 13**,** 39–44.

KRISHNASWAMY, R., FUGITT, F. L. & KIDDER, D. L. 1994. Spiral phosphatic coprolites from the Pennsylvanian of southeastern Ohio. *Geological Society of America, Abstracts with Programs,* 26**,** 27.

KRZYKAWSKI, T., SZOPA, K., BRACHANIEC, T. & SALAMON, M. A. 2014. Carboniferous coprolite in the siderite concretion from Sosnowiec-Zagórze Lagerstätte, Poland – preliminary data *Paläontologie, Stratigraphie, Fazies* 22**,** 101-107.

KÜHL, G., BARTELS, C., BRIGGS, D. E. G. & RUST, J. 2012. *Visions of a vanished world: The extraordinary fossils of the Hunsrück Slate,* New Haven, Yale University Press.

LAOJUMPON, C., MATKHAMMEE, T., WATHANAPITAKSAKUL, A., SUTEETHORN, V., SUTEETHORN, S., LAUPRASERT, K., SRISUK, P. & LE LOEUFF, J. 2012. Preliminary report of coprolites from the Late Triassic of Thailand. *New Mexico Museum of Natural History and Science Bulletin,* 57**,** 207-214.

LEBLANC, A. R. H., BRINK, K. S., CULLEN, T. M. & REISZ, R. R. 2017. Evolutionary implications of tooth attachment versus tooth implantation: A case study using dinosaur, crocodilian, and mammal teeth. *Journal of Vertebrate Paleontology***,** e1354006.

LEBLANC, A. R. H. & REISZ, R. R. 2015. Patterns of tooth development and replacement in captorhinid reptiles: a comparative approach for understanding the origin of multiple tooth rows. *Journal of Vertebrate Paleontology***,** e919928.

LEBLANC, A. R. H., REISZ, R. R., BRINK, K. S. & ABDALA, F. 2016a. Mineralized periodontia in extinct relatives of mammals shed light on the evolutionary history of mineral homeostasis in periodontal tissue maintenance. . *Journal of Clinical Periodontology,* 43**,** 323–332.

LEBLANC, A. R. H., REISZ, R. R., EVANS, D. C. & BAILLEUL, A. M. 2016b. Ontogeny reveals function and evolution of the hadrosaurid dinosaur dental battery. *BMC Evolutionary Biology,* 16**,** 152.

LIU, H. P., BERGSTRÖM, S. M., WITZKE, B. J., BRIGGS, D. E. G., MCKAY, R. M. & FERRETTI, A. 2017. Exceptionally preserved conodont apparatuses with giant elements from the Middle Ordovician Winneshiek Konservat-Lagerstätte, Iowa, USA. *Journal of Paleontology,* 91**,** 493-511.

LOMAX, D. R., ROBINSON, P., CLEAL, C. J., BOWDEN, A. & LARKIN, N. R. 2016. Exceptional preservation of Upper Carboniferous (lower Westphalian) fossils from Edlington, Doncaster, South Yorkshire, UK. *Geological Journal,* 51**,** 42-50.

LUO, M., SHI, G. R., CHEN, Z.-Q., HU, S., HUANG, J., ZHANG, Q., ZHOU, C. & FANG, Y. 2018. Youngest ambient inclusion trails from Middle Triassic phosphatized coprolites, southwestern China: New insights into an old intriguing phenomenon. *Gondwana Research,* 55**,** 60-73.

MACUNGO, Z., LOIDE, I., ZUNGUZA, S., NHAMUTOLE, N., MAHARAJ, I. E. M., MUGABE, J., ANGIELCZYK, K. D. & ARAÚJO, R. 2020. Endothiodon (Therapsida, Anomodontia) specimens from the middle/late permian of the Metangula Graben (Niassa Province, Mozambique) increase complexity to the taxonomy of the genus. *Journal of African Earth Sciences,* 163.

MAISEY, J. G. & MELO, J. H. G., 2005, SOME MIDDLE DEVONIAN (EIFELIAN–GIVETIAN) FOSSIL FISH REMAINS FROM THE PIMENTEIRA FORMATION OF THE PARNAÍBA BASIN, NORTHEAST BRAZIL: ARQUIVOS DO MUSEU NACIONAL, V. 63, P. P. 495-505. 2005. Some Middle Devonian (Eifelian–Givetian) fossil fish remains from the Pimenteira Formation of the Parnaíba Basin, northeast Brazil. *Arquivos do Museu Nacional,* 63**,** 495-505.

MANSKY, C. F., LUCAS, S. G., SPIELMANN, J. A. & HUNT, A. P. 2012. Mississippian bromulites from the Blue Beach, Nova Scotia, Canada. *New Mexico Museum of Natural History and Science Bulletin,* 57**,** 161-170.

MANTELL, G. A. 1822. *The fossils of the South Downs; or Illustrations of the geology of Sussex.,* London.

MCALLISTER, J. A. 1985 Reevalution of the formation of spiral coprolites. *The University of Kansas Paleontological Contributions,* 114 1-12.

MCALLISTER, J. A. 1988. Preliminary description of the coprolitic remains from Hamilton Quarry, Kansas. *In:* MAPES, G. & MAPES, R. H. (eds.) *Regional geology and paleontology of Upper Paleozoic Hamilton Quarry area.* Kansas Geological Survey.

MCALLISTER, J. A. 1996. Coprolites. *In:* SCHULTZE, H.-P. & CLOUTIER, R. (eds.) *Devonian fishes and plants of Miguasha, Quebec, Canada.* München: Verlag Dr Friedrich Pfeil.

MILÀN, J., RASMUSSEN, E. S. & DYBKJÆR, K. 2018. A crocodilian coprolite from the lower Oligocene Viborg Formation of Sofienlund Lergrav, Denmark. *Bulletin of the Geological Society of Denmark,* 66**,** 181-187.

MONDAL, S. 2017. A short review of phanerozoic taxonomic and ecologic diversity of bivalves. *Indian Journal of Geology,* 86-87**,** 19-34.

MONTGOMERY, C. 2019. *Early Triassic Coprolite Morphotypes from the Burgersdorp Formation (Tarkastad Subgroup, Beaufort Group) of South Africa.* Unpublished MSc Thesis, University of the Witwatersrand.

MURCHISON, R. I. 1867. *Siluria (Fourth Edition),* London, John Murray.

NEVELING, J. 2002. *Biostratigraphic and sedimentological investigation of the contact between the Lystrosaurus and Cynognathus Assemblage Zones (Beaufort Group: Karoo Supergroup).* Unpublished PhD thesis, University of the Witwatersrand,.

NEVELING, J. 2004. Stratigraphic and sedimentological investigation of the contact between the Lystrosaurus and the Cynognathus Assemblage Zones (Beaufort Group: Karoo Supergroup). *Council for Geoscience Bulletin,* 137**,** 1-165.

NEVELING, J., HANCOX, P. J. & RUBIDGE, B. S. 2005. Biostratigraphy of the lower Burgersdorp Formation (Beaufort Group; Karoo Supergroup) of South Africa – implications for the stratigraphic ranges of the early Triassic tetrapods. *Palaeontologica Africana,* 41**,** 81-87.

NEWMAN, M. & DAVIDSON, R. Early Devonian fish from the Midland Valley of Scotland. IPC3 Pre-Conference Field Trip, 2010 Aberdeen, University of Aberdeen. 38.

NICOLAS, M. & RUBIDGE, B. S. 2010. Changes in Permo-Triassic terrestrial tetrapod ecological representation in the Beaufort Group (Karoo Supergroup) of South Africa. *Lethaia,* 43**,** 45-59.

NIEDŹWIEDZKI, G., BAJDEK, P., OWOCKI, K. & KEAR, B. P. 2016a. An Early Triassic polar predator ecosystem revealed by vertebrate coprolites from the Bulgo Sandstone (Sydney Basin) of southeastern Australia. *Palaeogeography, Palaeoclimatology, Palaeoecology,* 464**,** 5-15.

NIEDŹWIEDZKI, G., BAJDEK, P., QVARNSTRÖM, M., SULEJ, T., SENNIKOV, A. G. & GOLUBEV, V. K. 2016b. Reduction of vertebrate coprolite diversity associated with the end-Permian extinction event in Vyazniki region, European Russia. *Palaeogeography, Palaeoclimatology, Palaeoecology,* 450**,** 77-90.

NORTHWOOD, C. 1997. *Palaeontological interpretations of the Early Triassic fossil Arcadia Formation, Queensland. .* Doctors' in Philosophy, La Trode University.

NORTHWOOD, C. 2005. Early Triassic coprolites from Australia and their palaeobiological significance. *Palaeontology* 48**,** 49-68.

OLROYD, S. L., LEBLANC, A. R. H., ARAUJO, R., ANGIELCZYK, K. D., DUHAMEL, A., BENOIT, J. & AMARAL, M. 2021. Histology and muCT reveal the unique evolution and development of multiple tooth rows in the synapsid Endothiodon. *Sci Rep,* 11**,** 16875.

OLSON, E. C. 1962. Late Permian Terrestrial Vertebrates, U. S. A. and U. S. S. R. . *Transactions of the American Philosophical Society,* 52**,** 1-224.

OLSON, E. C. 1965. Relationships of *Seymouria*, *Diadectes*, and *Chelonia*. *American Zoologist,* 5**,** 295-307.

OWOCKI, K., NIEDZWIEDZKI, G., SENNIKOV, A. G., GOLUBEV, V. K., JANISZEWSKA, K. & SULEJ, T. 2012. Upper Permian Vertebrate Coprolites from Vyazniki and Gorokhovets, Vyatkian Regional Stage, Russian Platform. *Palaios,* 27**,** 867-877.

PAN, Y. H., HU, S. X., SHA, J. G., ZHANG, Q. Y., WANG, Y. Q., ZHOU, C. Y., WEN, W., HUANG, J. Y. & XIE, T. 2014. Early Triassic bivalves from the Feixianguan Formation in Xingyi, Guizhou and the Ximatang Formation in Qiubei, Yunnan (southern China). *Palaeoworld,* 23**,** 143-154.

PONOMARENKO, A. G. & MOSTOVSKI, M. B. 2005. New beetles (Insecta: Coleoptera) from the Late Permian of South Africa. *African Invertebrates,* 46**,** 253-260.

PRICE, P. H. 1927. The coprolite horizon of the Conemaugh Series in and around Morgantown, West Virginia. *Annals of the Carnegie Museum,* 17**,** 211-254.

QVARNSTRÖM, M., AHLBERG, P. E. & NIEDŹWIEDZKI, G. 2019a. Tyrannosaurid-like osteophagy by a Triassic archosaur. *Scientific Reports,* 9**,** 925.

QVARNSTRÖM, M., ANAGNOSTAKIS, S., LINDSKOG, A., SCHEER, U., VAJDA, V., RASMUSSEN, B. W., LINDGREN, J. & ERIKSSON, M. E. 2019b. Multi-proxy analyses of Late Cretaceous coprolites from Germany. *Lethaia,* 52**,** 550-569.

QVARNSTRÖM, M., FIKÁČEK, M., VIKBERG WERNSTRÖM, J., HULD, S., BEUTEL, R. G., ARRIAGA-VARELA, E., AHLBERG, P. E. & NIEDŹWIEDZKI, G. 2021. Exceptionally preserved beetles in a Triassic coprolite of putative dinosauriform origin. *Current Biology*.

QVARNSTRÖM, M., NIEDŹWIEDZKI, G., TAFFOREAU, P., ŽIGAITĖ, Ž. & AHLBERG, P. E. 2017. Synchrotron phase-contrast microtomography of coprolites generates novel palaeobiological data. *Scientific Reports,* 7**,** 2723.

QVARNSTRÖM, M., NIEDŹWIEDZKI, G. & ŽIGAITĖ, Ž. 2016. Vertebrate coprolites (fossil faeces): An underexplored Konservat-Lagerstätte. *Earth-Science Reviews,* 162**,** 44-57.

QVARNSTRÖM, M., SZREK, P., AHLBERG, P. E. & NIEDŹWIEDZKI, G. 2018. Non-marine palaeoenvironment associated to the earliest tetrapod tracks. *Scientific Reports,* 8**,** 1074.

QVARNSTRÖM, M., WERNSTROM, J. V., PIECHOWSKI, R., TALANDA, M., AHLBERG, P. E. & NIEDZWIEDZKI, G. 2019c. Beetle-bearing coprolites possibly reveal the diet of a Late Triassic dinosauriform. *R Soc Open Sci,* 6**,** 181042.

RAKSHIT, N., BHAT, M. S., MUKHERJEE, D., RAY, S. & CAVIN, L. 2019. First record of Mesozoic scroll coprolites: classification, characteristics, elemental composition and probable producers. *Palaeontology,* 62**,** 451-471.

RAKSHIT, N. & RAY, S. 2021. Mortality dynamics and fossilisation pathways of a new metoposaurid-dominated multitaxic bonebed from India: a window into the Late Triassic vertebrate palaeoecosystem. *Historical Biology,* in press**,** 1-23.

RAMETTE, A. 2007. Multivariate analyses in microbial ecology. *FEMS Microbiology Ecology,* 62**,** 142–160.

RAYNER, D. H. 1963. The Achanarras Limestone of the Middle Old Red Sandstone, Caithness, Scotland. *Proceedings of the Yorkshire Geological Society,* 34**,** 117-138.

RODRIGUES, M. I. C., DA SILVA, J. H., SANTOS, F. E. P., DENTZIEN-DIAS, P., CISNEROS, J. C., DE MENEZES, A. S., FREIRE, P. T. C. & VIANA, B. C. 2018. Physicochemical analysis of Permian coprolites from Brazil. *Spectrochim Acta A Mol Biomol Spectrosc,* 189**,** 93-99.

RODRIGUEZ-DE LA ROSA, R. A., VEVALLOS-FERRIZ, S. R. S. & SILVA-PINEDA, A. 1998. Paleobiological implications of Campanian coprolites. *Palaeogeography, Palaeoclimatology, Palaeoecology,* 142**,** 231-254.

ROLFE, W. D. I. 1973. Excursion 15: Silurian arthropod and fish assemblages from Lesmahagow, Lanarkshire *In:* BLUCK, B. J. (ed.) *Excursion guide to the geology of the Glasgow District.* Glasgow: Geological Society of Glasgow,.

ROMER, A. S. 1956. *Osteology of the reptiles,* Chicago, University of Chicago Press.

ROMER, A. S. 1966. *Vertebrate paleontology,* Chicago, University of Chicago Press.

RUBIDGE, B. S., ERWIN, D. H., RAMEZANI, J., BOWRING, S. A. & DE KLERK, W. J. 2013. High-precision temporal calibration of Late Permian vertebrate biostratigraphy: U-Pb zircon constraints from the Karoo Supergroup, South Africa. *Geology,* 41**,** 363-366.

RUBIDGE, B. S., JOHNSON, M. R., KITCHING, J. W., SMITH, R. M. H., KEYSER, A. W. & GROENEWALD, G. H. 1995. An introduction to the biozonation of the Beaufort Group. *In:* RUBIDGE, B. S. (ed.) *Biostratigraphy of the Beaufort Group (Karoo Supergroup).* South African Committee for Stratigraphy Biostratigraphic Series, 1.

RUMMY, P., HALACLAR, K. & CHEN, H. 2021. The first record of exceptionally-preserved spiral coprolites from the Tsagan-Tsab Formation (Lower Cretaceous), Tatal, western Mongolia. *Scientific Reports,* 11**,** 7891.

SCHWANKE, C. & SOUTO, P. R. D. F. 2007. Coprólitos espiralados da Formação Pedra do Fogo, Bacia do Parnaíba. *In:* CARVALHO, I. S., CASSAB, R. C. T., SCHWANKE, C., CARVALHO, M. A., FERNANDES, A. C. S., RODRIGUES, M. A. C., SARDENBERG, M., ARAI, M. & OLIVEIRA, M. E. Q. (eds.) *Paleontologia: Cenários da vida.* Interciência: Rio de Janeiro.

SEGESDI, M., BOTFALVAI, G., BODOR, E. R., ŐSI, A., BUCZKÓ, K., DALLOS, Z., TOKAI, R. & FÖLDES, T. 2017. First report on vertebrate coprolites from the Upper Cretaceous (Santonian) Csehbánya Formation of Iharkút, Hungary. *Cretaceous Research,* 74**,** 87-99.

SEILACHER, A., MARSHALL, C., SKINNER, H. C. W. & TSUIHIJI, T. 2001. A fresh look at sideritic “coprolites”. *Paleobiology,* 27**,** 7-13.

SELDEN, P. A. 1979. *Functional morphology of Baltoeurypterus.* Doctor of Philosophy University of Cambridge.

SELDEN, P. A. 1984. Autecology of Silurian eurypterids. *Special Papers in Palaeontology,* 32**,** 39-54.

SHABICA, C. W. & GODFREY, S. J. 1997. Coprolites and trace fossils (biogenic structures). *In:* SHABICA, C. W. & HAY, A. A. (eds.) *Richardson’s guide to the fossil fauna of Mazon Creek.* Chicago: Northeastern Illinois University

SHISHKIN, M. A., RUBIDGE, B. S. & HANCOX, P. J. Vertebrate biozonation of the upper Beaufort Series of South Africa – a new look on correlation of the Triassic biotic events in Euramerica and southern Gondwana *In:* SUN, A. & WANG, Y., eds. Sixth Symposium on Mesozoic Terrestrial Ecosystems, Short Papers, 1995 Beijing. China Ocean Press, 250.

SILANTIEV, V. N., SILANTIEV, V. V., S.P., Z. & VYRUCHAEVA, H. Y. 2000a. A new discovery of a phosphatic concretions in the Upper Permian of European Russia. *Otechestvennaya Geologia,* 2000**,** 27–32.

SILANTIEV, V. N., SILANTIEV, V. V., ZUDINA, S. P. & VYRUCHAEVA, H. Y. 2000b. Phosphatic concretions in the Upper Permian of East European platform; in Geology and Mineral Resources of European Russia and Ural. *Proceedings of the Regional Conference, Book 2.* Yekaterinburg.

SMITH, R. & BOTHA, J. 2005. The recovery of terrestrial vertebrate diversity in the South African Karoo Basin after the end-Permian extinction. *Comptes Rendus Palevol,* 4**,** 623-636.

SMITH, R. M. H. 1990. A review of stratigraphy and sedimentary environments in the Karoo Basin of South Africa. *Journal of African Earth Sciences,* 10**,** 117-137.

SMITH, R. M. H. 1995. Changing fluvial environments across the Permian-Triassic boundary in the Karoo Basin, South Africa and possible causes of tetrapod extinctions. . *Palaeogeography, Palaeoclimatology, Palaeoecology,* 117**,** 81-104.

SMITH, R. M. H. & BOTHA-BRINK, J. 2014. Anatomy of a mass extinction: Sedimentological and taphonomic evidence for drought-induced die-offs at the Permo-Triassic boundary in the main Karoo Basin, South Africa. *Palaeogeography, Palaeoclimatology, Palaeoecology,* 396**,** 99-118.

SMITH, R. M. H., RUBIDGE, B. S., DAY, M. O. & BOTHA, J. 2020. Introduction to the tetrapod biozonation of the Karoo Supergroup. *South African Journal of Geology,* 123**,** 131-140.

SMITH, R. M. H. & WARD, P. D. 2001. Pattern of vertebrate extinctions across an event bed at the Permian–Triassic boundary in the Karoo Basin of South Africa. *Geological Society of America,* Bulletin 29**,** 1147–1150.

SOUTO, P. R. D. 2010. Crocodylomorph coprolites from the Bauru basin, Upper Cretaceous, Brazil. *New Mexico Museum of Natural History and Science Bulletin,* 51**,** 201-208.

SOUTO, P. R. F. 2001. Tetrapod coprolites from the Middle Triassic of Southern Brazil. *GAIA,* 16**,** 51-57.

SOUTO, P. R. F. 2007. Os coprólitos da Bacia de São José de Itaboraí. Estado do Rio de Janeiro, Brasil. *In:* AL, I. D. S. C. E. (ed.) *Paleontologia: Cenários da vida.* Rio de Janeiro: Interciência.

SOUTO, P. R. F. 2008. Coprólitos do Brasil. *Principais ocorrências e estudo.* Rio de Janeiro: Publit.

SOUTO, P. R. F. & FERNANDES, M. A. 2015. Fossilized excreta associated to dinosaurs in Brazil. *Journal of South American Earth Sciences,* 57**,** 32–38.

SOUTO, P. R. F. & SCHWANKE, C. 2010. Ocorrência de coprólitos de vertebrados na bacia de Alagoas, Cretáceo Inferior. *Boletim Do Museu Paraense Emílio Goeldi.* Ciências Naturais.

STEWART, I. & NICOLL, R. S. 2003. Multi-element apparatus structure of the Early Ordovician conodont Oepikodus evae Lindström from Australia and Sweden *In:* MAWSON, R. A. T., J. A (ed.) *Contributions to the Second Australian conodont Symposium (AUSCOS II) held in conjunction with Palaeontology*

Down Under 2000. Orange, Australia: Courier Forschungsinstitut Senckenberg.

STRICKLAND, H., E. & HOOKER, J. 1853. On the distribution and organic contents of the “Ludlow Bone Bed” in the Districts of Woolhope and May Hill with a note on the seed-like bodies found in it. *Quarterly Journal of the Geological Society of London,* 9**,** 8-12.

THULBORN, R. A. 1991. Morphology, preservation and palaeobiological significance of dinosaur coprolites. *Palaeogeography, Palaeoclimatology, Palaeoecology,* 83**,** 341-366.

TOLMACHEVA, T. Y. New conodont clusters from the Lower Ordovician of central Kazakhstan. *In:* DZIK, J., ed. Sixth European Conodont Symposium, Abstracts, 1996 Warszawa. Instytut Paleobiologii PAN, 57.

TOLMACHEVA, T. Y. & PURNELL, M. A. 2002. Apparatus composition, growth, and survivorship of the Lower Ordovician conodont *Paracordylus gracilis* Lindström, 1955. *Palaeontology,* 45**,** 209-228.

TREWIN, N. H. 1986. Palaeoecology and sedimentology of the Achanarras fishbed of the Middle Old Red Sandstone, Scotland. *Transactions of the Royal Society of Edinburgh: Earth Sciences,* 77**,** 21-46.

TREWIN, N. H. 2008. *Fossils alive! Or new walks in an old field,* Edinburgh, Dunedin Academic Press.

TURNER, C. E. & PETERSON, F. 1999. Biostratigraphy of dinosaurs in the Upper Jurassic Morrison Formation of the Western Interior, U.S.A. *In:* GILLETTE, D. D. (ed.) *Vertebrate Paleontology in Utah.* Salt Lake City: Utah Geological Survey.

TURNER, S. 1999. The importance of coprolite events. *Ichthyolith Issues,* 20**,** 37-38.

TYLER, C. L. & KOWALEWSKI, M. 2014. Utility of marine benthic associations as a multivariate proxy of paleobathymetry: a direct test from recent coastal ecosystems of North Carolina. *PLoS One,* 9**,** e95711.

VAN EEDEN, O. R. 1972. Geology of the Republic of South Africa-an Explanation of the 1: 1 000 000 Map, 1970 Edition. *Special Publication, Geological Survey of South Africa,* 18**,** 85.

VIGLIETTI, P. A., SMITH, R. M. H., ANGIELCZYK, K. D., KAMMERER, C. F., FRÖBISCH, J. & RUBIDGE, B. S. 2016. The Daptocephalus Assemblage Zone (Lopingian), South Africa: A proposed biostratigraphy based on a new compilation of stratigraphic ranges. *Journal of African Earth Sciences,* 113**,** 153-164.

WAGNER, P. J., KOSNIK, M. A. & LIDGARD, S. 2006. Abundance distributions imply elevated complexity of Post-Paleozoic marine ecosystems. *Science,* 314**,** 1289-1292.

WASMER, M., HAUTMANN, M., HERMANN, E., WARE, D., ROOHI, G., UR-REHMAN, K., YASEEN, A. & BUCHER, H. 2012. Olenekian (Early Triassic) bivalves from the Salt Range and Surghar Range, Pakistan. *Palaeontology,* 55**,** 1043-1073.

WILLIAMS, M. E. 1972. The origins of "spiral coprolites". *The University of Kansas Paleontological Contributions,* 59**,** 1-27.

WOODWARD, J. 1695. *An essay towards a natural history of the earth, and terrestrial bodyes, especially minerals: as also of the sea, rivers, and springs. With an account of the universal deluge: and of the effects that it had upon the earth. ,* London:.

YAN, E. V., BEUTEL, R. G. & LAWRENCE, J. F. 2018. Whirling in the late Permian: ancestral Gyrinidae show early radiation of beetles before Permian-Triassic mass extinction. *BMC Evolutionary Biology,* 18.

YAN, E. V., LAWRENCE, J. F., BEATTIE, R. & BEUTEL, R. G. 2017. At the dawn of the great rise: †Ponomarenkia belmonthensis (Insecta: Coleoptera), a remarkable new Late Permian beetle from the Southern Hemisphere. *Journal of Systematic Palaeontology,* 16**,** 611-619.

YATES, A. M., NEUMANN, F. H. & HANCOX, P. J. 2012. The earliest post-paleozoic freshwater bivalves preserved in coprolites from the karoo basin, South Africa. *PLoS One,* 7**,** e30228.

ZAHER, H. & RIEPPEL, O. 1999. The phylogenetic relationships of *Pachyrhachis problematicus*, and the evolution of limblessness in snakes (Lepidosauria, Squamata). *Comptes Rendus Academie Sciencias Paris Sciences de la terre et des planetes,* 329**,** 831-837.

ZANGERL, R. & RICHARDSON, E. S. 1963. The paleoecological history of two Pennsylvanian black shales. *Fieldiana, Geological Memoirs, ,* 4 352.

ZATOŃ, M., BRODA, K., QVARNSTRÖM, M., NIEDŹWIEDZKI, G. & AHLBERG, P. E. 2017. The first direct evidence of a Late Devonian coelacanth fish feeding on conodont animals. *Naturwissenschaften,* 104**,** 26.

ZATOŃ, M., NIEDŹWIEDZKI, G., MARYNOWSKI, L., BENZERARA, K., POTT, C., COSMIDIS, J., KRZYKAWSKI, T. & FILIPIAK, P. 2015. Coprolites of Late Triassic carnivorous vertebrates from Poland: An integrative approach. *Palaeogeography, Palaeoclimatology, Palaeoecology,* 430**,** 21-46.

ZATOŃ, M. & RAKOCIŃSKI, M. 2014. Coprolite evidence for carnivorous predation in a Late Devonian pelagic environment of southern Laurussia. *Palaeogeography, Palaeoclimatology, Palaeoecology,* 394**,** 1-11.

ZIDEK, J. 1980. Acanthodes lundi, new species (Acanthodii) and associated coprolites from uppermost Mississippian Heath Formation of central Montana. *Annals of Carnegie Museum,* 49**,** 49-78.

ZUSCHIN, M., HARZHAUSER, M. & SAUERMOSER, K. 2006. Patchiness of local species richness and its implications for large-scale diversity patterns: an example for the middle Miocene of the Paratethys. *Lethaia,* 39**,** 65–80.